PURDUE UNIVERSITY
Purdue Research Foundation
Lafayette, Indiana

AN EXPERIMENTAL AND ANALYTICAL STUDY OF REAL SURFACE EFFECTS ON RADIANT HEAT TRANSFER

by

J. S. TOOR, R. VISKANTA AND
E. R. F. WINTER

May 1971

School of Mechanical Engineering
Heat Transfer Laboratory

AN EXPERIMENTAL AND ANALYTICAL STUDY OF REAL SURFACE EFFECTS ON RADIANT HEAT TRANSFER

by

J. S. TOOR, R. VISKANTA AND
E. R. F. WINTER

May 1971

AN EXPERIMENTAL AND ANALYTICAL STUDY OF REAL SURFACE EFFECTS ON RADIANT HEAT TRANSFER

by
J. S. Toor
R. Viskanta
E. R. F. Winter
School of Mechanical Engineering
Purdue University
Lafayette, Indiana 47907

Research Supported
by
Manned Spacecraft Center
National Aeronautics and Space Administration
Houston, Texas 77058

under
Contract No. NAS 9-8118

May 1971

FOREWORD

Except for minor changes, this report constitutes the doctoral dissertation of Mr. J. S. Toor which was submitted to the Faculty of Purdue University in partial fulfillment of the degree of Doctor of Philosophy.

ACKNOWLEDGMENT

This research was sponsored by Manned Spacecraft Center, National Aeronautics and Space Administration, under contract No. NAS 9-8118. The Technical Monitor was Mr. R. E. Durkee. Purdue Research Foundation provided financial support to Mr. J. S. Toor in the form of a David Ross Fellowship and Purdue University made available additional computer funds.

Certain members of the staff of the School of Mechanical Engineering of Purdue University contributed to the successful completion of this research. Special appreciation is expressed to Professor R. J. Schoenhals for his comments and careful reading of a draft of the report. The authors wish to acknowledge many helpful discussions with graduate students E. E. Anderson, R. W. Bergstrom, Jr., M. Abrams and B. W. Grange. Messrs. A. Clausen, C. Shanke and W. Walls made helpful suggestions during the experimental phase of the work. The help of Mr. J. Y. Baladi, in preparation of illustrations and other tasks is also acknowledged.

TABLE OF CONTENTS

Page

LIST OF TABLES v

LIST OF FIGURES. vii

LIST OF SYMBOLS. x

ABSTRACT xiii

1. INTRODUCTION 1

2. LITERATURE SURVEY. 4

2.1 Radiation Characteristics of Surfaces . . . 4
2.1.1 Radiation Characteristics of Ideal Surfaces 4
2.1.2 Theoretical Models for Optical Constants. 5
2.1.3 Radiation Characteristics of Real Surfaces 8
2.1.3.1 Reflectance, Emittance and Absorptance 8
2.1.3.2 Bidirectional Reflectance . 9
2.2 Analysis of Radiation Interchange 13
2.3 Experiments on Radiation Interchange . . . 18

3. FORMULATION OF THE PROBLEM AND METHOD OF SOLUTION . 23

3.1 Introduction 23
3.2 Radiation Interchange by 'Action at a Distance' Method 27
3.3 Choice of Configuration. 30
3.4 Reduction of Integral Equations 31
3.5 Radiation Characteristics of Surfaces . . . 33
3.5.1 Constant Property Models. 34
3.5.2 Specular Directional Property Models. 36
3.5.3 Diffuse Plus Specular Directional Property Models. 37
3.6 Solution of Integral Equations 39
3.7 Radiation Interchange by the Monte Carlo Method 41

Page

4. EXPERIMENTAL APPARATUS AND PROCEDURE 47

4.1 Introduction 47
4.2 General System Design 48
4.3 Test Chamber 50
4.4 Test Assembly 53
4.5 Test Surfaces 58
4.5.1 Choice of Test Surface Material and Size 58
4.5.2 Preparation of Surfaces 60
4.5.3 Measurement of Surface Roughness . . 60
4.6 Instrumentation 70
4.7 Experimental Procedure 72

5. RESULTS AND DISCUSSION 76

5.1 Independent Parameters 76
5.2 Comparison of Experiments and Analyses. . . 78
5.2.1 Comparison of Measured and Predicted Spectral Local Irradiation 82
5.2.2 Comparison of Measured and Predicted Total Local Irradiation 92
5.2.3 Comparison of Measurements and Predictions on Overall (Average) Basis 102

6. CONCLUSIONS AND RECOMMENDATIONS 107

7. REFERENCES 111

APPENDIX A: SPECULAR COMPONENT OF REFLECTIVITY . . . 121

APPENDIX B: DISCUSSION OF EXPERIMENTAL ERRORS . . . 135

APPENDIX C: TABULATION OF MEASURED AND PREDICTED IRRADIATION DATA 138

APPENDIX D: RECIPROCITY RELATION FOR RADIATION EXCHANGE. 144

LIST OF TABLES

Table		Page
1.	Survey of Experiments on Radiation Interchange	20
2.	Theoretical Models for Radiation Characteristics of Surfaces	35
3.	Typical Variation of the Temperature Across the Hot Surface.	57
4.	Description of Surfaces Used in the Experiment	63
5.	a. Location of the Thermopiles on the Cold Plate	70
	b. Location of the Thermocouples on the Hot Plate	70
6.	Overall Measured Irradiation and Fractional Departure from Experiment for Various Analyses on Spectral Basis, $\lambda = 3.08\mu$	103
7.	Overall Measured Irradiation and Fractional Departure from Experiment for Various Analyses on Spectral Basis, $\lambda = 4.51\mu$	104
8.	Overall Measured Irradiation and Fractional Departure from Experiment for Various Analyses on Total Basis	105

Appendix
Table

A-1.	Overall Specular Component of Reflectivity of Perfectly Reflecting Surface 1. The Intensity of Radiation Leaving Surface 3 is Diffuse with the Spectral Distribution Corresponding to Blackbody Emission at the Indicated Temperature. Varies Linearly with ξ, $I_{3\lambda}(\xi, \eta) = a + b\xi$.	134

Appendix Table

C-1. Measured and Predicted Local Irradiation G^*_λ on Spectral Basis, $\lambda = 3.08\mu$ 138

C-2. Measured and Predicted Local Irradiation G^*_λ on Spectral Basis, $\lambda = 4.51\mu$ 140

C-3. Measured and Predicted Local Irradiation G^* on Total Basis 141

LIST OF FIGURES

Figure		Page
1.	Comparison of Experimental Data and Simple Drude Theory of Normal Reflectance of Ultra High Vacuum Silver, Gold and Aluminum from 3-30μ, from Reference [8]	6
2.	Geometry of Radiation Incident and Leaving a Differential Area	25
3.	Configuration Studied	25
4.	View of Complete Experimental System	49
5.	Schematic Diagram of Test Assembly	51
6.	View of the Reflector Plate and the Moving Mechanism	52
7.	View of Arrangement of Test Surfaces	54
8.	Design Sketch of Cold Block, Reflector Block, Hot Test Plate and Cold Test Plate	55
9.	Roughness Profile of Test Surfaces, a,b) Bi-directional Surface, B-3; c) Bidirectional Surface, B-2; d) Diffuse Surface, D-3	62
10.	Autocorrelation Coefficient and Roughness Height Density of Test Surfaces	65
11.	Micrographs and Roughness Profiles of Test Surfaces S-2 and B-2 by Scanning Electron Microscope	67
12.	Micrographs and Roughness Profiles of Test Surfaces B-3 and D-3 by Scanning Electron Microscope	68
13.	Typical Thermopile Calibration Curve	74
14.	Comparison of Total Absorption Factors for Different Models, Surface Arrangement S-S-B, $\delta = 1$, $\eta = 1/8$.	81

Figure | Page

15. Comparison Between Measured and Predicted Irradiation for Different Models, Surface Arrangement S-S-S, $\lambda = 3.08\mu$, $\delta = 1$, $\gamma = 1/6$. . 83

16. Comparison Between Measured and Predicted Irradiation for Different Models, Surface Arrangement S-S-S, $\lambda = 3.08\mu$, $\delta = 1$, $\gamma = 1/2$. . 84

17. Comparison Between Measured and Predicted Irradiation for Different Models, Surface Arrangement S-S-B, $\lambda = 4.51\mu$, $\delta = 1$, $\gamma = 1/6$. . 87

18. Comparison Between Measured and Predicted Irradiation for Different Models, Surface Arrangement S-S-B, $\lambda = 4.51\mu$, $\delta = 1$, $\gamma = 1/2$. . 88

19. Comparison Between Measured and Predicted Irradiation for Different Models, Surface Arrangement S-B-S, $\lambda = 3.08\mu$, $\delta = 1$, $\gamma = 1/6$. . 90

20. Comparison Between Measured and Predicted Irradiation for Different Models, Surface Arrangement S-B-S, $\lambda = 3.08\mu$, $\delta = 1$, $\gamma = 1/2$. . 91

21. Comparison Between Measured and Predicted Total Irradiation for Different Models, Surface Arrangement S-S-S, $\delta = 1$, $\gamma = 1/6$. . . 93

22. Comparison Between Measured and Predicted Total Irradiation for Different Models, Surface Arrangement S-S-S, $\delta = 1$, $\gamma = 1/2$. . . 94

23. Comparison Between Measured and Predicted Total Irradiation for Different Models, Surface Arrangement S-S-B, $\delta = 1$, $\gamma = 1/6$. . . 96

24. Comparison Between Measured and Predicted Total Irradiation for Different Models, Surface Arrangement S-S-B, $\delta = 1$, $\gamma = 1/2$. . . 97

25. Comparison Between Measured and Predicted Total Irradiation for Different Models, Surface Arrangement S-S-B, $\delta = 1$, $\gamma = 1/2$, $\eta = 1/8$ 99

26. Comparison Between Measured and Predicted Total Irradiation for Different Models, Surface Arrangement S-B-S, $\delta = 1$, $\gamma = 1/6, 1/2$. 100

Figure Page

27. Comparison Between Measured and Predicted Total Irradiation for Different Models, Surface Arrangement S-B-B, $\delta = 1$, $\gamma = 1/2$. . . 101

Appendix Figure

A-1. Specular Component of Reflectivity of Spectral Intensity for a Perfectly Reflecting Material . 123

A-2. Effect of Directional Variation of Spectral Intensity on the Specular Component of Reflectivity for a Perfectly Reflecting Material, Eq. (A·2) 125

A-3. Specular Component of Reflectivity of Blackbody Intensity for a Perfectly Reflecting Material, Eq. (A·7) 128

A-4. Specular Component of Reflectivity of Perfectly Reflecting Surface 1. Intensity of Radiation Leaving Surface 3 is Diffuse and Uniform with the Spectral Distribution Corresponding to Blackbody Emission at the Indicated Temperature. 133

LIST OF SYMBOLS

Symbol	Definition
A	Surface area
a	Correlation distance
a_m	Mechanical correlation distance
B	Bidirectional
B_{di-j}	Absorption factor, defined by Eq. (3·34)
CP	Constant property
D	Diffuse or density of surface roughness heights
DP	Directional property (emission and absorption according to Fresnel's equations)
E	Total energy emitted per unit time and per unit area
EXP	Experimental
f	Reflection distribution function, defined by Eq. (3·11)
G	Irradiation, defined by Eq. (3·6)
g	Specular component of reflectance predicted by Beckmann or Davies model, Eq. (3·31)
I	Leaving intensity of radiation
I'	Incident intensity of radiation
J	Radiosity, defined by Eq. (3·7)
K	Kernel function, defined by Eq. (3·14)
L,W,H	See Figure 3
N	Number of energy bundles
n	Number of surfaces in the enclosure
Q	Overall heat transfer rate, Eq. (3·39)
q	Local heat flux, Eq. (3·1)
R	Local specular component of reflectance
$\overline{R}$	Area averaged specular component of reflectance
S	Specular

Symbol	Definition
S-B-S	Surfaces in position 1,2,3 respectively
T	Temperature
UR	Uniform radiosity
x,y,z	Coordinates
z	Surface roughness height from the mean

Greek Symbols

α	Absorptance, absorptivity
γ,δ	H/L, W/L, respectively
ε	Emittance, emissivity
θ	Polar angle
λ	Wavelength
λ_m	Mean wavelength
μ	Microns
ξ,η	Dimensionless coordinates, x/L and y/L, respectively
ρ	Reflectance, reflectivity
σ	Stefan-Boltzman constant or rms roughness
σ_m	Mechanical rms roughness
τ	Transmittance
ϕ	Azimuthal angle
Ω	Solid angle
$\vec{\Omega}$	Direction (θ,ϕ), Figure 2

Subscripts

b	Refers to blackbody
G	Gray
i,j	Dummy indices
SG	Semigray
λ	Refers to spectral values
∞	Refers to perfectly reflecting surface
$\supset$	Integration over hemisphere

Symbol	Definition
	Superscripts
d	Diffuse component of reflectance
s	Specular component of reflectance
'	Incident direction
*	Dimensionless irradiation

ABSTRACT

This study was undertaken with the purpose of critically examining the validity of the commonly used simplified models for predicting local as well as overall radiation interchange among real surfaces. The directional and spectral effects have been examined separately by comparing the experimental data with the predictions based on simple and more detailed models for the radiation properties of surfaces. These comparisons have been made spectrally and on a total basis.

Because of the mathematical difficulties associated with the numerical solution of a system of integral equations for the intensity of radiation leaving a surface, the problem has been solved by the Monte Carlo method. Solutions for the local incident flux were obtained for several models approximating the radiation characteristics of the surfaces. The models ranged from simple diffuse and specular to more detailed nongray diffuse plus specular directional property models with the specular component of reflectance calculated from the bidirectional Beckmann model. The directional property variations were evaluated from Fresnel's equations with the optical constants predicted from simple Drude theory.

The configuration studied consisted of three plane parallel surfaces of finite extent. This permitted critical examination of the influence of various parameters on radiation interchange. The test surfaces were gold with rms roughnesses varying from 0.02μ to 7.1μ. Enclosure surface temperatures varied from 77°K to 760°K. The local incident flux was measured at wavelengths of 3.08μ and 4.51μ and on the total basis.

Comparisons between the experimental data and predictions are presented in an attempt to ascertain the adequacy of the models for providing the local and overall irradiation on spectral and total bases. For the most part, the prediction of the overall irradiation using appropriate constant property models agrees well with the experimental results to within the combined experimental and theoretical uncertainties. In general, it is concluded that for accurate prediction of local irradiation the directional property variation and specularity of surfaces should be taken into account. The results based on gray and semigray analyses agree equally well with experimental data provided that the directional effects are considered and the direction independent specular component of reflectance is evaluated properly. Additional conclusions, recommendations and procedures are also given.

1. INTRODUCTION

Radiant heat transfer has become increasingly important in modern day technology. Thermal problems encountered in the design of space vehicles capable of penetrating into unfamiliar environments include such widely divergent areas as long-life storage of cryogenic liquids, heat rejection systems, solar power generation devices, maintenance of safe and comfortable environments in living quarters and instrument compartments. Other areas where knowledge of radiant transfer is essential involve the design of furnaces, high temperature chemical equipment, high temperature energy conversion devices, reactor shielding and infrared surveillance. In these applications radiation heat transfer is quite important, and in some cases it is the only means of energy transfer. The inability to accurately predict radiant heat transfer has been illustrated by overheating of the Mariner II spacecraft. Temperatures not only exceeded the upper design tolerances but finally even the upper measuring range. Future generation spaceships with tighter thermal tolerances and much longer active life will demand improved thermal design and control. This calls for more reliability, greater precision and greater detail in radiant heat transfer predictions than were considered necessary in the past.

This demand has provided the impetus for the research effort in the various aspects of radiant heat transfer and has resulted in a number of new approaches for computation of radiation interchange between surfaces. A number of simplified models for approximating the radiation surface properties have been employed; however, the validity of these models and the accuracy of the methods of solution have

not been substantiated by more realistic and refined analysis or experiments.

In spite of the importance of radiation interchange, only a modest amount of analytical and experimental work has been reported. Analysis has been limited only to simple surface characteristic models and enclosures because of the complexity of the problem and due to the lack of accurate knowledge of radiation properties of surfaces. Experimental work has been limited by the difficulties associated with eliminating convection heat transfer and providing experimental environments which eliminate extraneous radiation. The small number of experiments carried out have reported the measurements on a total (integrated over the whole spectrum) basis only.

The existing experimental data are not conclusive and in some cases are contradictory. "Diffuse gray analysis is relatively good for all cases", "analysis which does not include bidirectional effects can lead to large error", "no general conclusions can be drawn" are the statements of some of the previous investigators who have measured the heat transfer on total basis and performed analyses on a gray or a semigray basis. This illustrates how incomplete our understanding is at the present time and demonstrates the inability to predict radiation exchange in real enclosures. Thus, additional research effort is needed, and this study was undertaken to meet this need.

It was conceived as an analytical and experimental study. Analysis was necessary to predict the radiation exchange between real surfaces using more realistic surface characteristic models so that the validity of simplified methods could be examined. And, experiment was needed to verify the predictions. Specifically, the following tasks were undertaken:

1. Measure the spectral and total local radiant heat transfer in an enclosure consisting of simply arranged surfaces.

2. Predict the spectral and total local radiant heat transfer in the enclosure using simple as well as detailed models.
3. Compare analytical predictions with experimental data and examine the validity of the commonly used methods of analysis.
4. Estimate the range of validity of the commonly used approximations for radiation exchange and suggest simplified models and procedures which should be employed for more realistic radiant heat transfer calculations.

In the next chapter literature pertaining to radiation interchange between surfaces is reviewed. In Chapter 3 the radiation interchange problem is formulated using both "action at a distance" and "Monte Carlo" methods. Solutions based on the integral equations and the Monte Carlo methods are discussed. Experimental apparatus and procedure are given in Chapter 4. The results are presented and discussed in Chapter 5, while Chapter 6 contains conclusions based on this study as well as the recommendations for future work.

2. LITERATURE SURVEY

In this chapter a review of the literature relevant to this study is presented. Emphasis is placed on papers describing the most recent achievements. Most of the earlier work is referred by way of textbooks or previous review articles. This survey covers three general areas: 1) radiation characteristics of surfaces, 2) analysis of radiation interchange, and 3) experiments on radiation exchange.

2.1 Radiation Characteristics of Surfaces

In the analysis of radiant energy interchange among surfaces knowledge of emission, absorption and reflection characteristics is needed. Depending on the nature of the application, various degrees of detail are required in specifying the radiation characteristics of a surface. These details depend upon the surface arrangement, temperatures, emissivities and the energy quantities to be calculated. For example, the calculation of the local (overall) radiant heat loss, as compared to local (overall) radiant interchange, may demand a different degree of detail of the radiation characteristics of surfaces. The determination of these characteristics from theoretical models and their evaluation by comparison with the experimental data is discussed below.

2.1.1 Radiation Characteristics of Ideal Surfaces

For an ideal (clean and optically smooth) surface, the monochromatic reflectivity for each component of polarization can be calculated by Fresnel's equations. With the aid

of Kirchhoff's law, the magnitude and directional distribution of the emissivity can be inferred. However, for accurate predictions of these characteristics, precise knowledge of optical constants of the surface material is required. Models for predicting these constants are discussed briefly below.

2.1.2 Theoretical Models for Optical Constants

From the many available models for predicting the optical constants of materials we shall discuss only those which are relevant to this study, i.e., for infrared radiation and materials of high electrical conductivity. The most widely used theories of this type are due to Drude [1]*, Hagen-Rubens [2] and Roberts [3-5] in addition to those based on the anomalous skin effect models [6, 7].

Drude has assumed that metals contain free electrons which oscillate under the influence of incident waves with the same frequency. The viscous damping forces, due to collisions between accelerated electrons and the atomic lattice, cause a phase difference between the oscillation of the electrons and the field. If the average time between these collisions (relaxation time) and the number density of free electrons is known, the optical properties of the metal can be predicted. These two parameters can be estimated from the electrical conductivity, the number of valence electrons per unit volume and the assumption of a spherical Fermi surface. This is called the "Drude Free Electron" model. In a recent study Bennett and Bennett [8] have shown (Figure 1) that the measured infrared reflectance† from carefully prepared silver, gold and aluminum surfaces is in excellent agreement with the predictions of Drude's theory.

---

* Numbers in brackets denote references.

† Radiation terms end with -ance for real surfaces and with -ivity for ideal surfaces.

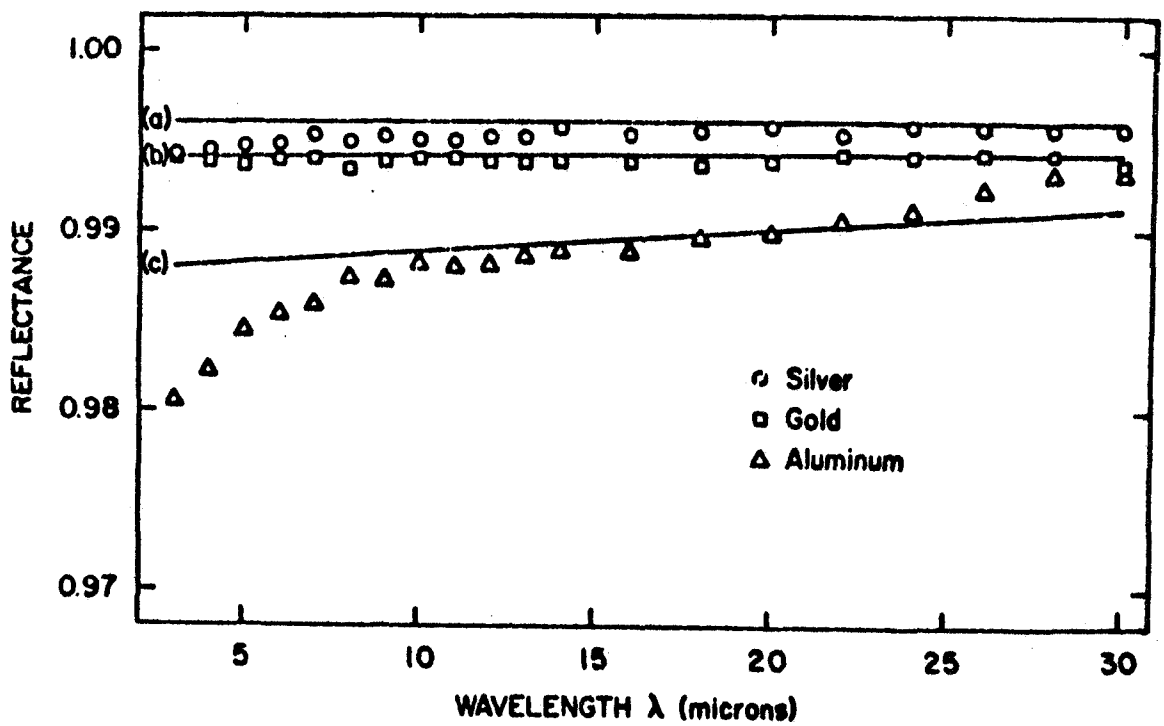

Figure 1. Comparison of Experimental Data and Simple Drude Theory of Normal Reflectance of Ultra High Vacuum Silver, Gold and Aluminum from 3-30μ, from Reference [8].

Also, in the near and far infrared the change of emittance with wavelength for metals is in good agreement [9] with the Drude model.

The simplest of all the atomic models is the one given by Hagen-Rubens [2]. This model assumes that the metal is a continuum and that the classical laws of electricity and magnetism can be applied. Again the optical properties of a metal for radiation of different wavelengths can be predicted from the DC electrical conductivity. This model is in fair agreement with experiments in the far infrared. For shorter wavelengths the electrons see a varying field during the time they traverse their mean free path; thus, the current density is no longer equal to the electrical conductivity times the electric field, a basic assumption in the derivation of the electromagnetic wave equations. Similarly, this relation is not appropriate when quantum skin effect is present.

Roberts [4] has extended Drude's model to account for more than one type of conduction electron. Mott [10] has recognized that both the s and d electrons contribute to the conduction of electricity and hence to the optical properties. Although Roberts' model is better than Drude's or Hagen-Rubens' [11-13] in the visible and near infrared, it has the objectionable feature in that, in addition to being more complicated, it is semiempirical and certain coefficients have to be determined experimentally.

When the mean free path of the electrons becomes large as compared to the wavelength and the penetration depth of the EM wave, the scattering of the electrons is mostly due to the surface of the metal rather than the interior of the metal. Thus, the absorptance is no longer controlled entirely by the bulk conductivity but is also affected by the condition of the metal surface. This phenomenon is known as the anomalous skin effect. Depending upon the condition of the surface, the electrons are reflected from

the surface specularly, diffusely or semi-specularly. This theory is not discussed further as it is of little importance in the infrared [14, 15] even at cryogenic temperatures.

2.1.3 Radiation Characteristics of Real Surfaces

2.1.3.1 Reflectance, Emittance and Absorptance

Real surfaces differ from the ideal ones in that the surfaces are not ideally smooth and optical properties of the material are not the same as those of the bulk material. The latter is due to work hardening, oxidation, etc.

The roughness of the surfaces also influences the radiation characteristics of materials, and the predictions based on ideal surface of the same material may not be valid. The influence of roughness on these characteristics is discussed below. As a detailed survey is already available in the literature [16-20], these effects will be discussed only very briefly here.

It is well known that appreciable roughening of a smooth surface decreases its reflectance, but many investigators do not agree whether or not small roughness decreases the reflectance appreciably. The conclusions drawn on the basis of experiments reported [21-25] are contradictory. The decrease in reflectance is attributed to multiple reflections within the surface asperities and/or because of surface damage. Quantitative effects of surface roughness on reflectance have been reported [21-29].

The effect of roughness on emittance has been examined by Rolling [21] and others [22, 23, 30, 31]. Rolling has reported that for sample temperatures from 865°K to 1640°K the hemispherical emittance of roughened (0.0 and 2.4μ) annealed platinum did not show an appreciable increase. It did show, however, significant changes in the spatial distribution of emitted energy. Although normal emittance

increased only slightly with increasing surface roughness (which agrees with the conclusions of others [22, 23]), the directional emittance increased more rapidly with increasing polar angle up to 70° and decreased for large angles of emission. Also, the spectral dependence of emittance on roughness was reduced as roughness increased and the temperature dependence was essentially eliminated. The conclusions of these experiments can be summarized by noting that, for small surface roughness without surface damage, the hemispherical emittance does not differ appreciably from that for an ideal surface, but the emittance increases with surface damage. Increasing surface roughness makes the surface behave more like a diffuse emitter. Large roughness increases the hemispherical emittance significantly due to multiple reflections. Since the spectral directional absorptance is equal to the spectral directional emittance, the above conclusions apply to absorptance also.

2.1.3.2 Bidirectional Reflectance

Although the effect of small roughness on the emittance and reflectance is relatively minor, it significantly affects the spatial distribution of reflected energy. Also, reflection from a surface may be considered perfectly specular in one limit, but the other limit, perfectly diffuse, does not exist [32]. The magnitude of the directional distribution of reflected radiation from a surface is governed not only by the surface conditions but also by the wavelength and direction of the incident energy.

In addition to the direction of incident radiation the spatial distribution of reflected energy depends on the root mean square roughness to wavelength ratio σ/λ and on the correlation distance to wavelength ratio a/λ. The former is a measure of the peak to valley distance while the latter is a measure of the density of the peaks. The

larger the distance between the peaks and the valleys, the larger is σ. Likewise, the larger the density of the peaks, the smaller is the value of a.

Bidirectional reflectance has been measured and predicted by numerous investigators [21-38]. For the purpose of discussion the variation of σ/λ, called the optical roughness, is usually divided into three ranges: $\sigma/\lambda << 1$, $\sigma/\lambda \simeq 1$ and $\sigma/\lambda >> 1$.

The slightly rough surface, $\sigma/\lambda << 1$, has been studied in detail by Houchens and Hering [33]. They have examined the Davies [34] and the Beckmann [35] models for predicting the spatial distribution of reflected energy. Both of the models assume that the surfaces are randomly rough and can be described statistically by the Gaussian distribution of the surface heights and the autocorrelation coefficient. Electrical conductivity of the material is assumed to be infinite, i.e., it is perfectly reflecting. Both models have identical expressions for the coherent component but differ in the incoherent part of the reflection distribution function. They [33] have shown that the Davies prediction does not conserve energy outside of a narrow range of parameters. The Beckmann model has been found to be superior because the specular and diffuse components of reflectance sum up to unity over a wide range of the σ/λ and a/λ parameters. The predictions of this model compare favorably with the experimental data of Birkebak and Eckert [36] and that of Smith and Hering [37]. For small roughness, this model predicts that the specular component of reflectance increases with decreasing optical roughness σ/λ, and increases with the angle of incidence. Also, in general, the reflected intensity peaks in the specular direction. The specular component of reflected energy depends only on the angle of incidence and on the optical roughness. The correlation distance a affects only the spatial distribution of incoherently reflected energy. The larger the value of a, the more the incoherently

reflected energy is concentrated around the specular direction. One limitation of this model is that it assumes the material to be of infinite conductivity, i.e., perfectly reflecting. To account for the finite conductivity of materials the reflectance distribution function is multiplied by the reflectance of the optically smooth material. This is an approximation, but it predicts the bidirectional reflectance reasonably well despite the fact that it violates reciprocity. These predictions have been confirmed by the experiments reported in [33, 36-38], to mention only a few references. It may be noted that violation of reciprocity relation occurs only for incoherent component [39].

For large optical roughness, $\sigma/\lambda >> 1$, multiple reflections occur between surface asperities resulting in decreased reflectance as compared to that of optically smooth surface of the same material. Since surface roughness is much larger than the wavelength of the energy, the methods of geometrical optics may be applied to predict bidirectional reflectance. Different models for predicting the distribution of reflected energy by these methods have been proposed [32, 40-42]. Treat and Wildin [43] have recast the model proposed by Torrance and Sparrow [32] to satisfy the reciprocity condition. In this model it is assumed that the reflecting surface is made up of pairs of opposing facets which form V-shaped grooves whose azimuthal orientation is random and whose opening half-angles follow a Gaussian distribution. The model satisfactorily predicts the off specular peaks observed [32] for $\sigma/\lambda >> 1$; however, its drawback is that certain parameters must be determined from experimental data.

When σ is of the same order as the wavelength λ, $\sigma/\lambda \simeq 1$, the previously discussed models can be extended to cover this range also. There is not a single derivation of the reflection distribution function based on solid theoretical grounds. Treat and Wildin [43] claim that their reformulated model of

Torrance and Sparrow [32] can be extended to σ/λ values significantly less than unity. Recently, Look and Love [44] have proposed a model which consists of one-dimensional, statistically constructed, asymmetric, smooth, rounded V-grooves. Incident energy bundles are traced by the Monte Carlo method. The quantum mechanical wavepackets are assumed to be spheres, and due to uncertainty principle, the incident energy in the groove is nonuniform. The predictions of this one-dimensional model agree well with the experimental data [28, 36, 38, 45] in the plane of incidence.

Radiation characteristics of one-dimensional periodic surfaces ($\sigma/\lambda >> 1$) have been reported in references [46-59]. The behavior of a periodic surface and the effect of interreflections and shadowing for the case of $\sigma/\lambda >> 1$ are of interest. Sparrow and Lin [46] have calculated the directional absorptance of a symmetric V-groove cavity with either diffusely or specularly reflecting walls when the cavity is illuminated by diffuse or collimated energy. Hemispherical [46-50] and directional emittances [47] have also been reported for this system without diffuse walls. Experimental data [48] for the hemispherical emittance and directional absorptance [51] show excellent agreement with the predictions. The experimental results reported by Zipin [52, 53] also show good agreement with the predictions. Trapezoidal cavities [54, 55] and asymmetrically grooved surfaces [56, 57] have also been studied. Hering and Smith [58] have extended the above analyses for V-shaped symmetric grooves to walls having any arbitrary specular component of reflectance. All of these analyses assume that local surface properties are constant. The only analysis of periodic dielectric surface appears to be that of Nelson and Goulard [59] who have studied a sinusoidal periodic surface and predicted the off specular peaks.

2.2 Analysis of Radiation Interchange

In radiant heat exchange calculations the postulate that the surfaces are non-polarizing, gray and diffuse has remained standard until recently, in spite of the experimental evidence to the contrary [30, 60, 61]. The justification for retaining the diffuse assumption is computational simplicity. A number of procedures have been devised for calculating radiation interchange between non-black diffuse surfaces. A review and comparison of these methods has been given by Sparrow and Cess [62]. If an approximation is made that the temperature, radiation surface characteristics and radiosity are uniform on each surface (or zone), the standard methods permit the calculation of radiant heat exchange between n surfaces with no greater difficulty than solving a system of n algebraic equations. However, the accuracy of the results obtained is uncertain due to departure of the basic assumptions from reality [60, 63]. Another deficiency of the method is that only the overall heat transfer for each surface (or a zone) can be calculated; local heat flux cannot be obtained.

Newer applications of radiation heat transfer knowledge to modern technology have placed emphasis on precision and greater detail which has brought forth new approaches and more realistic methods for computing radiant heat transfer. The first step in this direction relaxed the assumption that the radiosity over a given surface is uniform by formulating the radiation exchange problems in terms of integral equations and then solving these equations. A number of solutions for different geometrical arrangements have been reported in the literature. A summary of some of these studies is reported in the review article by Sparrow [63] and in the textbook by Sparrow and Cess [62].

An alternate to the diffuse model, which also lends itself to analytical treatment for some enclosures, has been proposed. An image method for calculating radiation interchange between plane surfaces, which emit diffusely and reflect specularly, has been developed by Eckert and Sparrow [64] and extended by Sparrow, et al. [65]. This method has been employed in a number of studies to facilitate computation of radiation interchange in axisymmetric configurations formed by specularly reflecting surfaces [66]. A more complete review of this model can be found elsewhere [62].

Real surfaces are neither purely diffuse nor purely specular reflectors. A model which probably approaches more closely to physical reality was suggested first by Münch [67], but is generally attributed to Seban [68]. It involves a subdivision of the hemispherical reflectance into diffuse, ρ^d, and specular, ρ^s, components, such that

$$\rho = \rho^d + \rho^s$$

This approximation, coupled with the assumption of diffuse emission, also lends itself readily to analytical treatment for some enclosures. This model has been adopted by many investigators [46, 69-72] for calculating radiation interchange between surfaces. This approach is more realistic than the methods discussed previously.

For angles of incidence between 0° and 60° the approach suggested by Kholopov [73] of approximating the bidirectional reflectance seems more realistic. It is based on the observation that, "in directional scattering, the axis of the reflected beam is directed in conformance to the law of mirror reflection, while the shape of the scattered energy resembles an ellipsoid of revolution for angles of incidence less than 60°". Some results corresponding to emittances of non-diffuse cavity-type sources have been presented [73, 74]. The bidirectional reflectance was approximated

by a portion of an ellipsoid of revolution, sliced by the reflecting surface, the major axis of which coincides with the direction of specular reflection. Although for some problems this kind of reflectance function seems more realistic, it has the serious drawback that it cannot be used for large angles of incidence. In addition, no correlation between surface roughness and the ratio of major to minor axis of ellipsoid of revolution has been proposed. Also, the actual shape of the reflected energy resembles more an ellipsoid rather than ellipsoid of revolution, the axis in the plane of incidence being larger than perpendicular to it.

It is well known that emission from surfaces is not diffuse and is often assumed only for computational simplicity. Investigations [70, 71] have shown that, for specularly reflecting surfaces, ignoring directional effects yielded local irradiation in some instances three times larger than that predicted by more realistic property models [70] and four times larger than experimentally measured values [71]. Hence, the correct accounting for the variation of properties with direction for specularly reflecting surfaces is very important [70, 71].

The directional emission and directional absorption model has also been used [17, 39, 70, 75] for nonspecularly reflecting surfaces for which the reflectance distribution function has been approximated as the sum of diffuse and specular reflectances which are both dependent on direction:

$$\rho(\theta') = \rho^{d}(\theta') + \rho^{s}(\theta')$$

Calculations based on this model show better agreement [39] with experiments. Results have also been reported [17, 70] for this model by assuming $\rho^{s}(\theta')/\rho(\theta') = \text{constant}$. However, a method for calculating the value of this constant is not available in the literature.

As was discussed in Section 2.1, the incoherent component of energy is not reflected diffusely but has been assumed so only for computational convenience. The incoherent part of the reflection distribution function, as predicted by Beckmann [35], has also been taken into account for the calculation of radiant heat transfer [17, 70, 72]. However, this function is too complicated to be of general use in engineering calculations. Results based on the Beckmann rough surface model have also appeared in the literature [17, 76]. For surfaces having large roughness, multiplication of the reflection distribution function by the reflectance of a smooth surface of the same material to correct for finite conductivity of the material may cause an appreciable error. This model is also too lengthy for the purpose of engineering calculations. The results reported in Reference [77] support the above conclusions. In addition, it is mentioned that the choice of the model is more critical when surfaces are of finite rather than infinite extent. Comparison of radiation exchange analyses with the above-mentioned models shows [39, 77] that the choice of the model and the level of detail needed to describe the radiation characteristics of participating surfaces are more important in predicting local radiant energy quantities, as opposed to the overall quantities.

The calculations carried out by all of the above-mentioned investigators are either on gray or semigray basis. There is no difficulty in formulating the exact problem for enclosures consisting of real surfaces. However, it is a formidable task to solve the problem so formulated. Bevans and Edwards [78] have reduced the exactly formulated problem, with some assumptions, and have developed three approximations which permit the use of angular-dependent properties in an approximate manner. The calculations can be done either on a gray basis or on a band basis.

There are only a few studies [79-81] which have considered spectral effects in the calculations of radiant heat transfer, and all are limited to infinite parallel plates. Goodman [79] has computed the net radiant heat exchange utilizing a diffuse emission model. The nongray predictions were about 30 percent higher for inconel and 17 percent higher for aluminum as compared with the gray surface analysis. Branstetter [80] has performed a similar analysis for molybdenum, tantalum and tungsten. The gray predictions of heat exchange with different combinations of materials varied from 60 to 106 percent of nongray analysis. Holt, et al. [81] has also calculated the radiation exchange between infinite parallel plates. They have included directional as well as the spectral effects. For all combination of materials (gold, iron and stainless steel) the predictions of the net radiation exchange with spectral and directional properties were higher than those obtained with the constant property gray analysis. The maximum difference (about 300 percent) occurred at very low temperatures and for large temperature differences between the plates of gold. For most of the situations considered, differences between the two analyses were 50 to 100 percent, the constant property gray analysis always predicting lower value. Although the above studies show that spectral and directional effects are important, extension of these conclusions to enclosures with finite surfaces is not justified. As an example, for the two infinite parallel plate configuration the constant property models predict essentially the same heat exchange irrespective of the bidirectional model, while sizable differences are calculated with various models for enclosures composed of finite surfaces.

As already mentioned, the numerical solution of rigorously formulated radiation heat exchange problems is often impractical even on very fast digital computers. As an alternate to the analytical formulation statistical methods

are being used more often for evaluation of radiation interchange in complex systems having direction-dependent surface characteristics. The Monte Carlo method and its application to radiation interchange problems has been reviewed by Howell [82]. A more complete survey of the literature dealing with the application of the Monte Carlo method is given in [77].

The survey of literature has shown that radiant heat transfer calculations with spectral and directional effects [81] have been carried out only for the infinite parallel plate geometry, and that these effects are important: Inclusion of bidirectional effects makes the problem too complicated, and furthermore the magnitude of these effects is not well known. The choice of the model and the level of detail needed to describe the radiation characteristics of participating surfaces is more important in predicting local radiant energy quantities. This is most critical for highly reflecting surfaces of finite extent and with large temperature differences. For complex systems having direction-dependent surface characteristics the Monte Carlo method is superior to the solution based on the integral equation approach.

2.3 Experiments on Radiation Interchange

The experimental measurement of radiant energy quantities of interest, i.e., irradiation, radiosity, heat flux and others has received very little attention. The experimental effort in the past has been mostly devoted to the determination of radiation surface characteristics such as the hemispherical emittance for which the overall radiant heat interchange was measured between simply arranged surfaces and the emittance determined. In other experiments [83] the equilibrium temperatures of surfaces which are exchanging heat by radiation only have been measured. A

summary of the pertinent experimental studies is given in Table 1.

Measurements of radiant heat exchange have been made by only a few investigators [67, 71, 75, 83-86, 88, 89]. The overall heat transfer between two eccentric spheres having different surface properties was measured by Elser [84]. He found that heat transfer increased with eccentricity and attributed this finding to the increased importance in specular reflection. A similar test arrangement was employed by Münch [67]. With the inner sphere made of oxidized copper and the other of oxidized brass, Münch has found that the overall radiant heat transfer increased slightly with eccentricity and that the radiation interchange factor based on the diffuse-specular model for reflection agreed well with the experimental data. Radiant heat interchange between two square plates of stainless steel at different temperatures was measured by Love and Gilbert [85]. For closed spacings the measured overall heat transfer agreed well with diffuse type of analysis.

Bevans, et al. [83] have measured the equilibrium temperatures of various surfaces comprising an enclosure when a constant heat flux was imposed at one of the surfaces. The enclosure consisted of square plates arranged in either an adjoint configuration or a parallel configuration separated with or without a third surface called a reflector. The heated surface was painted with a black paint while the cooled surface was either black or painted with aluminum paint. The measured equilibrium temperature of the sink was found to be always larger than predicted. The greatest discrepancies between the predictions and the experiments occurred for situations in which both the sink and the reflector were highly reflecting. Predictions based on the simple diffuse analysis, the specular analysis and the diffuse-specular gray directional property analysis using second approximation of Bevans and Edwards [78] were equally

TABLE 1

Survey of Experiments on Radiation Interchange

Surface shape	Configuration	Measured	Ref.	Year	Remarks
Sphere	Two concentric and eccentric spheres	Overall heat transfer	84, 67	1949, 1955	No external radiation sources. Emission only
Square plate	Parallel and adjoint plates; Rectangular cavity	Equilibrium temperature	83	1965	
Square plate	Parallel plates	Overall heat transfer	85	1966	
Long plate	Parallel and adjoint plates	Local irradiation	75	1968	
Long plate	Rectangular cavity	Local irradiation	71	1970	
V-grooved and flat plate, Length/width = 2	Parallel plates	Overall heat transfer	89	1970	
	LEM model	Overall directional radiosity	86	1967	System exposed to an external collimated flux. No emission.
Long plate	Three sided cavity; one angle 90° and the other variable.	Local radiosity	88	1970	

in error as compared with the experimental data. The authors attributed this discrepancy to the lack of accurate knowledge of radiation properties, the gray radiation assumption, and approximations inherent in the analysis.

Schornhorst and Viskanta [75] have measured the local irradiation on two long narrow plates maintained at different temperatures in parallel and perpendicular configurations. After using several plate materials and surface roughnesses the authors have concluded that even for highly polished surfaces the gray diffuse analysis predicts the local irradiation within 20 percent of the measured values; however, the predictions of the appropriate constant property specular model for polished surfaces were higher in some cases from experimental data by a factor of two. They have concluded that the direction-dependent property model with reflectance represented by $\rho^d(\theta') + \rho^s(\theta')$ provides an excellent compromise between a realistic level of description of properties and a practical level of computational detail. Also, the choice of the property model was found to be more critical for evaluating the local irradiation than the local heat flux for highly reflecting surfaces.

Engstrom, et al. [71] have measured the local irradiation in a rectangular cavity formed by two long plates separated by an adiabatic surface. They have concluded that the diffuse analysis (where appropriate) yields relatively good approximations for radiant heat transfer. However, for highly reflecting surfaces approaching the optically smooth limit the predictions of the constant property specular model were in some cases higher than the experimental data by about a factor of four. The diffuse plus specular direction-dependent model recommended in [75, 77] was examined in detail by Toor, et al. [39]. It was found that the predictions based on this model were in better agreement with experimental results than those of the diffuse model; however, no general conclusions could be drawn.

Zapf [86] has simulated the "sunlit Apollo Lunar module" and measured the luminance in various directions. The analysis of Neu and Dummer [87] based on the bidirectional property model compares favorably with the experimental data, but in this case no interreflections were involved. Howell and Durkee [88] have measured the distribution of energy within a cavity exposed to a source of collimated incident radiation. They have concluded that the distribution of energy can be strongly dependent upon the bidirectional reflectances of the cavity surfaces, and analyses that do not include directional effects in their formulation can lead to large errors in predicting the distribution of energy. They have attributed the discrepancy between analysis and experiment of reference [75] either to certain assumptions or to experimental difficulties on which they did not elaborate. However, all the evidence so far suggests another possibility that radiation interchange among surfaces demands a different level of detail of surface properties when the system is irradiated by a collimated external flux compared to when the system walls themselves emit radiation. It has already been shown by Toor, et al. [90] and by Houchens and Hering [17] that the two cases lead to different conclusions.

The review of literature has revealed that larger discrepancies between experiment and analysis occur when the surfaces are highly reflecting. The few attempts made to analyze radiant heat transfer between surfaces with direction and wavelength dependent properties are limited by the gray assumption. The validity of the simplified methods of analysis have not been verified either by more realistic nongray calculations or by experimental measurements on a spectral basis. It is clear that there is a definite need for analysis on a nongray basis and for experimental measurements, on both a spectral as well as a total basis, to check the validity of the models for predicting radiation heat interchange.

3. FORMULATION OF THE PROBLEM AND METHOD OF SOLUTION

3.1 Introduction

It is the purpose of this chapter to formulate the radiation interchange problem in an enclosure (accounting for the spectral, directional and roughness effects) with as few idealizing assumptions as possible. Before proceeding with the details of the analysis it is desirable to present and discuss the basic postulates. The following assumptions are made in the analysis:

1. Planck's and Kirchhoff's laws are valid.
2. The geometric optics theory is valid for the analysis of radiant heat interchange. The two fundamental postulates of the theory are:
   a) the various effects and quantities are additive and
   b) the directional change of radiation is negligible.

   Postulate (a) implies that the phenomenon of diffraction, interference and coherence are excluded [91].
3. The radiation characteristics of surfaces are independent of the polarization state of the incident intensity.
4. The medium separating the surfaces is of unit index of refraction and does not participate in the exchange of radiation.

Assumption 1 implies that only thermal radiation is considered. The body which is exchanging heat is close to a state of thermodynamic equilibrium defined by temperature T. This means that emission, absorption and reflection

characteristics are those which may be measured or calculated at the equilibrium state and that the relation $\alpha_\lambda(\theta) = \varepsilon_\lambda(\theta)$* is assumed to be valid. Assumption 2 implies that the radiation from each element is propagating as a plane wave when it reaches the irradiated element and that the radiation is incoherent relative to that from any other element. This requires that the dimensions of the surface elements, as well as the distances between the surfaces, be much larger than the wavelength of radiation. The fact that assumption 3 is not generally valid is well recognized [91] and has been examined in detail by Edwards and Bevans [92] and others [61, 90]. No conceptual difficulties would be introduced by omitting assumptions 3 and 4; however, they have been retained in the present treatment for the sake of reducing the nonessential mathematical complications. Assumptions 1 and 2 are not expected to seriously impair the relevancy of the analysis for engineering applications, while the use of assumption 3 can be expected to cause some deviation of the resulting predictions from reality.

In radiant heat transfer the quantities of interest such as local or overall heat flux, irradiation and radiosity can be calculated by considering a radiation balance at an elementary surface dA on an opaque surface specified by a position vector $\vec{r}$ as shown in Figure 2. The local spectral heat flux, $q_\lambda(\vec{r})$, can be expressed from the viewpoint of an observer just inside the body as

$$q_\lambda(\vec{r}) = \varepsilon_\lambda(\vec{r})E_{b\lambda}(\vec{r}) - \alpha_\lambda(\vec{r})G_\lambda(\vec{r}) \qquad (3\cdot1)$$

where ε_λ and α_λ are given by

---

* Under non-thermodynamic equilibrium $\alpha_\lambda(\theta) \neq \varepsilon_\lambda(\theta)$ strictly because of induced emission.

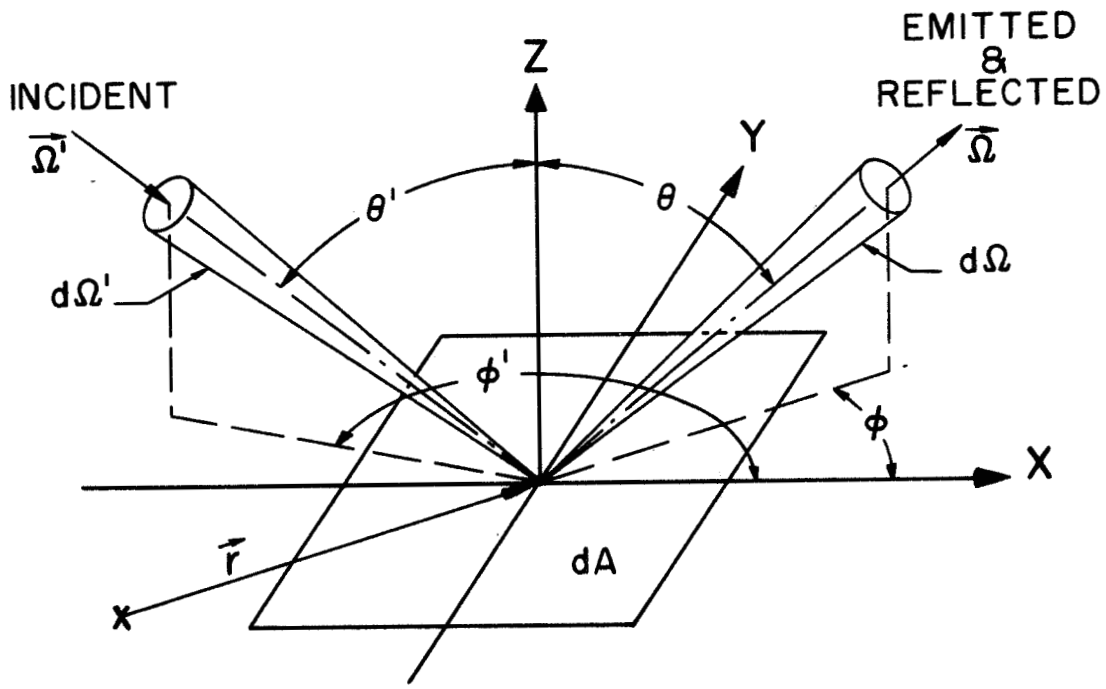

Figure 2. Geometry of Radiation Incident and Leaving a Differential Area.

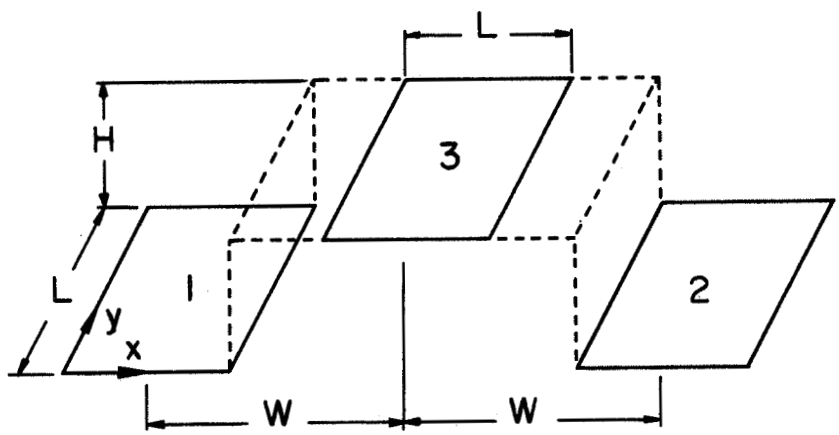

Figure 3. Configuration Studied.

$$\varepsilon_\lambda(\vec{r}) = \frac{E_\lambda(\vec{r})}{E_{b\lambda}(\vec{r})} = \frac{\int_\Omega \varepsilon_\lambda(\vec{\Omega},\vec{r}) I_{b\lambda}(\vec{r})\cos\theta d\Omega}{\int_\Omega I_{b\lambda}(\vec{r})\cos\theta d\Omega}$$

$$= \frac{1}{\pi}\int_\Omega \varepsilon_\lambda(\vec{\Omega},\vec{r})\cos\theta d\Omega \qquad (3\cdot2)$$

and

$$\alpha_\lambda(\vec{r}) = \frac{\int_{\Omega'} \alpha_\lambda(\vec{\Omega}',\vec{r}) I'_\lambda(\vec{\Omega}',\vec{r})\cos\theta' d\Omega'}{\int_{\Omega'} I'_\lambda(\vec{\Omega}',\vec{r})\cos\theta' d\Omega'} \qquad (3\cdot3)$$

The spectral directional emissivity $\varepsilon_\lambda(\vec{\Omega},\vec{r})$ is simply the ratio of the spectral energy actually emitted by the elementary surface area in the direction $\vec{\Omega}$ to that emitted in the same direction if the surface were black. Mathematically this is stated as

$$\varepsilon_\lambda(\vec{\Omega},\vec{r}) = I_\lambda(\vec{\Omega},\vec{r})/I_{b\lambda}(\vec{r}) \qquad (3\cdot4)$$

Also, by definition, the spectral directional absorptivity is the fraction of the spectral energy incident from a certain direction on an elementary surface area which is absorbed by that elementary surface area.

The local spectral heat flux can also be expressed from the viewpoint of an observer just outside the body as the difference between the spectral radiosity and the spectral irradiation,

$$q_\lambda(\vec{r}) = J_\lambda(\vec{r}) - G_\lambda(\vec{r}) \qquad (3\cdot5)$$

By definition of the spectral irradiation, $G_\lambda(\vec{r})$, is the spectral energy flux incident on an area and can be written as

$$G_\lambda(\vec{r}) = \int_{\Omega'} I'_\lambda(\vec{\Omega}',\vec{r})\cos\theta' d\Omega' \qquad (3\cdot6)$$

Similarly the spectral radiosity, $J_\lambda(\vec{r})$, is the spectral energy flux leaving an area and is expressed as

$$J_\lambda(\vec{r}) = \int_{\Omega} I_\lambda(\vec{\Omega},\vec{r})\cos\theta d\Omega \qquad (3\cdot7)$$

The total (integrated over the entire spectrum) local quantities can be calculated from the spectral values. For example, the total local radiant heat flux is written as

$$q(\vec{r}) = \int_0^\infty q_\lambda(\vec{r})d\lambda \qquad (3\cdot8)$$

The overall values can be obtained from the local values by integrating over the area. The overall (average) total heat transfer rate per unit area can be written as

$$\bar{q} = \frac{1}{A}\int_A q(\vec{r})dA \qquad (3\cdot9)$$

It can be observed from Eqs. (3·1) through (3·5) that the evaluation of the radiant energy quantities of interest demands the knowledge of the spectral and directional distributions of intensity of radiation leaving and incident on surfaces.

3.2 Radiation Interchange by 'Action at a Distance' Method

Under the assumptions mentioned in Section 3.1 problems of radiation interchange in an enclosure consisting of n surfaces can be easily formulated. Consider, for example, a radiation balance at an elementary surface dA_i located at some point $\vec{r}_i$ (Figure 2) of an enclosure formed by n surfaces. The spectral intensity of radiation leaving the surface element in the direction $\vec{\Omega}_i$ is denoted by $I_{i\lambda}(\vec{\Omega}_i,\vec{r}_i)$. It is the sum of the contributions due to emission and reflection of energy incident from all directions.

Introducing the reflection distribution function of McNicholas [93] and Polyak [94], the spectral intensity of radiation leaving the element of area dA_i in the direction $\vec{\Omega}_i$ is expressed as

$$I_{i\lambda}(\vec{\Omega}_i,\vec{r}_i) = \varepsilon_{i\lambda}(\vec{\Omega}_i,\vec{r}_i)I_{bi\lambda}(\vec{r}_i) + \int_{\Omega'} f_i(\vec{\Omega}_i',\vec{\Omega}_i,\vec{r}_i,\lambda)I'_{i\lambda}(\vec{\Omega}_i',\vec{r}_i)\cos\theta_i' d\vec{\Omega}_i' \quad (3\cdot10)$$

The first term on the right hand side of Eq. (3·10) accounts for emission and the second for reflection of incident radiation. The reflection distribution function relates the distribution of reflected intensity to the incident intensity from a certain direction according to

$$I_\lambda(\vec{\Omega},\vec{r}) = f(\vec{\Omega}',\vec{\Omega},\vec{r},\lambda)I'_\lambda(\vec{\Omega}',\vec{r})\cos\theta' d\Omega' \quad (3\cdot11)$$

Hence, if the incident intensity distribution is known, the reflected intensity distribution can be determined. The reflection distribution function is a basic property of the surface, and all other radiation characteristics of surfaces such as the emittance or reflectance can be calculated from it [95]. A correct reflection distribution function should 1) be symmetrical about the plane of incidence for an isotropic surface, 2) satisfy reciprocity conditions, 3) conserve energy and 4) agree with the experimental results.

When referred to the source surfaces Eq. (3·10) can be written as

$$I_{i\lambda}(\vec{\Omega}_i,\vec{r}_i) = \varepsilon_{i\lambda}(\vec{\Omega}_i,\vec{r}_i)I_{bi\lambda}(\vec{r}_i) + \sum_{j=1}^{n}\int_{A_j} f_i(\vec{\Omega}_i',\vec{\Omega}_i,\vec{r}_i,\lambda)I_{j\lambda}(\vec{\Omega}_j,\vec{r}_j)K_{ij}dA_j \quad (3\cdot12)$$

$$i = 1,2,\cdots n$$

where the configuration kernel K_{ij} is defined as

$$K_{ij} = \cos\theta_i' \cos\theta_j / |\vec{r}_i - \vec{r}_j|^2$$

Note that the angles involved in the sources of radiation have now been referred to the source surfaces. The integration indicated in Eq. (3·12) extends only over those parts of surface j which are directly 'visible' from dA_i. The summation over all surfaces includes even the contributions from surface i itself if other portions of surface i are 'visible' from dA_i. Incidence or emergence of radiant energy through imaginary surfaces can be treated similarly; however, the spectral intensity of radiation incident on a surface must be completely specified. Since an imaginary surface is perfectly transparent to radiation, the radiation incident from some external source on the outside of imaginary surface k is equal to the spectral intensity of radiation leaving the surface from inside, continued in the same direction.

For an enclosure consisting of n real surfaces, Eq. (3·12) contains n unknown functions I_1, I_2, $\cdots$ I_n. Since the unknowns appear under the integral sign, the resulting equations are integral equations. Once the solution for the I_i's has been determined from Eq. (3·12) for specified surface temperatures, other quantities of interest can be readily calculated. If, however, the local heat flux distribution is prescribed and it is necessary to calculate the temperature distribution, the problem is much more difficult since an iterative procedure must be employed to solve Eqs. (3·8) and (3·12) simultaneously.

Despite the ease of formulation of the radiation interchange problem, obtaining a closed form exact solution of the governing equations is not feasible. Hence, before the generally formulated radiation exchange problem, Eq. (3·12),

can be solved, it must be specialized to a definite configuration of surfaces.

3.3 Choice of Configuration

As mentioned in the INTRODUCTION, the objective of this study is to critically examine the validity of various commonly used models for radiation surface properties by comparing analytical predictions with experimental data. The configuration chosen must permit accurate predictions of heat transfer by retaining the essential features of the analysis while avoiding the distractions of complex geometrical relationships. Also, the predictions for the enclosure should be very sensitive to the choice of the model so that critical examination of various models can be made. The system should also be simple to construct and permit easy change of surface materials and geometrical parameters. For this study a system consisting of three rectangular parallel plates of finite extent, Figure 3, was selected. The following considerations have led to the choice of this configuration:

1. It has been studied previously [28, 72, 76, 92] and the analytical results have shown that it yields a very critical comparison between the predictions of the various models. This configuration was recommended by Bobco also for experimental investigation [96].
2. One surface can be adiabatic and the configuration can be made to represent both open and closed systems* by easy change of parameters.
3. By a proper arrangement of hot and cold surfaces the energy emitted from the hot surface is not directly incident on the radiation detectors located in the cold surface.

* The word "open" refers to such a system for which the ratio of heat loss to emission is large (near unity). On the other hand the word "closed" refers to a system for which this ratio is small.

4. The system has a simple geometrical character and is suitable for experiment and analysis.
5. The system arises in practical thermal control problems.

3.4 Reduction of Integral Equations

Assuming the temperatures and radiation properties to be uniform over each isotropic surface, Eqs. (3·12), which give the spectral leaving intensity for the configuration shown in Figure 3, reduce to the following system of integral equations:

$$I_{i\lambda}(x_i,y_i,\theta_i,\phi_i) = \varepsilon_{i\lambda}(\theta_i)I_{bi\lambda} + \int_{A_3} f_i(\theta_i',\phi_i',\theta_i,\phi_i,\lambda)I_{3\lambda}(x_3,y_3,\theta_3,\phi_3)K_{i3}dA_3 \quad i = 1,2 \tag{3·13a}$$

$$I_{3\lambda}(x_3,y_3,\theta_3,\phi_3) = \varepsilon_{3\lambda}(\theta_3)I_{b3\lambda} + \sum_{i=1}^{2} I_{bi\lambda}\int_{A_i} f_3(\theta_3',\phi_3',\theta_3,\phi_3,\lambda)\varepsilon_{i\lambda}(\theta_i)K_{i3}dA_i + \sum_{i=1}^{2}\int_{A_i}\int_{A_3} f_i(\theta_i',\phi_i',\theta_i,\phi_i,\lambda) f_3(\theta_3',\phi_3',\theta_3,\phi_3,\lambda)I_{3\lambda}(x_3,y_3,\theta_3,\phi_3)K_{i3}^2 dA_3dA_i \tag{3·13b}$$

Note that in Eq. (3·13) the function K_{12} is absent because surfaces 1 and 2 are coplanar. In terms of coordinates illustrated in Figure 3, the functions K_{ij} and angles can be expressed as

$$K_{ij} = H^2/[(x_i-x_j)^2+(y_i-y_j)^2+H^2]^2 \tag{3·14}$$

$$\theta_{ij} = \cos^{-1}\{H/[(x_i-x_j)^2+(y_i-y_j)^2+H^2]^{1/2}\} \tag{3·15}$$

$$\phi_{ij} = \tan^{-1}[(y_i-y_j)/(x_i-x_j)] \tag{3·16}$$

In terms of dimensionless distances,

$$\xi = x/L, \quad \eta = y/L \quad \text{and} \quad \gamma = H/L$$

Equations (3·13) can be expressed as

$$I_{i\lambda}(\xi_i,\eta_i,\theta_i,\phi_i) = \varepsilon_{i\lambda}(\theta_i)I_{bi\lambda} + \int_0^1\int_0^1 f_i(\theta_i',\phi_i',\theta_i,\phi_i,\lambda)I_{3\lambda}(\xi_3,\eta_3,\theta_3,\phi_3)K_{i3}d\xi_3 d\eta_3 \quad (3\cdot17a)$$

$$i = 1,2$$

$$I_{3\lambda}(\xi_3,\eta_3,\theta_3,\phi_3) = \varepsilon_{3\lambda}(\theta_3)I_{b3\lambda} + \sum_{i=1}^{2} I_{bi\lambda}\int_0^1\int_0^1 f_3(\theta_3',\phi_3',\theta_3,\phi_3,\lambda)\varepsilon_{i\lambda}(\theta_i)K_{i3}d\xi_i d\eta_i + \sum_{i=1}^{2}\int_0^1\int_0^1\int_0^1\int_0^1 f_i(\theta_i',\phi_i',\theta_i,\phi_i,\lambda)f_3(\theta_3',\phi_3',\theta_3,\phi_3,\lambda) I_{3\lambda}(\xi_3,\eta_3,\theta_3,\phi_3)K_{i3}^2 d\xi_3 d\eta_3 d\xi_i d\eta_i \quad (3\cdot17b)$$

where now the kernel function and the angles are given by

$$K_{ij} = L^2\gamma^2/[(\xi_i-\xi_j)^2+(\eta_i-\eta_j)^2+\gamma^2]^2 \quad (3\cdot14a)$$

$$\theta_{ij} = \cos^{-1}\{\gamma/[(\xi_i-\xi_j)^2+(\eta_i-\eta_j)^2+\gamma^2]^{1/2}\} \quad (3\cdot15a)$$

$$\phi_{ij} = \tan^{-1}[(\eta_i-\eta_j)/(\xi_i-\xi_j)] \quad (3\cdot16a)$$

This is a system of linear Fredholm integral equations of the second kind. Once it has been solved for $I_{3\lambda}$, it is easy to calculate both $I_{1\lambda}$ and $I_{2\lambda}$ from Eq. (3·17a). However, before one can proceed to solve these equations,

various parameters and functions appearing in the equations, for example, the radiation characteristics of surfaces, must be specified. This is done in the next section.

3.5 Radiation Characteristics of Surfaces

An analysis of radiation exchange among surfaces requires an acceptable description of the emittance, absorptance, and bidirectional reflectance of the participating surfaces. In the present application, where an attempt is made to evaluate the importance of real surface effects, considerable detail is required in specifying the radiation properties. However, the intent here is to adopt simple models that predict the radiant heat exchange realistically rather than to calculate the radiant exchange from more complicated models. Since the radiation characteristics of surfaces enter into the integral equation in a complicated manner, it is not possible to say, a priori, that a small (large) departure of these characteristics from reality will introduce only a small (large) error in the predictions of radiation heat transfer.

Previous studies have shown that, for better accuracy in the prediction of radiant interchange, directional effects [33, 70-72, 75] must be taken into account. However, these calculations were based on gray or semigray analyses. The predictions based on spectral and directional property models for infinite parallel plates in some cases were higher by a factor of four [81], which illustrates the importance of spectral and directional effects. Hence, for a meaningful comparison of the experimental data and the predictions, the analysis must include directional and spectral effects. Thus in the analysis dependence of radiation characteristics on direction, wavelength, temperature and surface roughness should be accounted for accurately. However, use of the incoherent part of the reflection

distribution function is too complicated for engineering calculations [70, 72], and such a detailed analysis is not justified in view of the fact that radiation characteristics of surfaces in general are not known accurately.

Since nongray effects make the problem rather complicated it is felt that for engineering calculations an alternative simple model should be explored. It should be based on the properties which can either be easily measured or can be calculated by incorporating the important spectral and directional effects. The predictions based on simplified models, then, must be compared with the predictions of nongray calculations and the experimental data to check the validity of the analysis. All the models used in the analysis are described below, and a summary is given in Table 2.

3.5.1 Constant Property Models

Diffuse Model, D. This is the commonly used diffuse model. The emittance and reflectance are considered to be independent of direction and wavelength. The total hemispherical and the spectral hemispherical properties are used for the total and spectral calculations, respectively. Thus, on a spectral basis

$$\varepsilon_\lambda = 1 - \rho_\lambda \tag{3·18}$$

and

$$f(\vec{\Omega}', \Omega, \lambda) = \rho_\lambda / \pi \tag{3·19}$$

Extensive calculations based on this model are found in the literature because it lends itself readily to analysis.

Specular Model, S. This is the simple specular model. The energy is assumed to be emitted diffusely and reflected specularly. The emittance and reflectance are considered to be independent of direction and wavelength. The reflection distribution function is expressed as

TABLE 2

Theoretical Models for Radiation Characteristics of Surfaces

Symbol	Model	Emission	Reflection	Reflection Distribution Function, $f(\vec{\Omega}', \vec{\Omega}, \lambda)$	Analyses	Some Previous Studies
D	Gray	Diffuse	Diffuse	ρ/π	Total, spectral	72,76
S	Gray	Diffuse	Specular	$\rho U(\delta)$	"	64,66
D+S	Gray	Diffuse	Diffuse + Specular	$\rho^d/\pi + \rho^s U(\delta)$	"	49,69-72
DP(S)	Spectral, Semigray, Gray	Directional	Specular	$\rho(\theta')U(\delta)$	"	70,71, 75,81,97
B(D+S)	Spectral	Directional	Diffuse + Specular	$\rho(\theta')[1-g(\theta',\sigma/\lambda)]/\pi+g(\theta',\sigma/\lambda)U(\delta)$	"	17,70,72
DP(D+S)	Semigray, Gray	Directional	Diffuse + Specular	$\rho^d(\theta')/\pi + \rho^s(\theta')U(\delta)$ $(\rho^s(\theta')/\rho(\theta') = \text{constant})$	"	17,70,71

$$f(\vec{\Omega}', \vec{\Omega}, \lambda) = \rho_\lambda U(\delta) \tag{3·20}$$

where

$$U(\delta) = \delta(\theta' - \theta)\delta[\phi' - (\phi + \pi)]/\cos\theta' d\Omega' \tag{3·21}$$

In Eq. (3·21), $\delta(x)$ is the Dirac delta function and is defined as follows:

$$\delta(x) = 0 \quad \text{for} \quad x \neq 0$$

$$= \infty \quad \text{for} \quad x = 0$$

and

$$\int_{-\infty}^{\infty} \delta(x)dx = 1$$

Diffuse plus Specular Model, D + S. This is the diffuse plus specular constant property model and is a combination of models D and S. The surfaces are considered to be diffuse emitters and to have both a diffuse and a specular reflectance component, such that

$$\rho_\lambda = \rho_\lambda^s + \rho_\lambda^d \tag{3·22}$$

and

$$f(\vec{\Omega}', \vec{\Omega}, \lambda) = \rho_\lambda^s U(\delta) + \rho_\lambda^d/\pi \tag{3·23}$$

This approach, suggested in [66, 67], is more realistic than the previous two models.

3.5.2 Specular Directional Property Models

Nongray, DP(S). For this nongray specular directional property model it is assumed that the surfaces are specular reflectors. The directional emittance and reflectance are predicted from Fresnel's equations, and from Kirchhoff's law

$$\varepsilon_\lambda(\theta') = 1 - \rho_\lambda(\theta') \tag{3·24}$$

The reflection distribution function is given by

$$f(\vec{\Omega}',\vec{\Omega},\lambda) = \rho_\lambda(\theta')U(\delta) \qquad (3\cdot25)$$

Calculations based on this model have appeared in the literature only for infinite parallel plates [81].

Semigray, DP(S). For this semigray model the surface is assumed to be a specular reflector, but the total emittance and absorptance are directional. The total directional emittance values used are calculated from the spectral emittances, the latter being predicted from Fresnel's equations. Thus,

$$\varepsilon(\theta') = \int_0^\infty \varepsilon_\lambda(\theta')E_{b\lambda}d\lambda/E_b \qquad (3\cdot26)$$

The total directional absorptance is calculated with the spectral distribution of incident intensity corresponding to the black body emission at the temperature of the emitting surface. Thus for calculating B_{ji} the directional absorptance of surface i is given by

$$\alpha_i(\theta') = \frac{\int_0^\infty \alpha_\lambda(\theta',T_i)E_{b\lambda}(T_j)d\lambda}{E_b(T_j)} \qquad (3\cdot27)$$

The reflection distribution function becomes

$$f(\vec{\Omega}',\vec{\Omega}) = \rho(\theta')U(\delta) \qquad (3\cdot28)$$

Gray, DP(S). This model is similar to the semigray model except that the total directional absorptance is assumed equal to the total directional emittance.

3.5.3 Diffuse Plus Specular Directional Property Models

Nongray Beckmann, B(D+S). This is the nongray diffuse plus specular directional property model. The emittance and reflectance are considered to be dependent on direction and

wavelength, while the reflection distribution function is taken to be the sum of the specular and the diffuse components. These two components are dependent on the direction and the wavelength of the incident radiation as well as on the surface roughness. According to this model the emittance is given by Eq. (3·24), and

$$f(\vec{\Omega}',\vec{\Omega},\sigma/\lambda) = \rho^{s}(\theta',\sigma/\lambda)U(\delta) + \rho^{d}(\theta',\sigma/\lambda)/\pi \qquad (3\cdot29)$$

Here $\rho^{s}(\theta',\sigma/\lambda)$ is the coherent component of reflectance predicted from the Beckmann or Davies model, with

$$\rho^{s}(\theta',\sigma/\lambda) = \rho_{\lambda}(\theta')g(\theta',\sigma/\lambda) \qquad (3\cdot30)$$

where $$g(\theta',\sigma/\lambda) = \exp\{-[4\pi(\sigma/\lambda)\cos\theta']^{2}\} \qquad (3\cdot31)$$

and $$\rho^{d}(\theta',\sigma/\lambda) = \rho_{\lambda}(\theta') - \rho^{s}(\theta',\sigma/\lambda)$$

Gray and semigray calculations based on this model have been reported [17, 70, 72], but the predictions with detailed consideration of spectral effects have not appeared in the literature.

Semigray, DP(D+S). For this model the total directional emittance and the total directional absorptance are evaluated from Eqs. (3·26) and (3·27) respectively. The specular component of reflectance is assumed constant and independent of direction. According to this model

$$f(\vec{\Omega}',\Omega) = \rho^{s}(\theta')U(\delta) + \rho^{d}(\theta')/\pi \qquad (3\cdot32)$$

where $$\rho^{s}(\theta')/\rho(\theta') = \text{constant}$$

The method of taking into account the spectral, directional and roughness effects for the evaluation of this constant is discussed in APPENDIX A.

Gray, DP(D+S). This model is similar to the previous model except that the total directional absorptance is assumed equal to the total directional emittance. Calculations with this model have been reported in the literature [17, 70, 71, 75] either for limiting values (0 or 1) of $\rho^{S}(\theta')/\rho(\theta')$ or for arbitrarily chosen values. There is no systematic method reported in the literature for calculating the specular component which takes into account the spectral, directional, and surface roughness effects as well as the system geometry. The method of calculating the specular component of reflectance is discussed in APPENDIX A.

3.6 Solution of Integral Equations

An exact analytical solution of Eq. (3·17) is not possible because the kernel is a complicated function and a numerical solution is the best that can be obtained. The methods for solving linear Fredholm integral equations of the second kind are well documented in the literature [98]. Sparrow [62] has given a review of some of the methods pertinent to the solution of integral equations arising in problems of radiant interchange. With a few exceptions, closed form solutions to these equations are not possible. Therefore, variational, finite difference and successive substitution or successive approximation methods are used. Variational methods are limited in that the form of the solution must be chosen, and also higher-order approximations are very tedious. Finite differencing of the integral equation results in a system of linear algebraic equations. This technique requires simultaneous solution of a large number of equations, which may be ill conditioned [85, 99]. The method of successive substitution lends itself readily to numerical computation, but the amount of effort involved in the method of successive approximations [100] is considerable. This is justified only when the convergence of the

method of successive substitution is very slow. In the present study, the solution was obtained by the method of successive substitution, but with one difference. Instead of using the values of the nth iteration as a group for (n + 1)st iteration, the values of I were used immediately after computation.

Calculations were performed on a CDC 6500 digital computer. The kernels which were needed repeatedly were stored in the core of the computer. Simpson's rule was used for the integration. Wherever possible the symmetry of the configuration was invoked to calculate the parameters. The area of each surface was divided into nodes. Iterations were terminated when the reflected intensity, the quantity under the integral sign, satisfied the convergence criteria:

$$\left| \frac{I_i - I_{i-1}}{I_i} \right| < 0.001$$

The convergence criteria for the reflected intensity is more severe than on the leaving intensity, especially for low values of reflectance and large spacing of surfaces.

For a specularly reflecting enclosure the leaving intensity was used in the convergence criteria because the reflected intensity in some directions was zero. For enclosures consisting of specular or near-specular surfaces it was found that the 7×7 grid was unsatisfactory. For the arrangement of plates considered it was found that a 9×9 grid was satisfactory. With this grid size and with bidirectionally reflecting surfaces, even though symmetry was invoked and the absolute minimum number of values were stored, the problem solution still exceeded the 150K memory of a CDC 6500 digital computer. To overcome this difficulty some of the values were stored on tapes, but reading from the tapes was very time consuming, and the approach was

abandoned since the Monte Carlo method was found to be more efficient.

3.7 Radiation Interchange by the Monte Carlo Method

In the Monte Carlo method the energy emitted by a surface is divided into a number of energy parts called 'energy bundles'. Application of the Monte Carlo method consists of emitting these energy bundles in various directions from a surface (or an elementary area) proportional to the actual energy emitted from the surface in those directions. The energy bundles then play the game of chance according to the actual deterministic and random features of the physical processes step by step [101]. In other words, the energy bundles are followed and the events in their life history are noted until the bundles are almost completely absorbed or escape from the system. The directions of the bundles are modified by the surfaces of the system according to the actual reflection and transmission characteristics. After tracing the histories of a sufficiently large number of bundles and summing (or averaging) the events, one can determine what fraction of the emitted energy has been absorbed and reflected at each surface or has escaped from the system through an opening. In terms of these fractions the other radiation quantities of interest can be readily written as shown below.

Consider radiation interchange in an enclosure consisting of n surfaces and direct attention to the emission of radiation from an elementary area dA_i located on surface i at a point denoted by the position vector $\vec{r}_i$. According to the definition of the spectral emitted flux, the amount of spectral radiant energy emitted from dA_i in the spectral interval λ and $\lambda + d\lambda$ is

$$E_{i\lambda}(\vec{r}_i)dA_i d\lambda = \int_{\Omega} \varepsilon_{i\lambda}(\vec{\Omega}_i,\vec{r}_i) I_{bi\lambda}(\vec{r}_i)\cos\theta_i d\Omega_i dA_i d\lambda \qquad (3\cdot33)$$

This emitted spectral energy is subdivided into N_{di} individual "energy bundles" and of these, according to the Monte Carlo method, $N_{di\to j}$ are eventually absorbed at surface A_j directly or after interreflections. The spectral absorption factor $B_{\lambda di-j}$ can be defined as

$$B_{\lambda di-j} = \lim_{N_{di}\to\infty} (N_{di\to j}/N_{di}) \qquad (3\cdot34)$$

The factor $B_{\lambda di-j}$ is a generalization of the absorption factor introduced by Gebhart [102]. The spectral absorption factor between two finite surfaces is defined in an analogous manner

$$B_{\lambda ij} = \lim_{N_i\to\infty} (N_{i\to j}/N_i) \qquad (3\cdot35)$$

Once the spectral absorption factors $B_{\lambda di-j}$ and $B_{\lambda ij}$ have been determined, the spectral local or overall values of heat transfer rate at a surface, the radiant interchange between two surfaces and the local radiant heat flux can be computed.

Recalling that the spectral local radiant heat transfer rate can in general be expressed as the difference between energies emitted and absorbed, for an elementary surface dA_i one can write

$$q_{i\lambda} = dQ_{i\lambda}/dA_i = \varepsilon_{i\lambda}E_{bi\lambda} - \left(\sum_{j=1}^{n} A_j\varepsilon_{j\lambda}E_{bj\lambda}B_{\lambda j-di}\right)/dA_i \qquad (3\cdot36)$$

The net spectral radiant interchange between an elementary surface dA_i and a finite surface A_j is given as

$$Q_{\lambda di\rightleftarrows j} = dA_i\varepsilon_{i\lambda}E_{bi\lambda}B_{\lambda di-j} - A_j\varepsilon_{j\lambda}E_{bj\lambda}B_{\lambda j-di} \qquad (3\cdot37)$$

The irradiation is obtained by dividing the energy absorbed by the absorptance of the surface, and the local spectral irradiation can be written as

$$G_{i\lambda} = \left(\sum_{j=1}^{n} A_j \varepsilon_{j\lambda} E_{bj\lambda} B_{\lambda j-di} \right) / \alpha_{i\lambda} dA_i \qquad (3\cdot38)$$

where α_λ has already been defined in Eq. (3·3). The total and overall radiation quantities can be calculated in an analogous manner by using the corresponding absorption factors. For example, the total overall radiant heat transfer rate from surface i can be expressed as

$$Q_i = A_i \varepsilon_i E_{bi} - \sum_{j=1}^{n} A_j \varepsilon_j E_{bj} B_{ji} \qquad (3\cdot39)$$

The calculation of radiant energy quantities from the above relations, Eqs. (3·36) through (3·39), is straightforward; however, these equations can be cast into a more convenient form by using the reciprocity relation

$$dA_i \varepsilon_{i\lambda} B_{\lambda di-j} = A_j \varepsilon_{j\lambda} B_{\lambda j-di} \qquad (3\cdot40)$$

The resulting equations then become

$$q_{i\lambda} = dQ_{i\lambda}/dA_i = \varepsilon_{i\lambda} \left(E_{bi\lambda} - \sum_{j=1}^{n} E_{bj\lambda} B_{\lambda di-j} \right) \qquad (3\cdot41)$$

$$Q_{\lambda di \rightleftarrows j} = dA_i \varepsilon_{i\lambda} B_{\lambda di-j} (E_{bi\lambda} - E_{bj\lambda}) \qquad (3\cdot42)$$

$$G_{i\lambda} = \sum_{j=1}^{n} \varepsilon_{i\lambda} E_{bj\lambda} B_{\lambda di-j} / \alpha_{i\lambda} \qquad (3\cdot43)$$

Note that Eq. (3·43) is not in a convenient form because in general α_λ is not equal to ε_λ and its evaluation demands the knowledge of the incident radiation field. However, this difficulty can be by-passed if the absorption factors

$B_{\lambda di-j}$ are calculated by considering emission from dA_i as diffuse. This amounts to introducing, at the desired location, a fictitious surface dA_i having constant properties. With this Eq. (3·43) reduces to

$$G_{i\lambda} = \sum_{j=1}^{n} E_{bj\lambda} B_{\lambda di-j} \qquad (3\cdot44)$$

It is evident that the introduction of this fictitious surface dA_i does not alter the character of the enclosure because in all the interreflections it is the real surface which participates in the radiation interchange.

Note that Eqs. (3·41) through (3·43), in general, are not valid on a total basis. The reason for this is that the reciprocity relation, Eq. (3·40), in general is not valid on a total basis. This is discussed in detail in APPENDIX D. There it is proven that Eqs. (3·40) through (3·43) are also valid on total basis, provided that in calculating the absorption factors B_{di-j} the energy emitted from dA_i corresponds to radiation characteristics of dA_i at temperature T_i and the black body emission corresponds to temperature T_j. It can be easily shown that Eq. (3·44) is also valid on total basis.

Equations (3·41) through (3·44) have been purposely cast in this form because now the radiant energy quantities can be calculated more efficiently. In the Monte Carlo calculations it is advantageous to predict B_{di-j} rather than B_{j-di} because the local radiant quantities can be calculated directly at a few points of interest. For constant surface property models all the B_{di-j}'s can be calculated simultaneously resulting in considerable saving in computer time. In general, B_{di-j} is much larger than B_{j-di} and it is on this factor that the accuracy of the Monte Carlo method depends. The larger the B_{di-j}, the more accurate is the result for the same number of energy bundles traced. Also,

"directed emission" [77] can be used more fruitfully for a single point than for an entire area.

For the enclosure studied here the irradiation, Eq. (3·44), can be written as

$$G_{i\lambda} = \sum_{j=1}^{3} E_{bj\lambda} B_{\lambda di-j} \tag{3·45}$$

The local spectral heat flux at surface i can be calculated from Eq. (3·41) or from

$$q_{i\lambda} = \varepsilon_{i\lambda}\sigma T_i^4 - \alpha_{i\lambda} G_{i\lambda} \tag{3·46}$$

where $\alpha_{i\lambda}$ is the spectral hemispherical absorptance calculated from Eq. (3·3).

The results on the total basis can be obtained either by integrating the local values over the entire spectrum or by obtaining them directly from the absorption factors which are calculated on the total basis. The latter method, however, is much easier. This can be done by labeling the emitted energy bundles in such a manner so that the simulated emission represents the actual emission directionally as well as spectrally. This is discussed in [77].

The details of the simulation of radiant heat transfer by the Monte Carlo method are omitted for the sake of brevity. A complete discussion on the simulation of the problem, the importance of randomness of the random numbers used and a number of shortcut methods to increase the accuracy of this method without increasing the computer time are given elsewhere [77].

For calculation of absorption factors it is not possible to trace an infinite number of energy bundles as required in Eq. (3·34). The number of energy bundles to be traced was a compromise between the availability of computer time and the accuracy needed. The probability of accuracy P that the

calculated result with large sample size N lies within r percent of the exact value p is [77]

$$P \simeq \mathrm{erf}(\zeta)$$

where

$$\zeta = (r/100)[Np/2(1-p)]^{1/2}$$

This shows that, for the same accuracy, N should be large when p is small and vice versa; or with the same value of N, larger values of the result p carry greater weight of confidence. Note that the accuracy ζ of the Monte Carlo results is proportional to $N^{1/2}$. Since the computer time is directly proportional to the number of energy bundles traced, this method becomes very time consuming for small values of p. This is the reason why Eq. (3·38) was transformed to Eq. (3·43), in accordance with the fact that B_{di-j} is much larger than B_{j-di}.

The problem was simulated on CDC 6500 digital computer using pseudo-random numbers produced by a multiplicative congruential generator. The local absorption factor was calculated by tracing a history of 1000 energy bundles. The efficiency of calculations was increased by shortcuts like 'directed emission' [77]. As an example, directed emission from the location $\xi = 0$, $\eta = 1/8$ was equivalent to emission of 53 times the number of energy bundles actually emitted. This number varied from point to point. For an enclosure consisting of surfaces having bidirectional reflection characteristics the Monte Carlo method was found to be more flexible and demanded less time and computer storage than the method of successive substitution for solving the system of integral equations.

4. EXPERIMENTAL APPARATUS AND PROCEDURE

4.1 Introduction

As mentioned in the INTRODUCTION, the objective of this study was to critically examine the validity of the various commonly used radiation surface property models. This necessitates the comparison of predictions of radiant quantities from various models and further comparison with experimental data. The type of configuration chosen for experimentation and the reasons for this choice have already been discussed in Section 3.3. The experimental system must be capable of providing a proper environment for the configuration of surfaces in which the effects of conduction, convection, extraneous radiation sources and other losses can be carefully controlled or possibly eliminated. Hence the surfaces should be of reasonable size so that it can be accommodated in an enclosure of convenient dimensions. The overall system design, test chamber, test assembly, instrumentation, calibration and general procedure are discussed in the remainder of this chapter.

Although it is desirable to measure the local heat flux, there are extreme experimental difficulties associated with a measurement of net local heat flux. Also, presently there is no way of measuring the local heat flux on a spectral basis. Hence, the local irradiation (incident radiant flux) was measured in an attempt to experimentally evaluate the methods of radiant heat transfer analysis and accomplish the goals of the study. Various radiation detectors such as a spectrometer, heat gauges, bolometers and thermopiles are available which can be used to measure the local irradiation. The other radiant energy quantities of interest can be readily determined once the irradiation is known.

4.2 General System Design

Since it was desired that the local irradiation be measured due to interaction of the surfaces only, it was necessary that extraneous radiation influences from outside of the test surfaces be eliminated. Also, to decrease the convective heat transfer to the environment and to prevent cryodeposit formation on the LN_2 cooled test surface 3, it was necessary to evacuate the system. The external radiation sources were reduced by mounting the test assembly inside a black, LN_2 cooled spherical chamber which is described in the next section. The convective heat transfer was reduced to an insignificant fraction of the total heat transfer by evacuating the chamber to a pressure of 1.333×10^{-2} N/m^2 or lower during the testing. A view of complete experimental system is shown in Figure 4.

The local total irradiation measurements were made with thermopiles. For the local spectral irradiation measurements, narrow band pass interference filters were mounted in front of the thermopiles. Measurement of irradiation by thermopiles was the most convenient and efficient method since the thermopiles are small in size, flat in response and can be easily placed at the desired locations without decreasing the test surface area appreciably. The alternative of measuring directional radiosity from positions outside the chamber by means of a spectrometer was not practical because of the inaccessibility of the locations at which the measurements were desired. Heat gauges also could not be used as they do not permit convenient measurement of incident spectral flux. Temperatures were measured with Chromel-Alumel thermocouples attached to the back sides of the test surfaces.

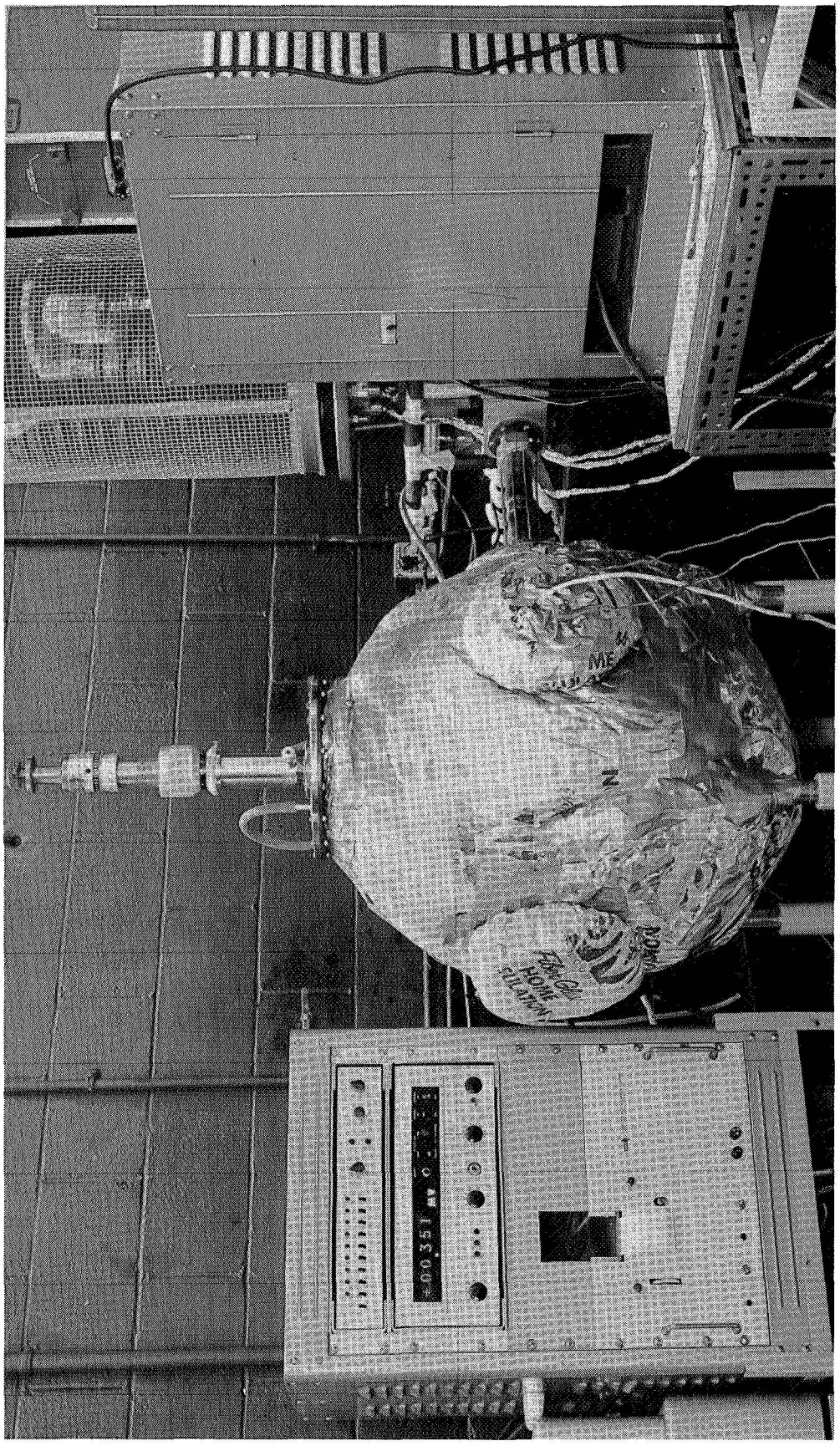

Figure 4. View of Complete Experimental System.

4.3 Test Chamber

The vacuum chamber in which the experiment was performed is shown in Figure 5. It consisted of two concentric spheres of aluminum with four 12.7 cm diameter ports on the sides, a 25.4 cm diameter port on the top and an air inlet valve at the bottom. The inner and outer spheres were respectively 60.96 and 63.5 cm in diameter with a 1.27 cm gap provided for heating or cooling by a circulating fluid.

This enclosure effectively eliminated external radiation from the outside environment. The low temperature of the chamber (77°K) ensured very low emission. The inside wall of the chamber was painted with a black paint to minimize reflection. A stand with four adjustable legs was used to support the chamber. The chamber and the stand were manufactured by Research Service, Inc. of St. Paul, Minn., and were used in a previous study [103]. The entire chamber was insulated on the outside with aluminum backed thick blanket of glass wool to reduce the heat gain from the environment.

Two of the four 12.7 cm ports had metallic flanges blackened on the inside through which various electrical and coolant feedthroughs were introduced. A 2.54 cm thick plate glass window was installed in the third port for visual inspection, and the fourth port was used to connect the chamber to the high vacuum pump by a 5.08 cm diameter pipe and a flexible coupling. Liquid nitrogen feedthroughs and the shaft supporting the reflector plate passed through the top 25.4 cm flange which was also blackened on the inside. This shaft could be operated from outside the chamber to lower or raise surface 3 without breaking the vacuum. The moving mechanism and the shaft are shown in Figures 5 and 6. With the help of the graduated scales on this mechanism the distances could be measured very accurately.

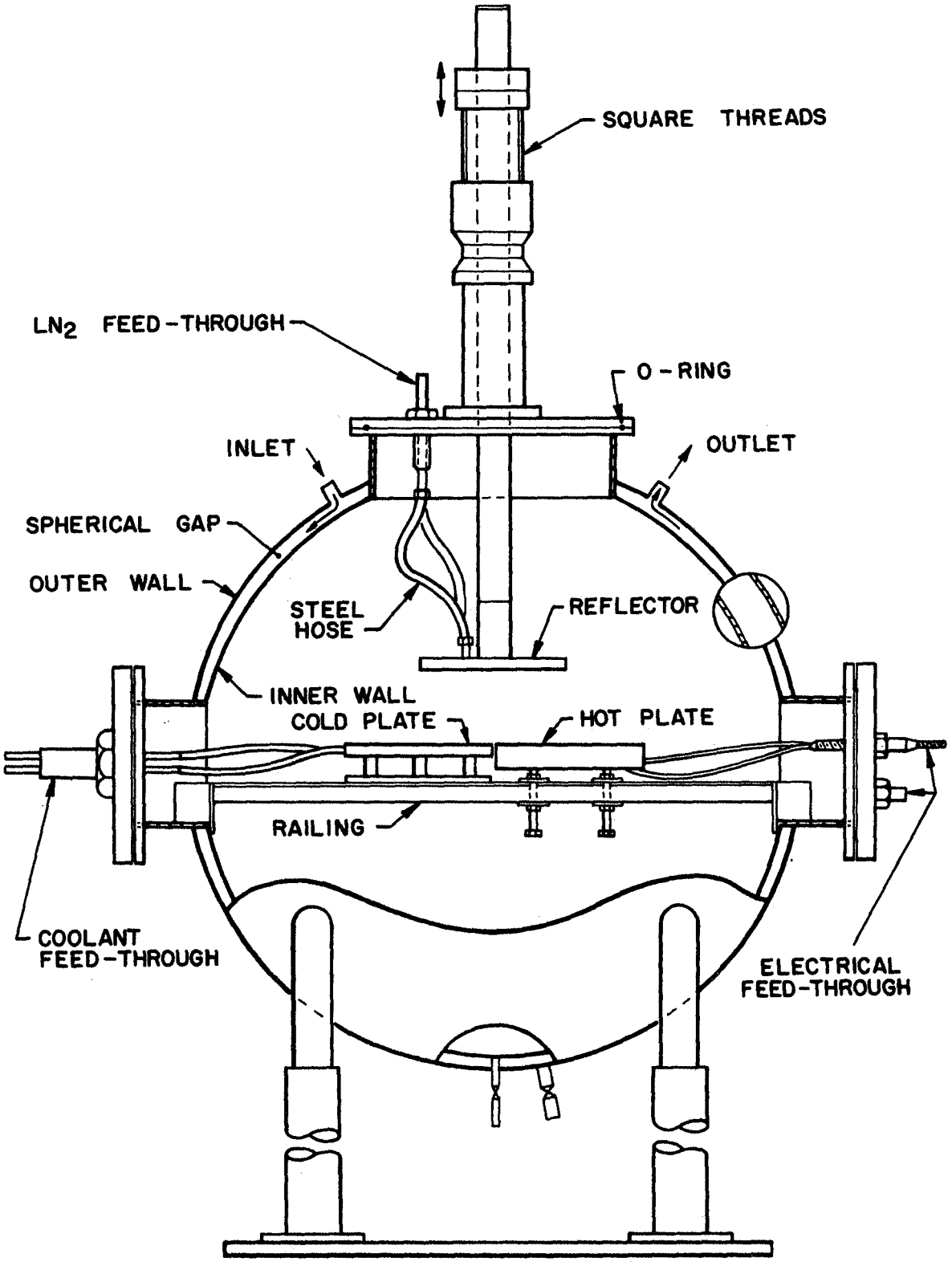

Figure 5. Schematic Diagram of Test Assembly.

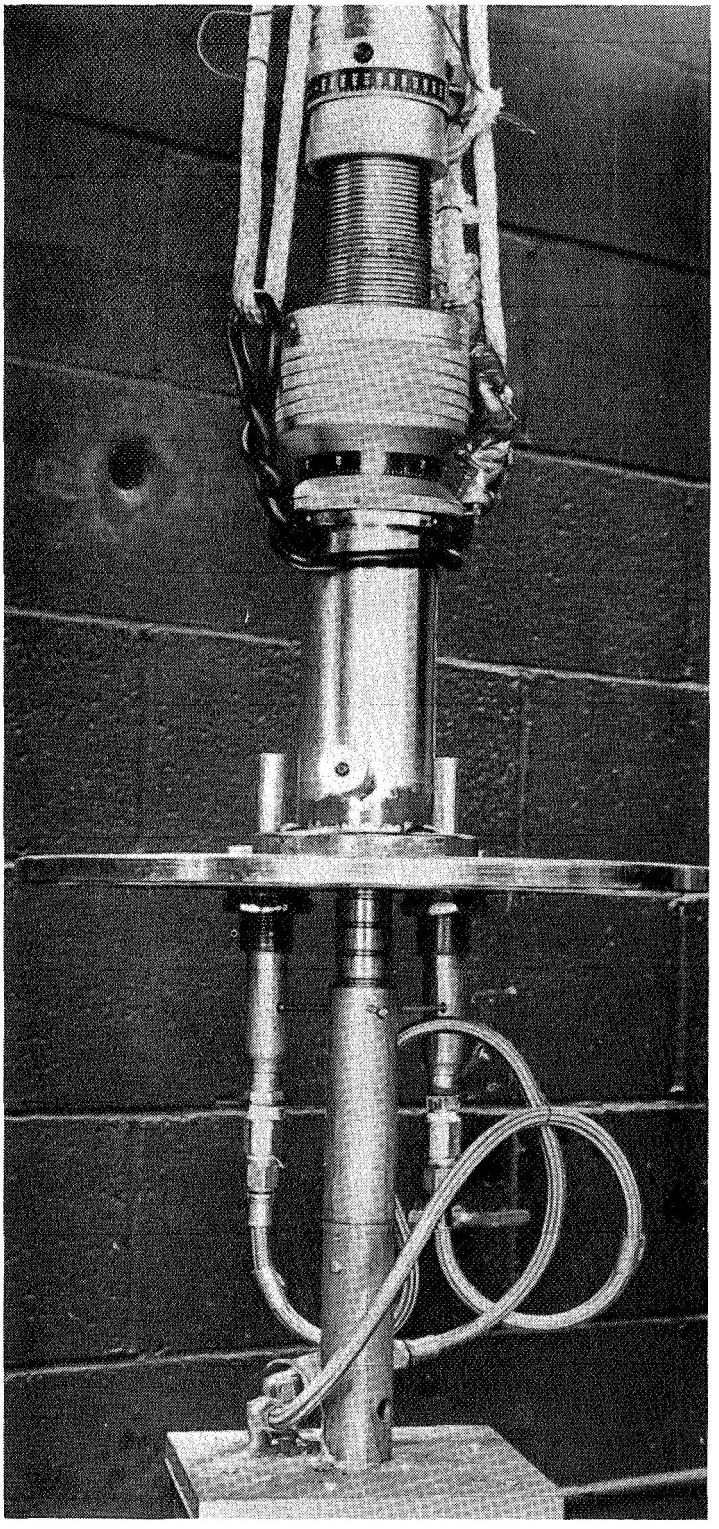

Figure 6. View of the Reflector Plate and the Moving Mechanism.

The chamber was evacuated by a Consolidated Vacuum Corporation, Type PSE-43, High Vacuum Pumping System. This unit includes a mechanical roughing pump, a high vacuum diffusion pump, a LN_2 cooled baffle and a Type GIC-110A ionization vacuum gauge. The system was capable of producing a vacuum of less than 1.333×10^{-5} N/m^2 as detected by the ionization gauge tube installed above the valve to the diffusion pump.

4.4 Test Assembly

The test assembly was to provide a means of mounting the test surface specimens in several configurations and allow for rapid interchange of geometries and test surfaces. Both the hot and cold surfaces were supported on a railing, see Figure 5, each end of which was supported in the chamber openings. Surface 3 was suspended by means of a shaft through the port at the top of the chamber. A view of arrangement of test surfaces inside the test chamber is shown in Figure 7 (for the sake of clarity the picture was touched). Details of each of the surface supports and method of attachment are given below.

Cold Block

The objective of the cold block design was to provide the system with a heat sink, fitted with interchangeable front surfaces, to ensure uniform test surface temperature. A composite view is shown in Figure 5, and the labyrinth coolant channel is illustrated in Figure 8. The coolant channels were grooved in a 15.24 × 15.24 cm block of copper and then covered with copper bars and soldered, making the channels vacuum tight. The labyrinth coolant channel was selected because it reduces the temperature gradients across the plate and minimizes the danger of the coolant by-passing part of the plate as in a manifold type of cooler. Holes were drilled through the block to accommodate

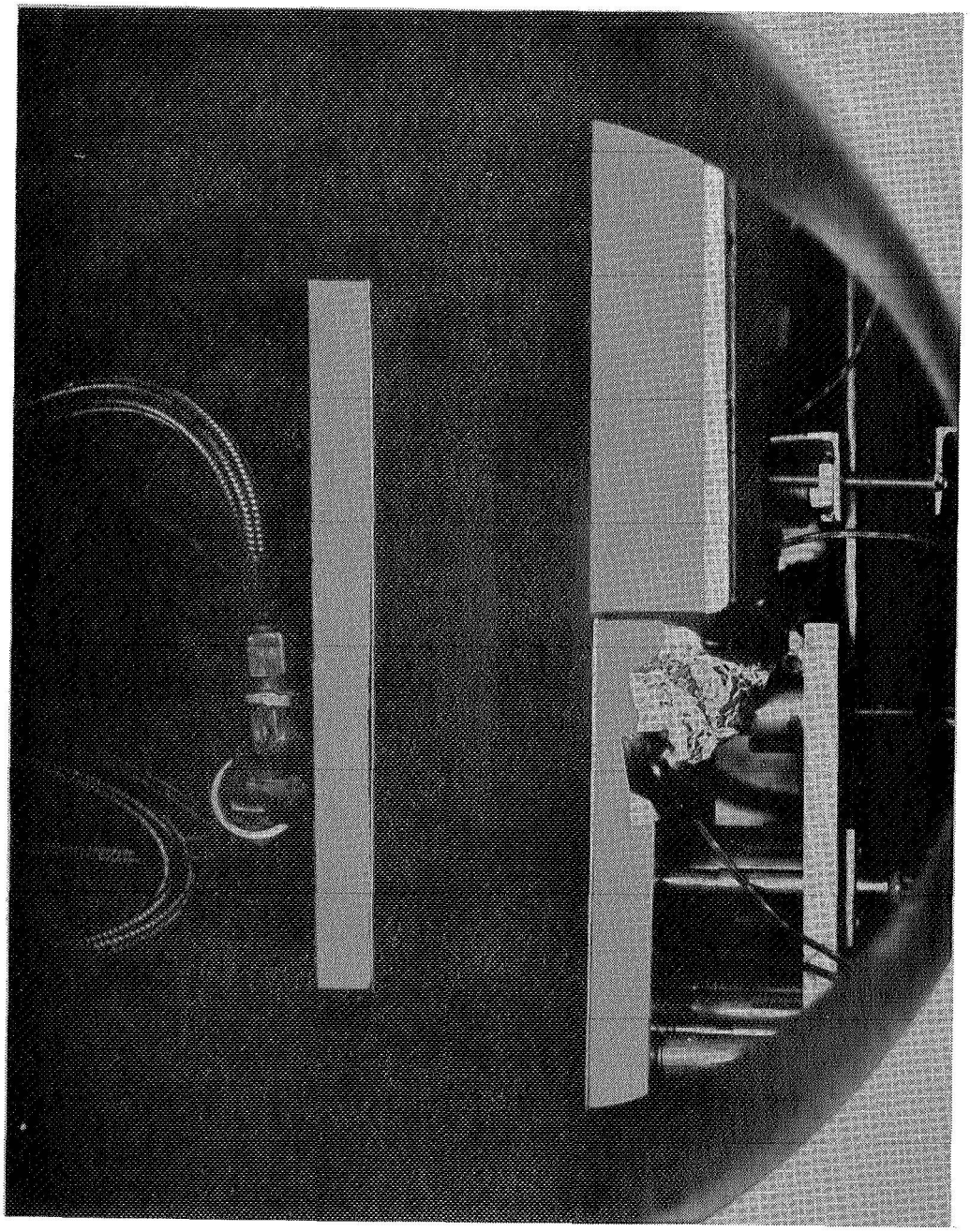

Figure 7. View of Arrangement of Test Surfaces.

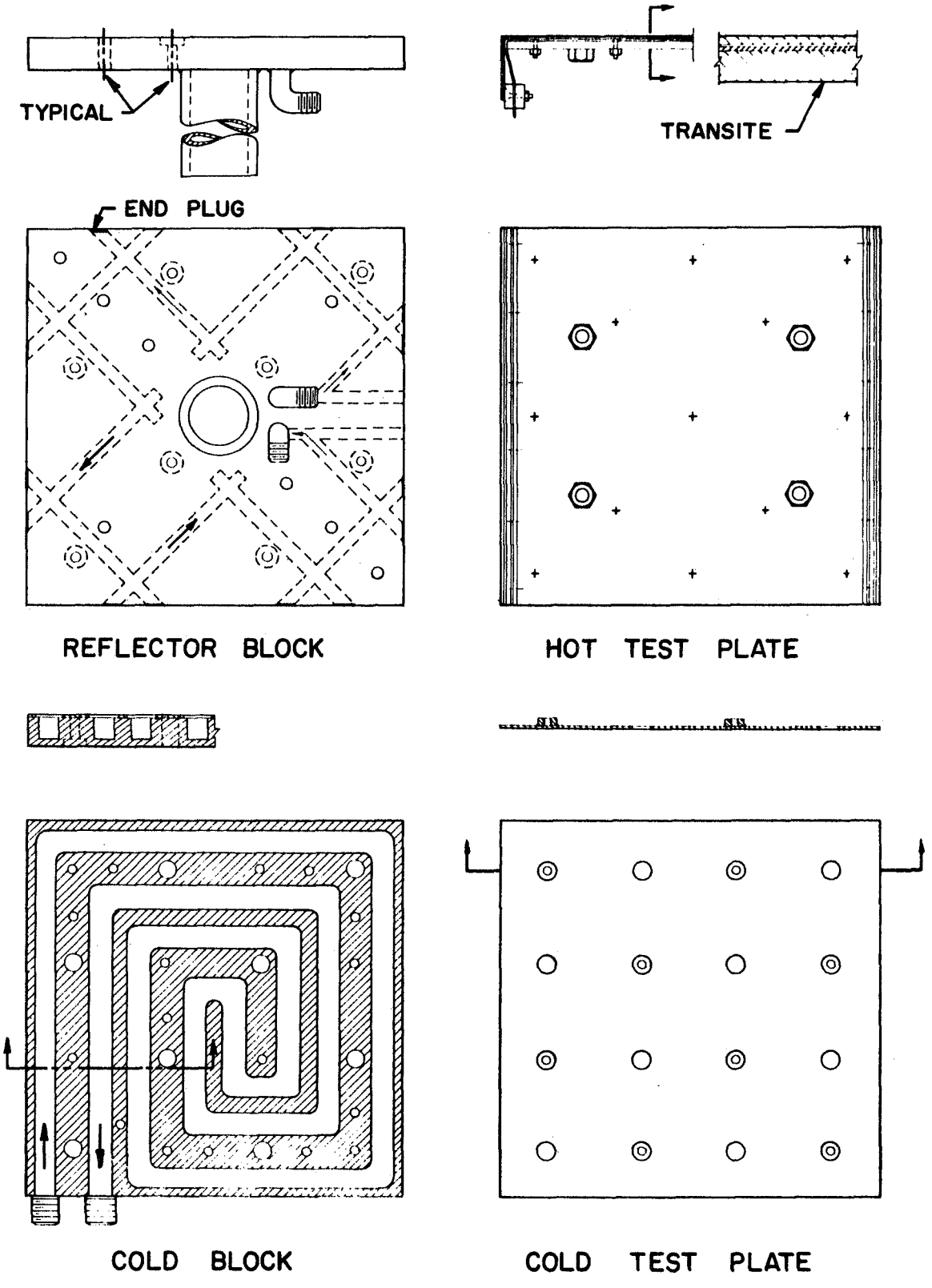

Figure 8. Design Sketch of Cold Block, Reflector Block, Hot Test Plate and Cold Test Plate.

the thermopiles, for fixing the test surface, and for thermocouples attached to the back of the cold test plate. The cold test plate is also shown in Figure 8.

Hot Plate

The thermal inertia of a good heater should be small enough so that a desired uniform temperature over the test surface can be reached in a reasonable period of time, and the system should be thermally stable enough to maintain this temperature. Materials of low thermal conductivity do not dissipate energy easily and thermal equilibrium is readily obtained, but this also has the disadvantage of creating hot spots, which in turn limit the uniformity of the surface temperature of the heater face.

For the design of the heater many ideas were conceived and tried. Electrical heating of the 15.24 cm square plate would have required very large currents, even for thin sheets, thus limiting the temperature level. Resistance coil heating by radiation from below was tried but resulted in a very nonuniform temperature distribution over the surface, especially at higher temperatures. Closely spaced chromel ribbon embedded in Sauereisen Cement 78 (which is an electrical insulator) was tried but this block cracked after a few cycles of heating and cooling. Finally, bonding of graphite cloth (HITCO-G-1550, Materials Division of HITCO) to the back of the test plate with Sauereisen Cement gave very satisfactory results. Typical variation of the surface temperature across the hot surface is illustrated in Table 3. The graphite cloth was of very uniform 0.41mm thickness with a resistance of 0.4 ohms per square and could withstand temperatures up to 3600°K in an inert atmosphere. One difficulty of working with graphite cloth was that the strands flared out when it was cut to the required size. This difficulty was overcome by spraying it with Pyromark paint, after which it became stiff and workable on drying. To

TABLE 3

Typical Variation of the Temperature Across the Hot Surface

Location		Temperature, °K	
η	ξ	$\gamma = 1/6$	$\gamma = 1/2$
a) High Temperature Level			
1/12	11/12	753.4	756.1
1/2	1/12	761.3	762.0
1/2	1/2	756.5	760.2
1/2	11/12	754.4	759.2
11/12	1/12	759.2	760.1
b) Low Temperature Level			
1/12	11/12	593.9	584.2
1/2	1/12	598.5	588.5
1/2	1/2	596.3	587.7
1/2	11/12	594.5	585.3
11/12	1/12	597.0	587.0

stiffen this thin assembly a transite plate, as shown in Figure 8, was bolted so that the graphite cloth became sandwiched in between the test plate and the transite plate. Four nuts were fixed on the back side of the transite plate to support it on the railing by means of screws and to adjust its level. The ends of the carbon cloth were sandwiched between two copper strips to ensure good contact between the copper and the graphite.

Reflector Block

The reflector block was designed to maintain one test surface at a very low temperature so that the emission from this surface could be essentially eliminated. This also was a 12.7 cm square and 1.27 cm thick copper block with holes drilled parallel to the surface for circulating LN_2 (Figure 8). Through holes across the block were used in bolting the test surface tightly against the copper block and for attaching the thermocouples. In the middle of this plate a hollow shaft was attached which was coupled to the shaft inserted through the top port. By means of this shaft the reflector plate could be raised or lowered without breaking the vacuum.

4.5 Test Surfaces

4.5.1 Choice of Test Surface Material and Size

As discussed in Section 2.3 the test surface material used in the experiments had to be of low emittance, easily available, solid and stable at high temperature over extended periods of time. Also it had to have very low vapor pressure at operating temperatures, as the experiments were conducted in vacuum. In addition, the experimental data of radiation properties of material used had to be available or predictable. Most of these conditions are met by the noble metals gold and silver, but the latter has

the disadvantage that it is chemically the most active of all the noble metals and reacts with sulphur or hydrogen sulphide (which is always present in air) to form silver tarnish [104]. On the other hand, gold is one of the least active metals chemically and does not tarnish in air. Also experiments [8, 9] have shown that the radiation properties of gold predicted from Drude's theory are in excellent agreement with experimental data for the wavelength range of interest (see Figure 1). Furthermore, use of gold for the test surfaces was of interest because of its practical applications. To mention a few, it is used as thin coating on high frequency conductors as are used in radar equipment and on metallic and glass surfaces for reflectors, particularly in the infrared. Its application on grids of vacuum tubes, in printed electrical circuits and in the chemical industry in autoclaves, piping etc. is also well known.

The choice of the model is more critical when surfaces are of finite rather than infinite extent [77], hence finite size surfaces were chosen. From the point of view of construction it was convenient to have all surfaces of equal size. The size requirement depended on the number of holes to be made for the thermopiles so that reduction in test surface area be negligible. Also, the area had to be large enough so that the irradiation could be detected, with errors introduced by the extraneous radiation and the local nonuniformities of temperature and radiation characteristics being negligible. Considering the above mentioned factors and the size of the chamber, the surfaces were made 15.24 × 15.24 cm in size. The surface roughness chosen was guided by the desire to cover the entire range of the specular component of reflectivity (from zero to one) for the selected configuration and the temperature levels considered.

4.5.2 Preparation of Surfaces

The test surfaces were prepared from stainless steel sheets 0.8mm or 1.6mm thick. Since the thicker material warps less upon sandblasting the 1.6mm thick steel sheet was used for surfaces which had to be sandblasted. The 'diffuse' surface was prepared by sandblasting with the standard "Mott" sandblast machine under 5.5×10^5 N/m^2 air pressure. The nozzle was held at a distance of about 5 to 8 cm perpendicular to the surface. The blasting grit used was approximately 80 mesh angular shaped hard steel. The 'bidirectional' surfaces were prepared on a standard glass bead blast machine. The air pressure was maintained at 2.8×10^5 N/m^2 and round shaped 120 mesh size glass beads were used. The nozzle was held perpendicular to the surface at a distance of 7 to 12 cm. The surfaces to be prepared as 'specular' were polished to a smooth finish. All the surfaces were electroplated with gold up to a thickness of approximately 5μ to ensure complete masking of the substrate.

Before gold plating the surfaces were cleaned by standard methods. After nickel and copper flashing these were gold plated in a horizontal position. The solution used for electroplating was Lea-Ronal P.C. 24K Hard Gold at a concentration of one ounce per gallon. Depending on the type of a surface, a continuous current at a density of 10 to 40 amperes per square meter was used. The solution was maintained at 43°C. The duration of gold deposition was from 20 to 30 minutes depending on the current and agitation.

4.5.3 Measurement of Surface Roughness

The root mean square roughness of the test surfaces was measured with a Type QB Amplimeter Model 13 (Serial 3623, manufactured by Bendix Industrial Metrology Division)

profilometer having a 2.5μ radius stylus mounted in an LK-2-2210 tracer. The calibration of the instrument was checked before use and it was set for 12.7mm stroke, STD damping, 0.762mm roughness-width cut off and 7.62mm/sec tracing speed. The 2.5μ radius stylus is the smallest size made by the manufacturer.

The surface roughness profiles (Figure 9) were traced by a Dektak having stylus of 25μ in diameter. This instrument was manufactured by Sloan Instruments Corporation. The manufacturer claims that it has a "capability to accurately measure vertical dimensions of a surface profile over a wide range from 25 Angstroms to 10^6 Angstroms". The profile scanning speed was set at 0.1 cm/min, but the chart speed varied from 10 cm/min to 50 cm/min. The correlation distances [35] were calculated from the surface profile by measuring 400 ordinates at 4μ intervals. The surface was assumed to be statistically repeatable. The root mean square roughness σ_m was calculated from these ordinates, and it compared favorably with the profilometer reading, in spite of the large difference in diameter of stylli. Intuitively, it is felt that the large diameter stylus should give lower rms roughness as it can not reach the bottom of the valleys; however, the small diameter stylus tends to break the ridges of the asperities. A good comparison of the effect of stylus size on the measured value is given in [105].

The values of measured roughness and the correlation distance calculated from the surface roughness profile along with the identification of the surfaces are summarized in Table 4. In each case the roughness reported is the average of five measurements made over each test surface of 12.7 cm square, since the roughness was not uniform; however, the maximum variation from the mean was less than 6 percent. The surfaces were found to be isotropic. Measurements at the same location from different

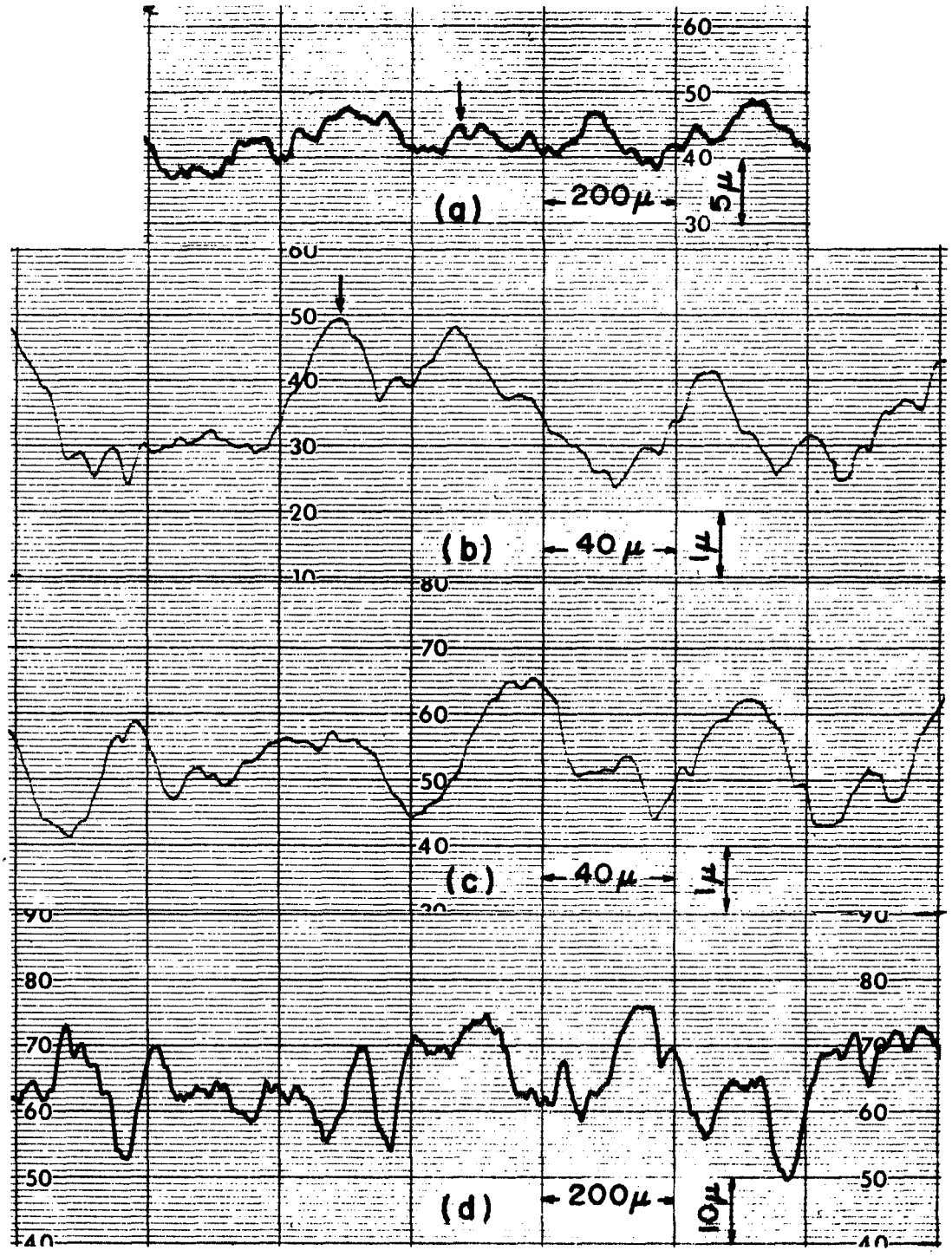

Figure 9. Roughness Profile of Test Surfaces, a,b) Bi-directional Surface, B-3; c) Bidirectional Surface, B-2; d) Diffuse Surface, D-3.

TABLE 4

Description of Surfaces Used in the Experiment

Designation of Surfaces	Roughness σ_m (microns)	Correlation Distance a_m (microns)	Method of preparation. Goldplated after being:
S-1	0.02	-	Polished
S-2	0.03	-	Polished
S-3	0.02	-	Polished
B-2	1.50	40.0	Blasted with glass beads
B-3	0.75	14.0	Blasted with glass beads
D-3	7.10	25.0	Blasted with steel grit

Symbols D, S, B denote diffuse, specular and bidirectional, respectively.

Numbers 1, 2, 3 denote the position of the surface in the configuration.

directions resulted in essentially the same roughness values.

The correlation distance for surface B-3 was calculated from the autocorrelation coefficient shown in Figure 10a. The mathematical definitions are omitted for the sake of brevity and can be found in a number of books, for example in [35]. For comparison purposes the assumed normal distribution in the derivation of Beckmann reflection function is also shown. The autocorrelation coefficient for surfaces B-2 and D-3 is not shown because it is similar. It is clear from the figure that the calculated autocorrelation coefficient is close to the assumed one. However, for very large distances it oscillates in a random fashion with a decreasing amplitude about zero while the assumed coefficient approaches zero monotonically.

The measured roughness height density for surfaces B-2 and B-3 and also the Gaussian distribution, assumed in the derivation of Beckmann reflection function, are plotted in Figures 10b and 10c. In both cases the ordinate and abscissa scales have been normalized with σ_m which was calculated from the ordinates measured at a 4μ interval from the surface roughness profile. For calculating the surface roughness height density D, the maximum peak to valley distance was divided into 20 equal parts. It can be seen from the figure that the calculated surface height density is not Gaussian and is skew to the left. The Gaussian distribution is symmetric about the mean and the maxima of surface height density lies at the mean value of surface height, at zero if all heights are measured from the mean value, as was done in this case. "Skew to the left" means that this maxima lies at some level below the mean. This can happen, for example, if the 'Gaussian' distribution profile is rounded off at the bottom of the valleys.

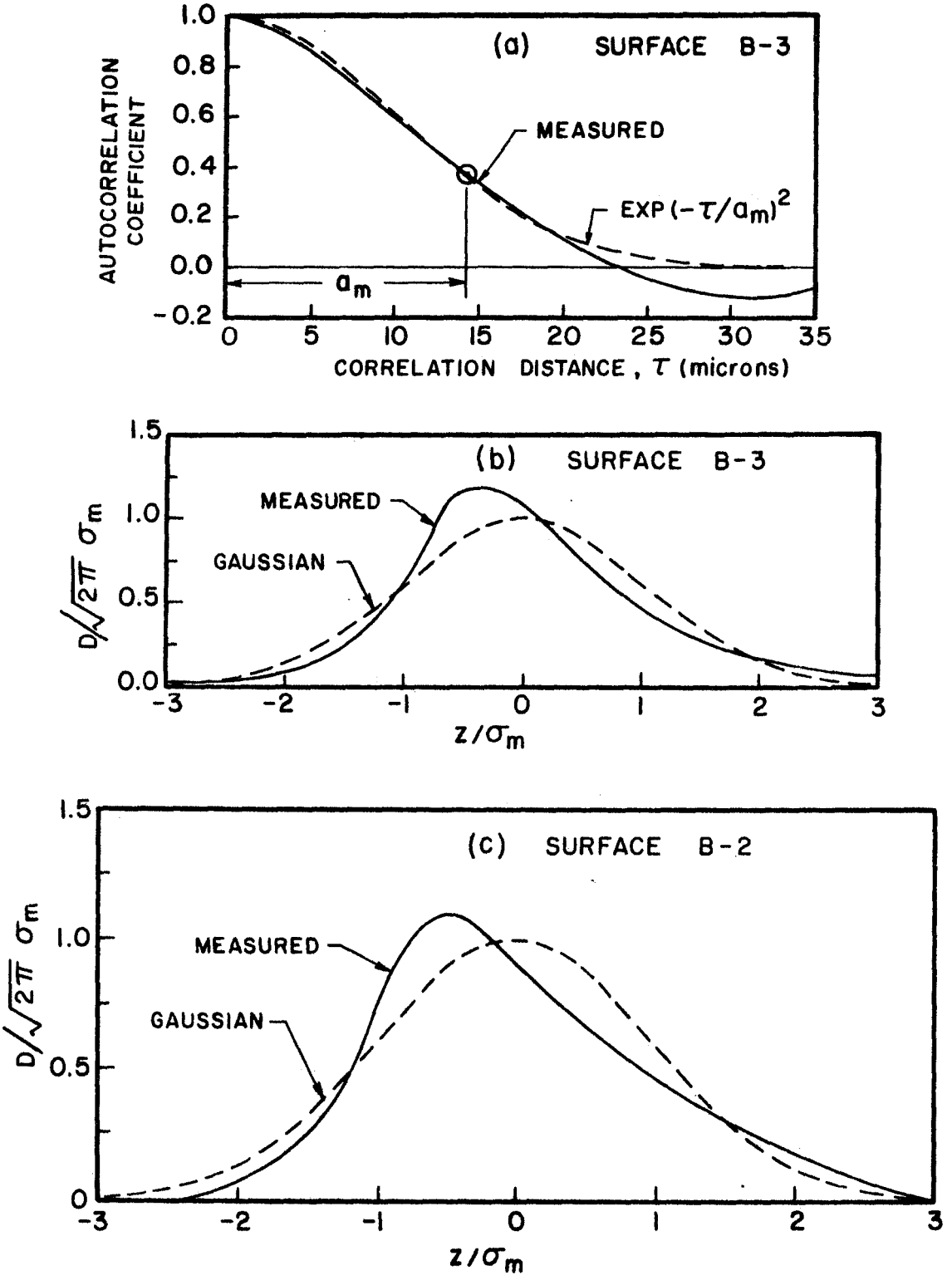

Figure 10. Autocorrelation Coefficient and Roughness Height Density of Test Surfaces.

The surface roughness profiles in Figures 9a and 9b are the same except for the scale, and the corresponding points are marked by arrows. The profiles, from which the ordinates were measured for calculation of the autocorrelation coefficients for bidirectional surfaces were to the same scale as shown in Figures 9b and 9c; however, for the 'diffuse' surface the profile was two times larger in the vertical and five times larger in the horizontal direction. It was expected, as is generally believed, that the finite size diameter stylus would distort the profile at the bottom of the valleys; however, the profile at the bottom of the valleys seems to be no different from what it is at the top of the hills. Either it is not perceptable to the eyes or the top of the hills are broken by the stylus and hence rounded off and appear similar to the bottom of the valleys.

After the test surfaces were used in the experiment they were checked for any impurities or visual defects on the surface. X-ray microprobe analysis with a scanning electron microscope* showed that various pieces cut from the test surfaces contained only the gold. To visualize the structure of the surface topography, micrographs of surfaces with different magnifications were taken with a scanning electron microscope. The surface profile was also traced on these very micrographs which are shown in Figures 11 and 12. For comparison purposes a 1μ diameter particle (approximately) is illustrated in Figure 11A.

Figure 11A shows the smoothness of the specular surface S-2. The grain structure is absent. This is due to slight buffing of the surface after electroplating. Some scratches and a few holes are present but these are of negligible size to affect the specularity of the surface. X-ray microprobe analysis of the holes showed the presence of gold ensuring

---

* Model JSM-2, Micro-METRICAL Laboratories Inc., Lafayette, IND.

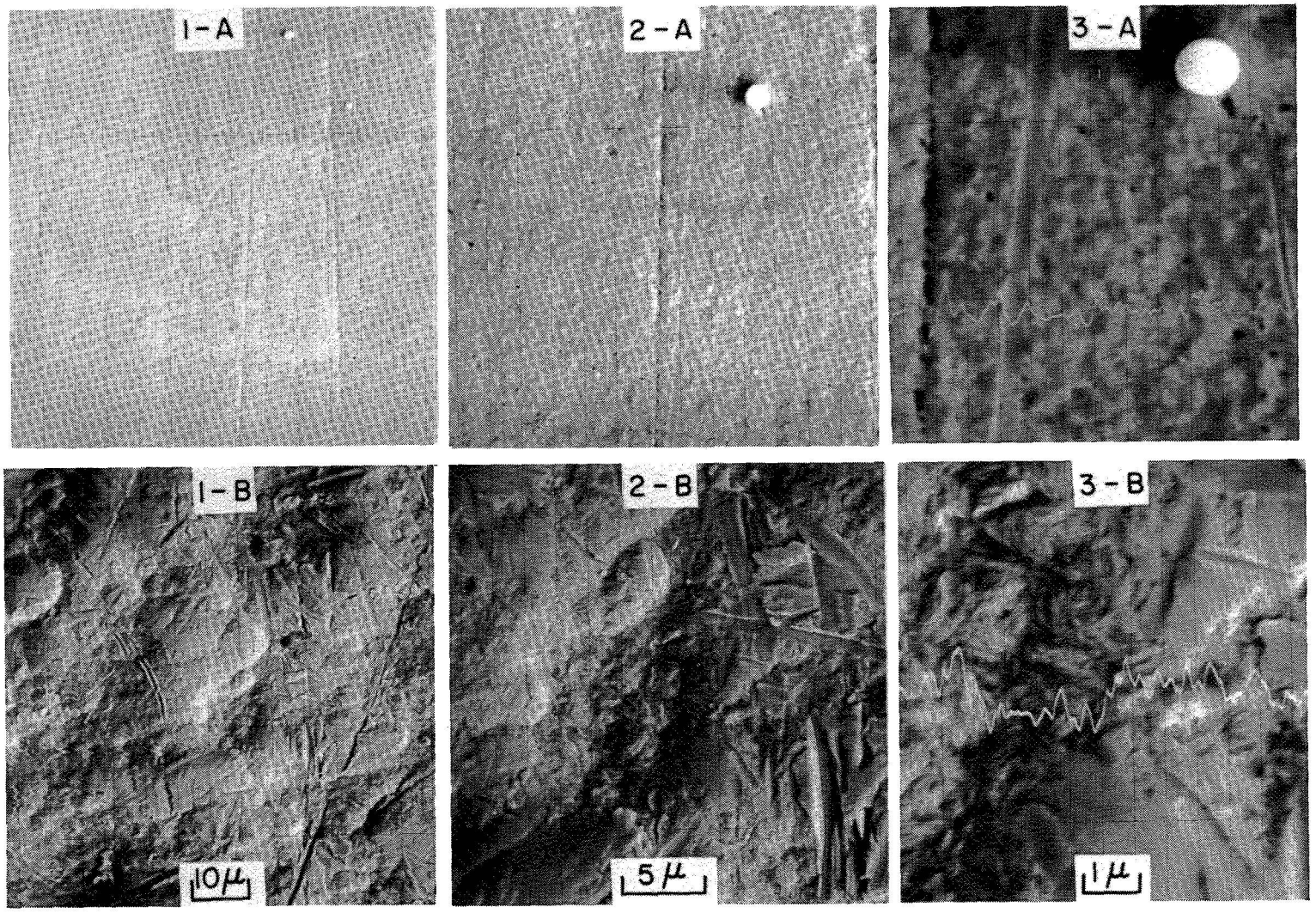

Figure 11. Micrographs and Roughness Profiles of Test Surfaces S-2 and B-2 by Scanning Electron Microscope.

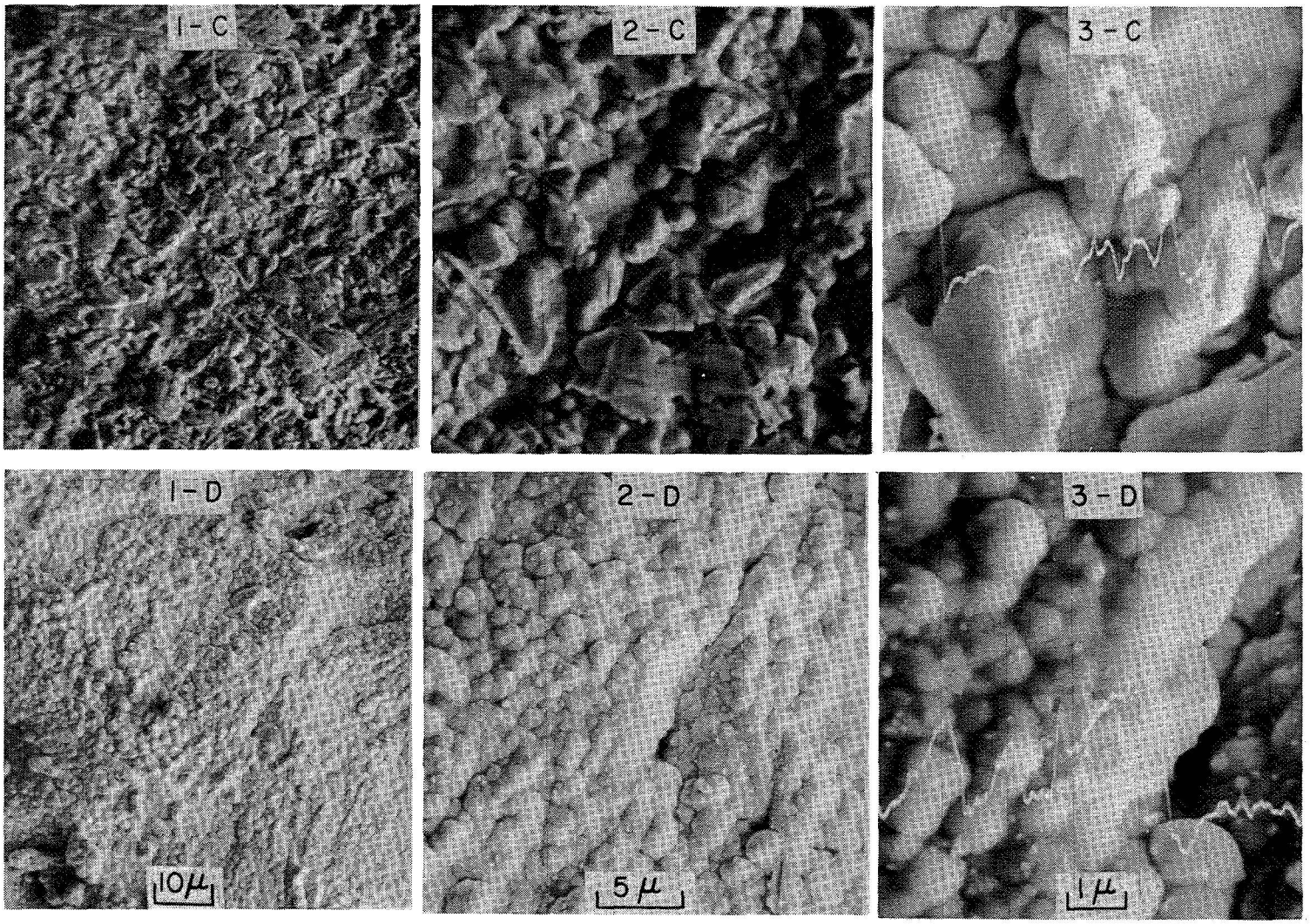

Figure 12. Micrographs and Roughness Profiles of Test Surfaces B-3 and D-3 by Scanning Electron Microscope.

that the substrate is completely masked. Fine details of the surface topography are shown on the traced profile. The rms roughness σ_m of this surface measured by the profilometer was 0.03μ. Thus, for all practical purposes this surface could be considered specular in the infrared. Photographs of the other specular surfaces were not taken, but they appeared to be very similar.

Surface B-2 is shown in Figure 11B. It has a roughness of 1.5μ. The asperities and valleys are clearly seen, but the grain structure is absent. Also, the surface appears to have been touched after electroplating as is clearly visible from the scratches. This possibly had occurred during the shipment or in handling because after receipt in the laboratory all precautions were taken to avoid any damage. The absence of grain structure even in the valleys suggests another possibility. This could happen due to the high temperature (760°K) to which this surface was heated many times during the experiment. Since no photographs were taken before the experiment it is impossible to determine whether or not this was caused by heating. The large correlation distance of 40μ for this surface may be due to the absence of grain structure.

Surface B-3, shown in photograph 12C, was not heated above the room temperature. Some grains seem to have been touched and flattened, and some holes can be seen in the picture. X-ray microprobe analysis of these holes again showed the presence of gold.

The roughest surface, D-3, is shown in Figure 12D. The grain structure can be clearly seen. Again, the valleys of the holes showed the presence of gold. Note that the grain size for this surface is finer than for surface B-3.

It is interesting to compare the surface roughness profile traced by the scanning electron microscope, Figures 11 and 12, with that traced by Dektak. There are a large number of small roughness details which are apparent in

Figures 11 and 12, but are missing in Figure 9. Thus, the values of correlation distance and rms roughness calculated from the two profiles is not expected to be the same. Also, the grain structure in Figure 12 clearly shows that the surface is not smooth locally but is made up of a large number of small spherical grains. In other words, the surface has a secondary roughness unlike that assumed in the derivation of Beckmann reflection distribution function. The influence of this secondary roughness on the spatial distribution of reflected energy, of course, also depends on the wavelength of the incident radiation; however, no attempt was made to look into this effect.

4.6 Instrumentation

Only two types of measurements were required for the experiment: temperature and local incident flux. The local total incident flux was measured with eight thermopiles located in the cold plate and mounted flush with the test surface. The location of the thermopiles is given in Table 5a. For spectral measurements the tubular filters (a tube at the end of which the filter was mounted) were slipped onto the thermopiles.

TABLE 5

a. Location of the Thermopiles on the Cold Plate

η	1/8	1/8	3/8	3/8	5/8	5/8	7/8	7/8
ξ	1/8	5/8	3/8	7/8	1/8	5/8	3/8	7/8

b. Location of the Thermocouples on the Hot Plate

η	1/12	1/2	1/2	1/2	11/12
ξ	11/12	1/12	1/2	11/12	1/12

The thermopiles were 6mm in diameter, uncompensated, of the end on pencil type with KBr windows manufactured by the Charles M. Reeder Company of Detroit, Michigan. The 6mm diameter size was large enough for the required number of junctions and small enough not to reduce the area of cold test surface appreciably. The KBr window was desirable for two reasons. Firstly, the KBr window sealed the evacuated thermopiles and increased its sensitivity. Secondly, any pressure changes inside the test chamber during the experiments were not communicated to the detector and hence did not effect the sensitivity of the instrument.

The filters were narrow-band pass interference type manufactured by the Optical Coating Laboratory, Inc., of Santa Rosa, California. They were the standard NO3080-5A and NO4510-4A filters. The number after the N denotes the center wavelength in angstroms of the transmission scan at normal incidence. The bandwidths of the 3.08μ and 4.51μ filters at normal incidence were 0.069μ and 0.194μ, respectively. To insure that the filters corresponded to the mentioned specifications, the transmission scan at two angles of incidence were also obtained from the manufacturer. The 3.08μ and 4.51μ filters were selected because the maxima of the black body radiation curve at the expected operating temperatures was near these wavelengths. The thermopiles were calibrated, with and without filters as an integral part of the experiment, which is discussed in Section 4.7. The emf's produced by the thermopiles were measured with a Vidar Digital Voltmeter.

The temperatures were measured with chromel-alumel thermocouples made of gauge 28 wire manufactured by Omega Engineering Inc., Stanford, Connecticut. Location of the thermocouples on the hot plate is shown in Table 5b. The thermocouple wire meets the NBS requirements of ± 2.22°C up to 55°K and ± 3/4 percent from 550°K to 1533°K. All the thermocouples were made from the same roll of wire and were

checked at the boiling point of water and the melting points of cadmium as well as antimony. The emf's produced by the thermocouples with the cold junction maintained at ice temperature were measured with the Vidar Digital Voltmeter.

4.7 Experimental Procedure

The first step in the procedure was to calibrate the thermopiles. Either the relative or the absolute method were possible. For this study the former was preferred, and the reasons for doing so are given later. The thermopiles were calibrated in position by using surfaces of known properties so that the irradiation could be accurately calculated. Then a calibration curve of thermopile emf versus local irradiation was constructed for the range of conditions of interest. The surfaces chosen were 3M Black Velvet Paint for the cold surface, behind which the thermopiles were mounted, and Pyromark Black Paint for the other surface, which was heated to a higher temperature. Surface 3 was a very smooth goldplated surface cooled by LN_2 so that it could be considered a nonemitting specular reflector. The Pyromark paint was chosen since it is known to be a gray, diffuse emitter [106], a good absorber and can withstand high temperatures while 3M Black Velvet is diffuse, gray and a very good absorber [107, 108]. The local irradiation for calibration purposes was predicted using the above radiation properties of the test surfaces. Even if the painted surfaces were not perfectly diffuse reflectors, the error introduced was small since little energy was reflected because of the high absorptivities of the paints.

The step by step procedure for calibration was as follows:

1. The set of test surfaces was instrumented and installed in the test chamber to form the desired configuration.

2. All the electrical connections inside the chamber were made and checked. To avoid the influence of stray EM waves on measurements, all the connection wires inside and outside the test chamber were properly shielded. Then all the ports were closed and the vacuum-roughing pump started.
3. After the pressure dropped below 6.6 N/m^2, the LN_2 baffle was charged and operation of diffusion pump was commenced.
4. The circulation of coolant from the Kryomat to the cold plate was started.
5. After the pressure dropped below 6.6×10^{-2} N/m^2, the chamber was cooled by LN_2 and later the cooling of surface 3 by LN_2 was also initiated. This precaution was taken to condense any condensables on the inside of the chamber rather than on surface 3.
6. Surface 2 was heated to the desired temperature level to obtain the range of incident fluxes on the thermopiles which would correspond approximately to those anticipated under the test conditions. The thermopile emf's and temperatures were recorded at a sufficient number of temperature levels.
7. The temperatures were corrected for the temperature gradient across the plate and were averaged over the entire surface. The local irradiation values corresponding to these temperatures were calculated and emf versus irradiation was plotted for each thermopile. A sample curve is shown in Figure 13.
8. For calibration on a spectral basis the procedure was exactly the same except that filters were installed on the thermopiles.

The above-mentioned procedure for calibration is a relative one. In this method the effects of thermopile mountings, KBr window, extraneous radiation, and other sources

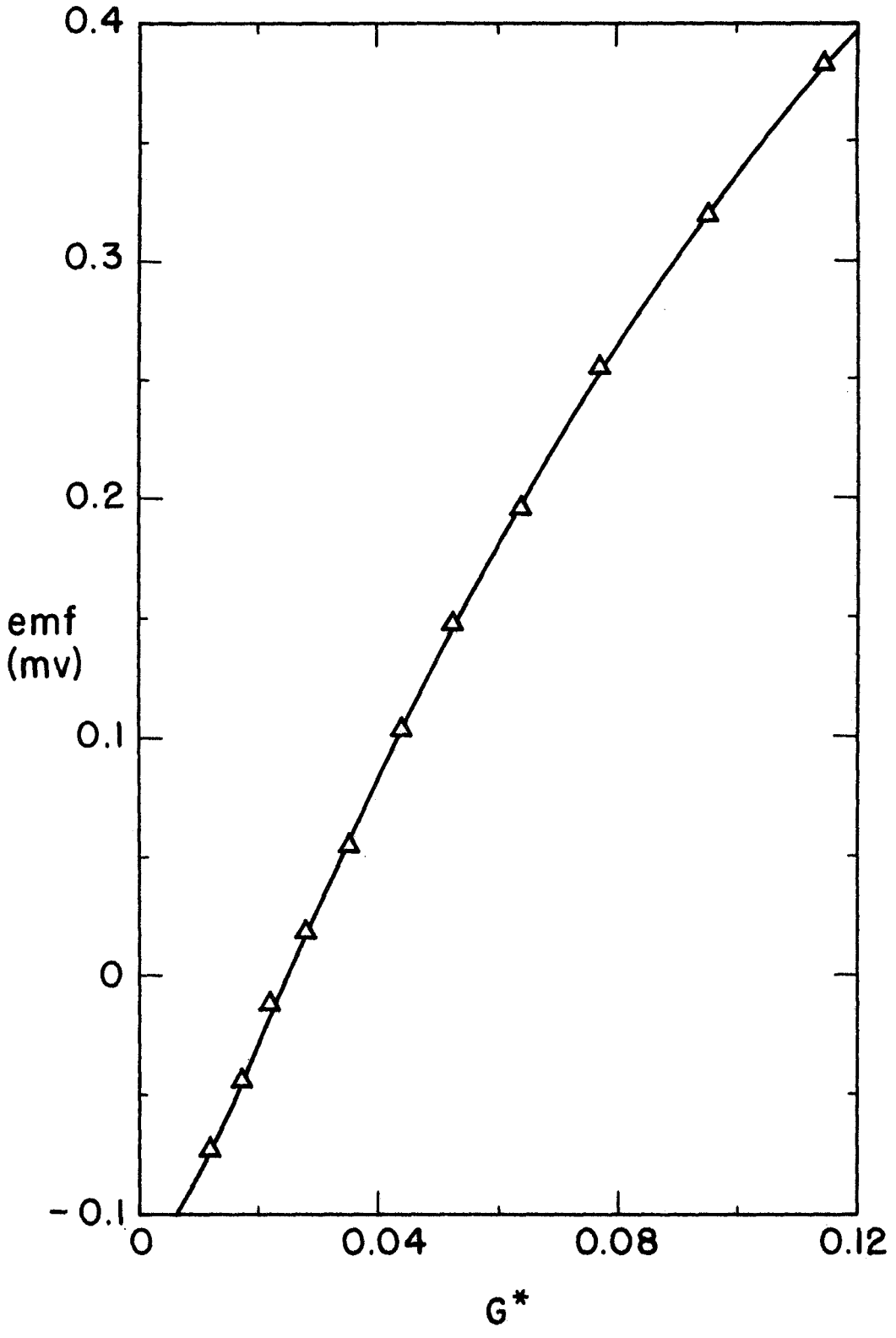

Figure 13. Typical Thermopile Calibration Curve.

of error are reduced, but are not completely eliminated. Possible errors may have arisen due to uncertainties in the radiation surface characteristics of paints. Also, the calibration of the thermopiles on an absolute basis would not have been meaningful since it was impossible to simulate the conditions under which they were to be used.

The procedure for taking the experimental data with test surfaces was exactly the same as for calibration. Care was taken to use the same filters and thermopiles in the same locations and orientations as during calibration.

5. RESULTS AND DISCUSSION

In this chapter experimental data are compared with the analytical predictions of radiant interchange, and the effects of various parameters on radiant heat transfer are discussed. Section 5.1 contains the discussion of these parameters and the radiation characteristics of the real surfaces used in the experiment. Comparisons of spectral and total experimental data with analytical predictions, on a local basis and on an overall basis, are presented in Section 5.2.

5.1 Independent Parameters

Before presenting and discussing the results, it is desirable to review the parameters which govern radiation interchange between simply arranged surfaces. In the broadest sense, the radiation interchange depends on the following: 1) the geometry of the system, 2) the radiation characteristics of surfaces and their dependence on direction and wavelength, and 3) the boundary conditions prescribed at the surfaces. There is, of course, an infinite number of combinations of the various independent parameters, and so it is necessary to be selective.

The reasons for selecting particular configuration used have already been given in Section 3.3. The dimensionless separation distance δ was maintained close to unity for lack of space in the chamber, while the dimensionless spacing γ between the plates was kept at 1/6 to 1/2. The smaller value ($\gamma = 1/6$) was limited by not having sufficient irradiation on the thermopiles in the extreme location

(ξ = 1/8), and the larger value (γ = 1/2) was limited by the available space in the chamber as well as the irradiation consideration.

For each spacing the data were taken at two temperature levels of the hot surface 2. The lower temperature was dictated by the need to have sufficient energy incident on the thermopiles at the desired wavelength. The higher temperature level was limited by other considerations such as the cooling capacity of the chamber and evaporation of materials at low pressure and high temperature. The cold surface was maintained at about room temperature by circulating coolant from the kryomat through the cold block. This was necessary for good performance of the thermopiles which passed through the cold block. Surface 3 was kept at the LN_2 temperature for two reasons. Firstly, at this temperature the emission from this surface is very small and can be neglected thus simplifying the predictions. Secondly, because the absorptance of gold at this temperature is very small it is practically an adiabatic surface. Previous studies [71, 83] have shown that it is in the presence of an adiabatic surface in an enclosure that a large discrepancy occurs between experiment and analysis.

For a meaningful comparison of the experimental and analytical results the radiation characteristics of surfaces must be known to an acceptable accuracy. The literature search has shown that for gold there is considerable discrepancy in these properties from one investigator to another. The methods of preparation of surfaces vary widely, and the available data do not cover the complete spectral and directional range of interest of this study. After carefully examining the available data, including that compiled by the Thermophysical Property Research Center of Purdue University [16], values of the total hemispherical emittance were selected which corresponded to samples prepared in a manner similar to that used in

this study. Complete bidirectional data could not be found in the literature. The only data available are for one or two angles of near normal incidence. The data reported on a spectral basis are mostly in the visible spectrum, and those available at the wavelengths of interest correspond to the samples prepared in a different fashion and hence are not acceptable.

In view of the above-mentioned lack of needed radiation property data, the values used in the analysis were based on those predicted by Fresnel's equations. The optical constants were calculated by the simple Drude theory. Previous investigators have shown that Drude's model is excellent for predicting the optical constants in the infrared spectrum for ultra high vacuum deposited gold. Since the emittance of pure metals is smaller [20, 109] than that deposited commercially, due to contamination and surface damage, the values predicted by Drude's theory were proportioned to yield the selected experimental total hemispherical emittance.

5.2 Comparison of Experiments and Analyses

In this section the experimental data are compared with the analytical predictions of various models. The purpose of these comparisons is to examine the validity of the commonly used simplified methods of radiant heat transfer analysis by comparing these with more detailed analyses as well as the experimental data. Comparisons are performed on a spectral as well as a total basis so that directional and spectral effects can be examined separately. Only some representative results are presented graphically. The remaining data are tabulated in APPENDIX C.

All the data presented are in terms of spectral or total irradiation at the cold surface. They have been nondimensionalized with respect to the spectral or total

emissive power of the cold surface. That is, the local total irradiation in dimensionless form is given by $G_1^* = G_1/\varepsilon_1\sigma T_1^4$. This is somewhat arbitrary; however, the procedure chosen is a logical extension of schemes previously employed. In the presentation of the data the subscript 1 has been dropped for convenience since all the data are for surface 1. The overall (average) irradiation results presented in Tables 6 through 8 were obtained from the local values.

It was mentioned in Section 3.7 that the numerical solution of integral equations with detailed properties was very time consuming and hence was abandoned in favor of the Monte Carlo method of solution. Although some results for the experimental situation were obtained by solving the integral equations, for the sake of consistency only the Monte Carlo results are presented. The accuracy of the Monte Carlo program was checked in some cases by comparing these results with those predicted from the integral equation solutions. The comparison was found to be very good. Since the Monte Carlo method is a statistical one, the results did have some scatter, but it was small. The curves shown in the figures were faired through the plotted points corresponding to the values calculated by means of the Monte Carlo method.

Before discussing the results it is appropriate to reexamine Eq. (3·44) which was obtained from Eq. (3·38) by the use of reciprocity relation, Eq. (3·40). If the reflection distribution function used in the calculations fails to satisfy the Helmholtz reciprocity relation, that is, if it is not symmetric with respect to the directions of incidence and reflection, $[f(\vec{\Omega}',\vec{\Omega},\lambda) \neq f(\vec{\Omega},\vec{\Omega}',\lambda)]$, the reciprocity relation for absorption factors, Eq. (3·40), is not valid. It is well known that when the Beckmann reflection function is corrected for finite conductivity of materials it fails to satisfy reciprocity. It was pointed

out [39] that the violation of the reciprocity relation occurs only for the incoherent component and not for the coherent component. Since in this study only the coherent component was predicted by the Beckmann model, the use of Eq. (3·44) to predict irradiation is perfectly justified.

Another quantity to be examined is the local irradiation at surface 1 due to emission from other surfaces. Rewriting Eq. (3·45) in dimensionless form on total as well as spectral basis yields, respectively,

$$G_1^* = [B_{d_1-1} + B_{d_1-2}(T_2/T_1)^4 + B_{d_1-3}(T_3/T_1)^4]/\varepsilon_1 \qquad (5\cdot1)$$

and

$$G_{1\lambda}^* = [B_{\lambda d_1-1} + B_{\lambda d_1-2}(E_{2b\lambda}/E_{1b\lambda}) + B_{\lambda d_1-3}(E_{3b\lambda}/E_{1b\lambda})]/\varepsilon_{1\lambda} \qquad (5\cdot2)$$

It is clear from Eq. (5·1) that the irradiation depends on the absorption factors and the temperatures. When B_{di-j} are of the same order of magnitude the main contribution to G_1^* is from B_{d_1-2} when $(T_2/T_1)^4$ is large. In the present study $(T_3/T_1)^4 \simeq 0.005$ and $(T_2/T_1)^4$ varies approximately from 20 to 50. In such a case (for all B_{di-j} equal), ignoring B_{d_1-3} results in a difference of less than 0.01 percent for the high temperature level and less than 0.025 percent for the low temperature level of the hot plate. For large values of $(T_2/T_1)^4$ even B_{d_1-1} may be ignored. For example, a difference of less than 2 percent (when B_{d_1-1} and B_{d_1-2} are equal) results in the value of G_1^* for $(T_2/T_1)^4 = 50$. Similar conclusions can be drawn for the calculation of $G_{1\lambda}^*$, and the neglect of the emission from surface 3 can be justified. Consequently, in the calculations surface 3 was assumed nonemitting. Some sample results are presented in Figure 14 to illustrate the order of magnitude of the absorption factors. The key to the various lines on all the figures is the same as that given in Figure 15 unless noted

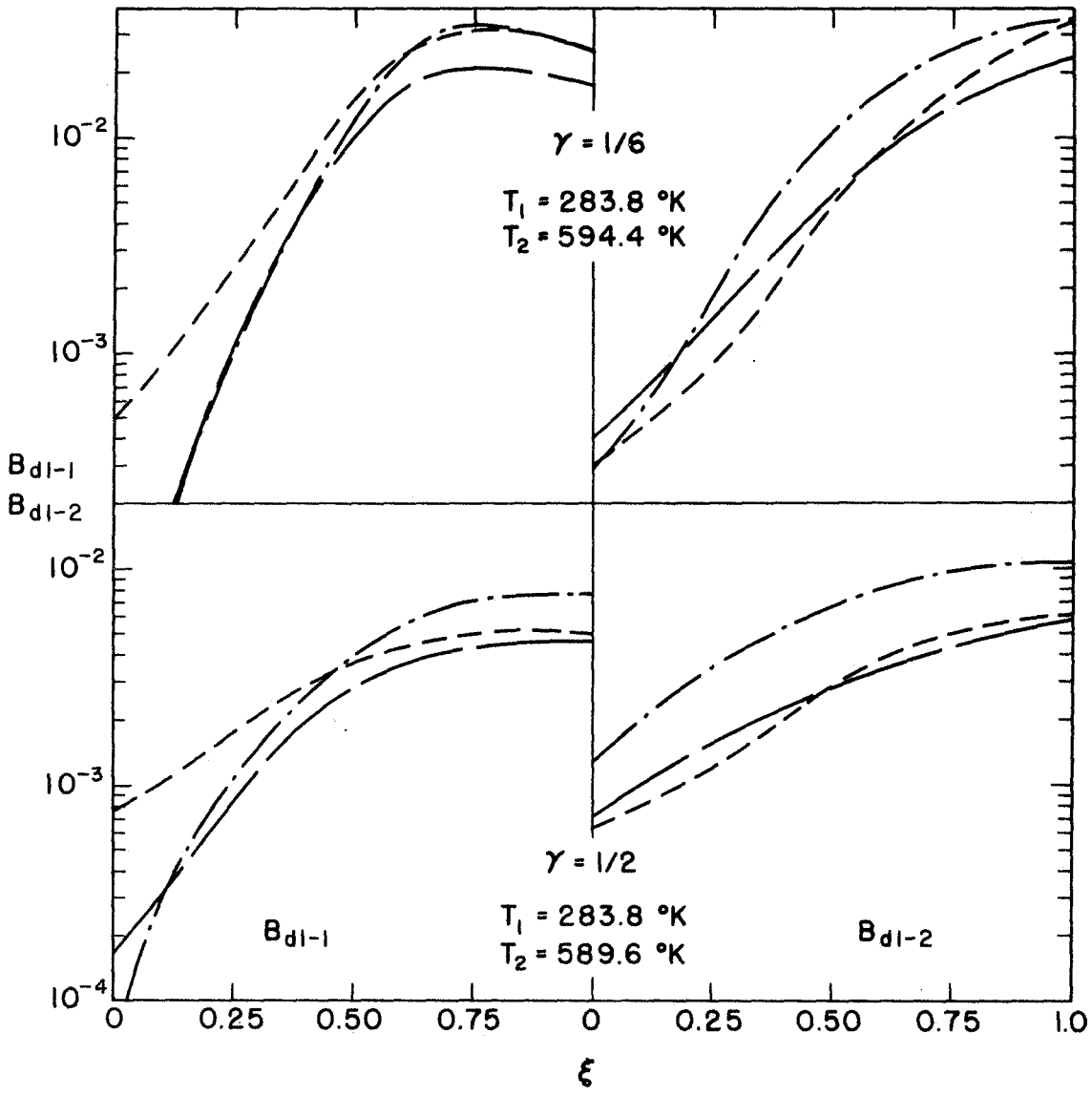

Figure 14. Comparison of Total Absorption Factors for Different Models, Surface Arrangement S-S-B, $\delta = 1$, $\eta = 1/8$.

otherwise. It is clear that the order of magnitude of B_{d1-1} and B_{d1-2} at corresponding points is the same. Since $(T_2/T_1)^4 >> 1$ it was expected that the trend of the irradiation curves should be similar to those of B_{d1-2}, which was confirmed later.

5.2.1 Comparison of Measured and Predicted Spectral Local Irradiation

In Figures 15 and 16 the analytical predictions for the constant property diffuse, specular, and directional property specular DP(S) models of spectral irradiation at $\lambda = 3.08\mu$ are compared with the experimental data (circles) when all the surfaces are specular ($\sigma_m/\lambda < 0.01$). Examination of the figures reveals that the experimental data are in best agreement with the predictions of DP(S) analysis; however, at some points (Figure 15) these predictions are about 40 percent lower than the data. The results based on diffuse analysis (Figure 15) are about 80 percent lower than the experimental data. At both temperature levels, for Figures 15 and 16, the predictions of the diffuse analysis are always lower than those of the constant property specular analysis. Since the local heat flux at the cold surface is given by

$$q^*_{1\lambda} = 1 - \varepsilon_{1\lambda} G^*_{1\lambda} \qquad (5\cdot3)$$

this means that the diffuse analysis would predict too high a heat flux. The lower irradiation shows that more of the energy leaves the enclosure for the diffuse than for the specular reflection model. This is typical of enclosures which exchange a large portion of their energy in near normal directions. As an example, for two parallel plates with a large separation distance, the irradiation based on the specular model is always higher [70, 72, 75] than that based on the diffuse model. This seems plausible due to the fact

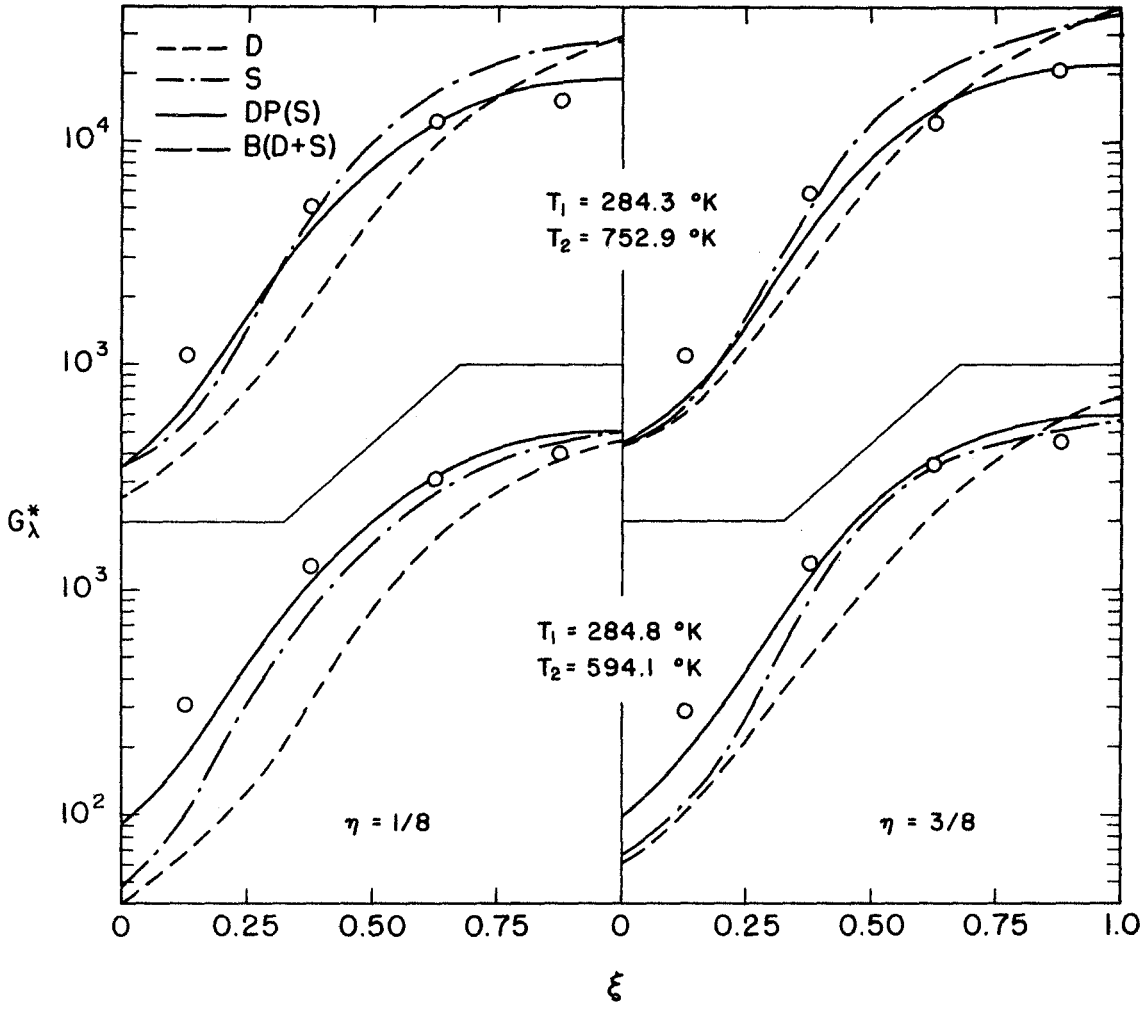

Figure 15. Comparison Between Measured and Predicted Irradiation for Different Models, Surface Arrangement S-S-S, $\lambda = 3.08\mu$, $\delta = 1$, $\gamma = 1/6$.

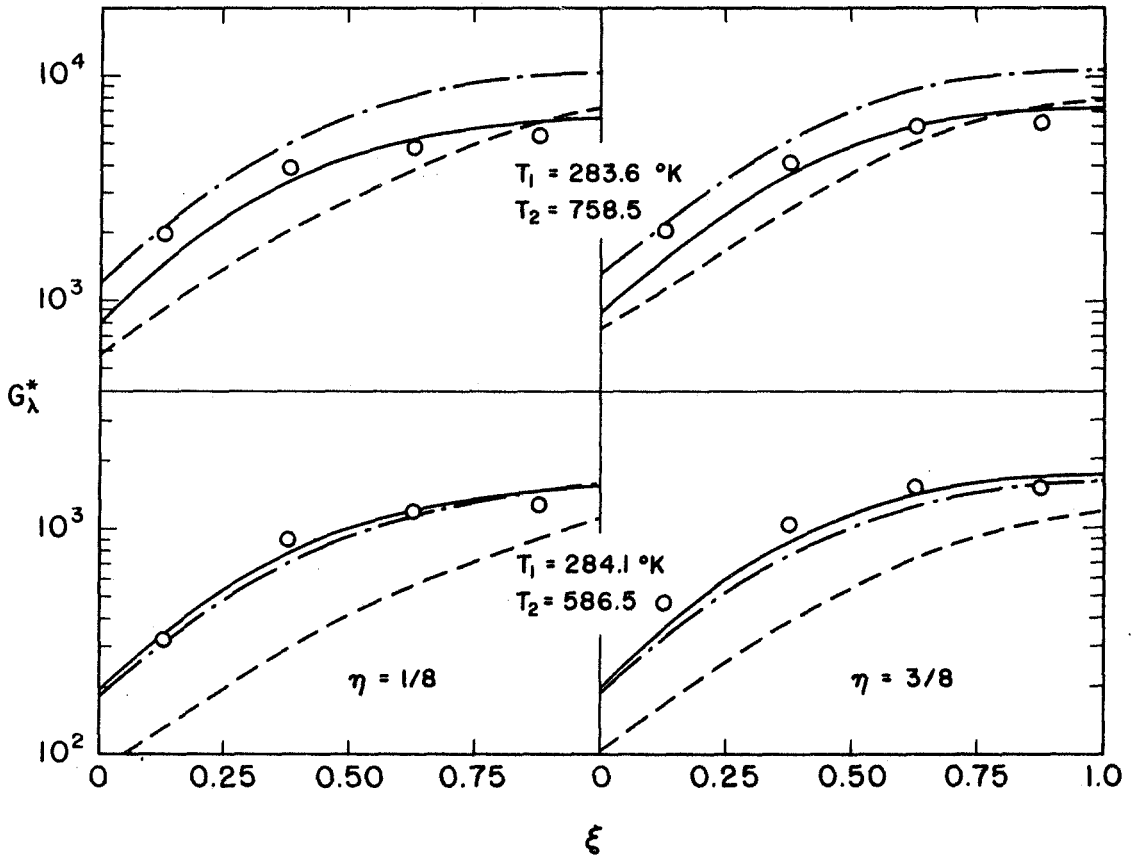

Figure 16. Comparison Between Measured and Predicted Irradiation for Different Models, Surface Arrangement S-S-S, $\lambda = 3.08\mu$, $\delta = 1$, $\gamma = 1/2$.

that at each reflection from a diffuse surface the energy is uniformly distributed with a constant intensity. On the contrary, when more of the energy exchange occurs in directions other than the normal, the diffuse analysis would predict higher irradiation. This observation is supported by calculations of the adjoint plate system [17, 75, 77] for opening angles larger than 15°. Rectangular cavity type enclosures [71, 72, 83] fall in the former category.

The largest discrepancy among the various analyses and with the experiments in Figure 15 occurs on the open end of the closed configuration ($\gamma = 1/6$). The temperature level appears to have little effect on the trends of the CP results. This is due to the fact that for both cases T_2/T_1 is sufficiently high so that G^*_λ is controlled by $B_{\lambda d_{1-2}}$. Hence, any further increase in temperature T_2 does not alter the shape of the curves. With the rise in temperature, the DP(S) analysis tends to fall in between the S and D analyses. The trends in Figure 16 ($\gamma = 1/2$) are the same as in Figure 15. The directional property analysis is in closest agreement with experimental data. For a more open configuration the irradiation is more uniform. The change in temperature level does not seem to have an appreciable effect on the trends of the results except to increase the irradiation and reduce G^*_λ based on the DP(S) model below that of the S model. This is due to the fact that most of the energy emitted at oblique angles leaves the system without being absorbed. Mostly, the energy emitted in the near normal directions contributes to irradiation, and the emission in the normal direction for metals is always higher for the CP model than for the DP model.

When surface 3 is replaced by a diffuse surface ($\sigma_m = 7.1\mu$), the difference between the predictions (in all predictions surface 3 is assumed diffuse) of the three models in general decreases and the experimental results agree best (within 40 percent) with the DP(S) analysis. These results

are presented only in tabular form in APPENDIX C. Over a large part of the surface the predictions of the S and D models are almost identical. However, at some locations the CP analyses yield values which are twice the measured values. The largest difference occurs at high temperatures and for the more open system ($\gamma = 1/2$). It is recognized however, that the diffuse limit does not exist. A part of the disagreement between analysis and experiments can be attributed to this reason.

With surfaces 1, 2 specular and surface 3 bidirectional ($\sigma_m/\lambda \simeq 0.17$) the results for $\lambda = 4.51\mu$ are presented in Figures 17 and 18. While the trends for the S and D models are the same as already discussed, the B(D+S) model predicts a lower irradiation than is indicated by the experimental data. The trend of the S and D analyses is expected to remain the same throughout because the results are for identical plate spacing. The differences are only in the temperatures and the radiation characteristics which are relatively small. Next to the B(D+S) analysis, the experimental results are in closer agreement with predictions based on the diffuse rather than the specular models. This seems to be due to small specular component of reflectance. For $\gamma = 1/6$ the overall specular components of reflectance are 0.045 and 0.17 for $\lambda = 3.08\mu$ and 4.51μ, respectively. A similar trend exists also for $\gamma = 1/2$ where again the specular components are small; 0.01 for $\lambda = 3.08\mu$ and 0.1 for $\lambda = 4.51\mu$.

In agreement with the conclusions of the previous studies [71, 75], the constant property specular model usually predicts higher irradiation, at some locations more than 3 times the values from the DP predictions. For $\gamma = 1/2$, predictions of the S analysis more than 100 percent higher than in the experiments is quite common. Consistently, the experimental data are higher than the B(D+S) analysis on the open end of the system. This may be due to the

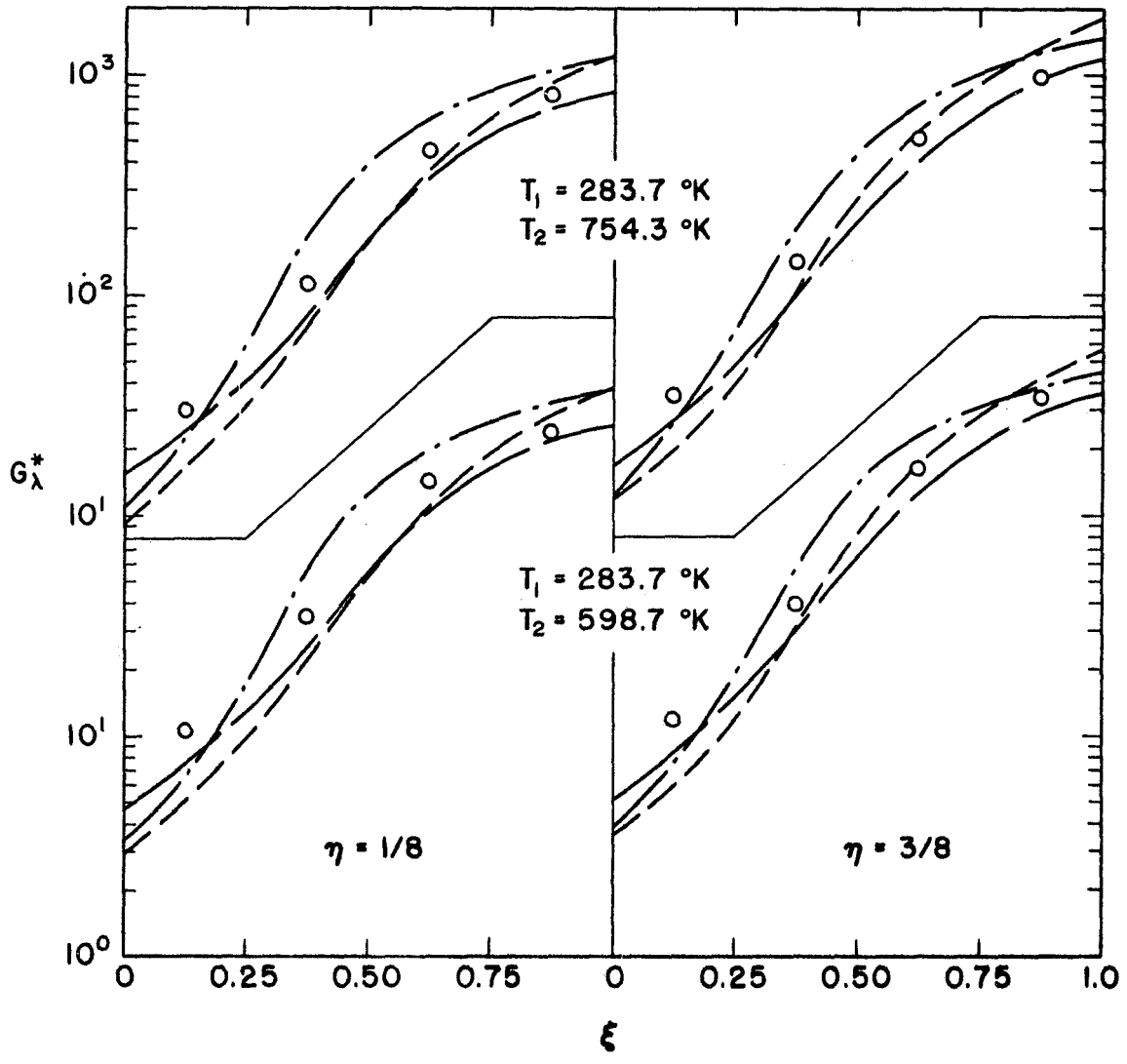

Figure 17. Comparison Between Measured and Predicted Irradiation for Different Models, Surface Arrangement S-S-B, $\lambda = 4.51\mu$, $\delta = 1$, $\gamma = 1/6$.

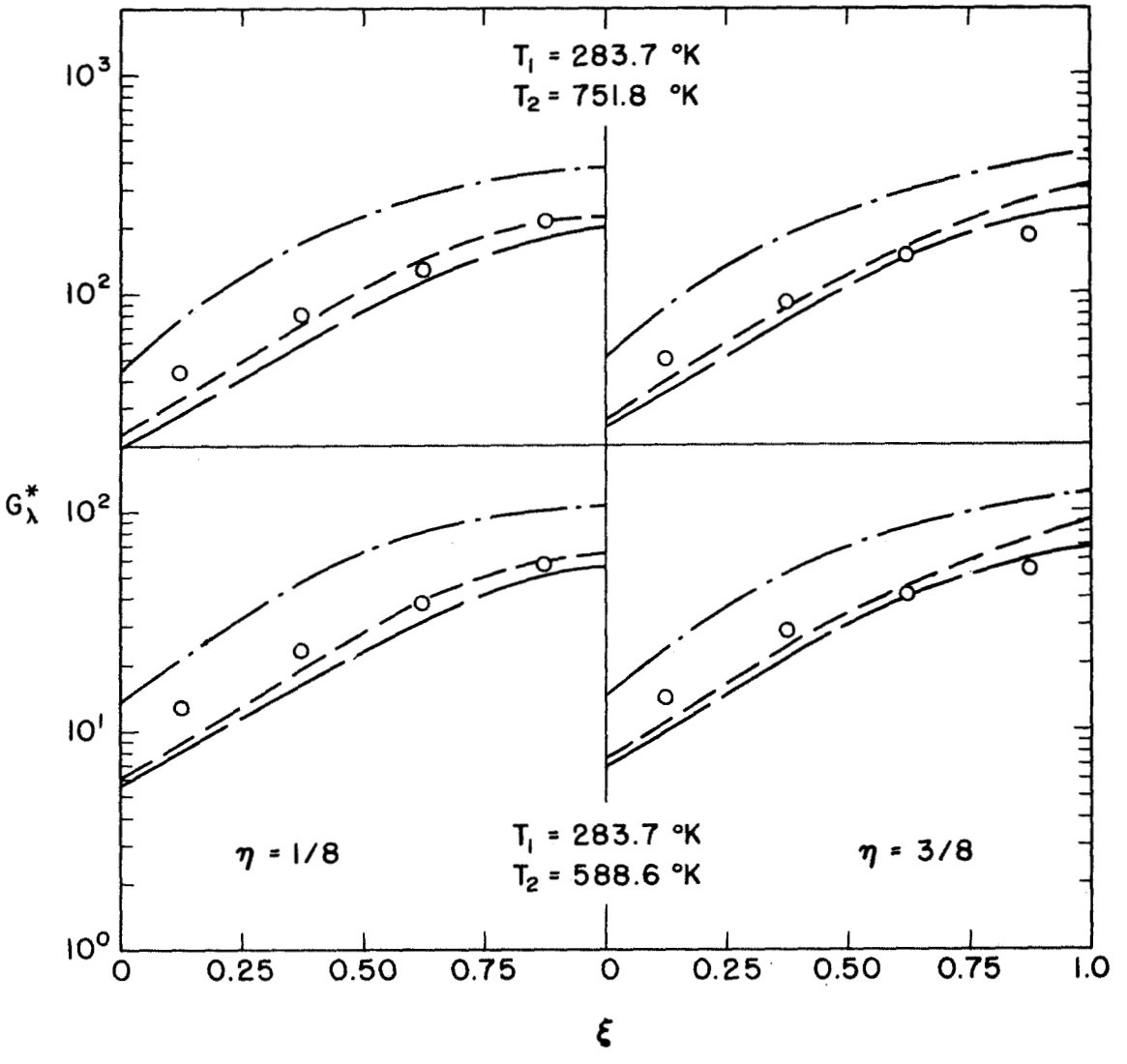

Figure 18. Comparison Between Measured and Predicted Irradiation for Different Models, Surface Arrangement S-S-B, $\lambda = 4.51\mu$, $\delta = 1$, $\gamma = 1/2$.

limitation in the model itself. Actually the incoherently reflected energy is peaked in the specular direction but this energy has been assumed to be reflected diffusely in the B(D+S) model. The overall direction of energy flow is from surface 2 to surface 1 via surface 3. Thus, the B(D+S) model would predict that less energy is reflected towards the open end of surface 1 than is actually reflected. Hence, the irradiation predicted from this model will be lower than the experimental data. This may be only one of the reasons. Possible errors in the experiments are discussed in APPENDIX B.

With a bidirectional surface 3 some calculations were performed for $\lambda = 4.51\mu$ with the D+S and DP(D+S) models. The results are given in APPENDIX C. In both cases the specular component was calculated by taking into account the wavelength, surface roughness and enclosure configuration (for details see APPENDIX A). Both of these analyses yielded results of comparable accuracy with that of the detailed B(D+S) analysis. Note that the results of the D+S analysis do not always lie between those of the D and S models.

Since the conclusions of the experimental data discussed so far at $\lambda = 3.08\mu$ and 4.51μ were the same, additional experimental data at $\lambda = 4.51\mu$ were not taken. The results presented in Figures 19 and 20 are when surfaces 1 and 3 are specular but surface 2 is bidirectional ($\sigma_m/\lambda \simeq 0.5$). The agreement between the predictions based on the B(D+S) model and the experimental data is much better than in the previous cases already discussed. In the worst cases the DP analysis is about 30 percent lower and the S analysis is 150 percent higher than the data. Note that for $\gamma = 1/6$ at $\xi = 1/8$ the experimental data are more than four times the predictions based on diffuse analysis.

The experimental results for a system consisting of a specular surface 1 and bidirectional surfaces 2 and 3 are

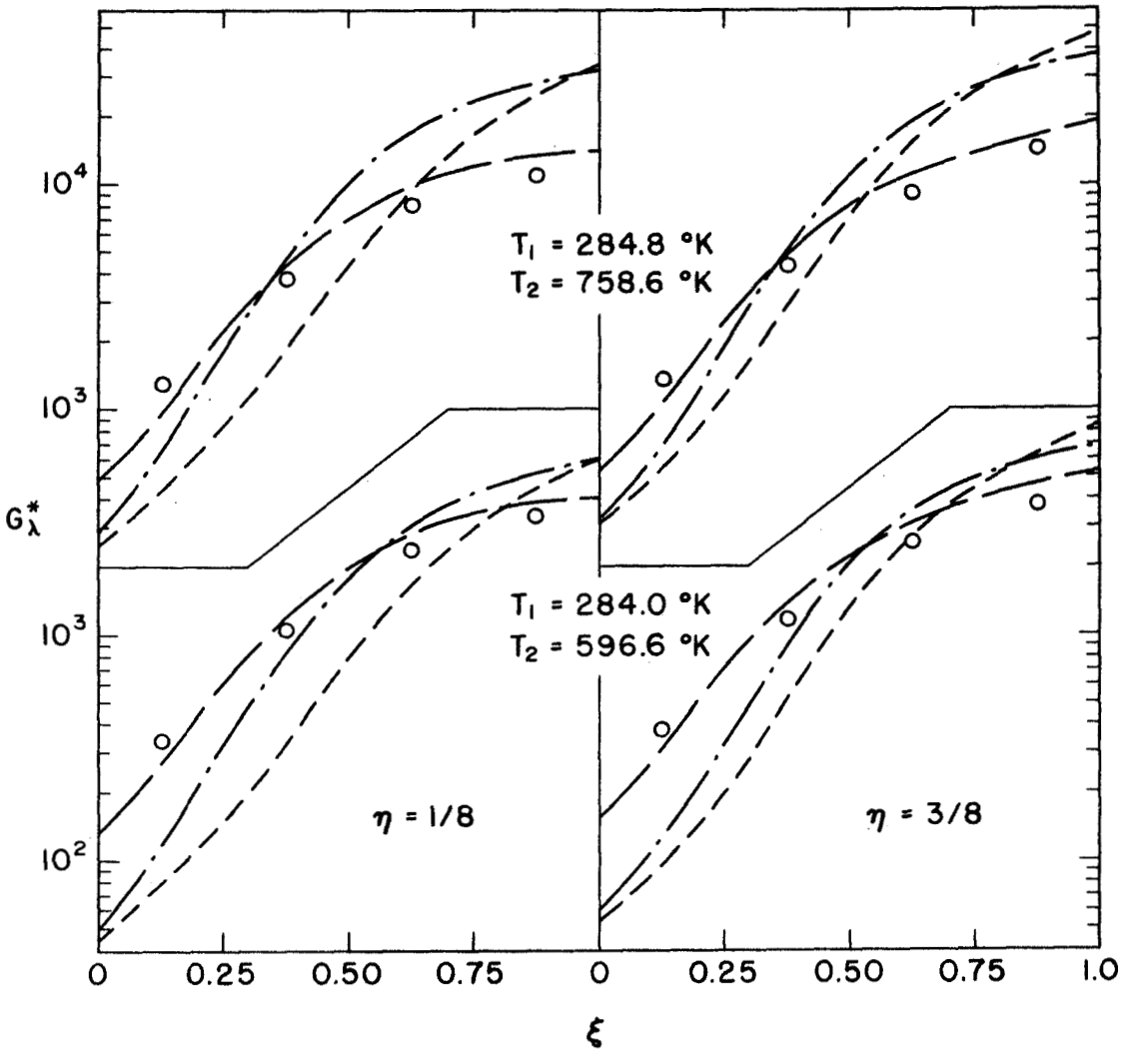

Figure 19. Comparison Between Measured and Predicted Irradiation for Different Models, Surface Arrangement S-B-S, $\lambda = 3.08\mu$, $\delta = 1$, $\gamma = 1/6$.

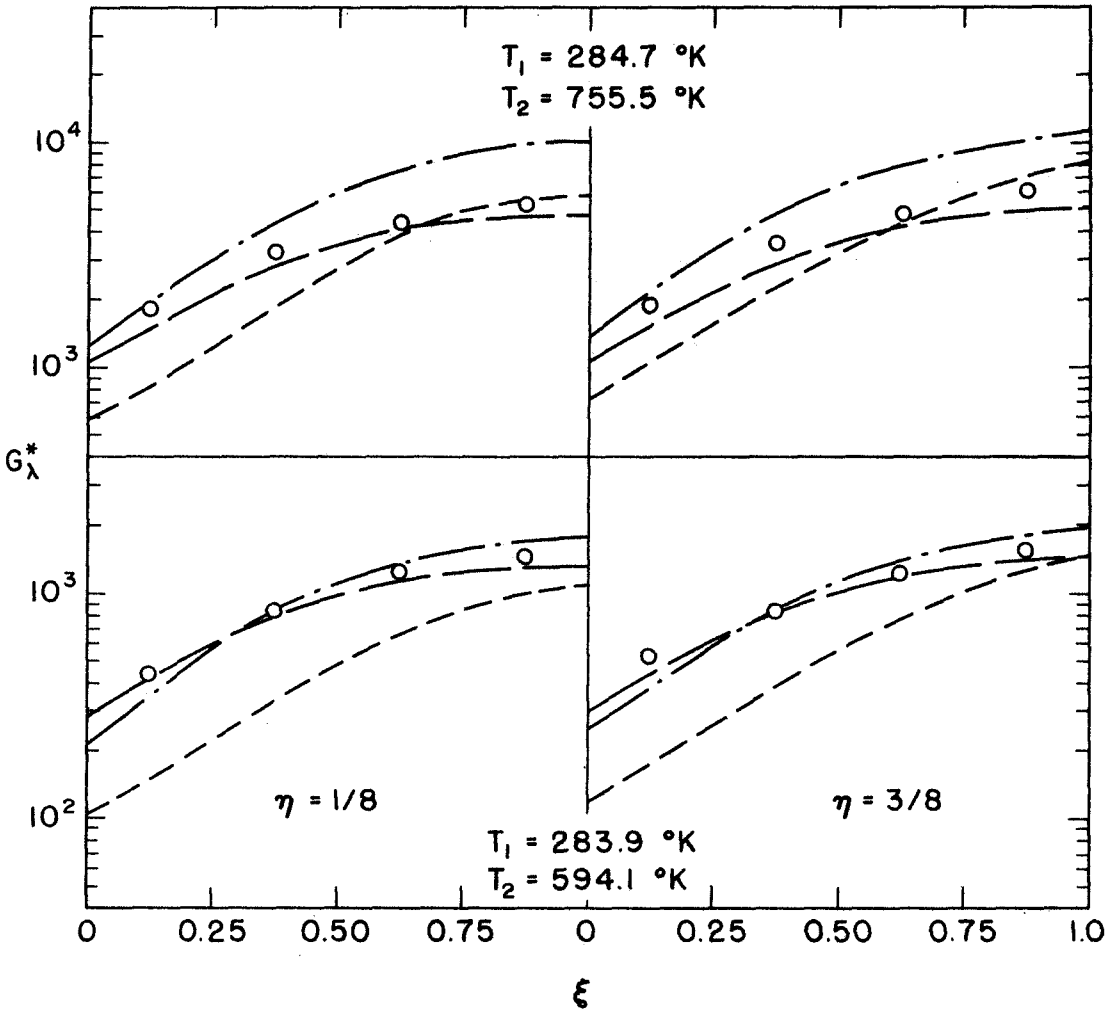

Figure 20. Comparison Between Measured and Predicted Irradiation for Different Models, Surface Arrangement S-B-S, $\lambda = 3.08\mu$, $\delta = 1$, $\gamma = 1/2$.

given only in the tabular form since they do not add anything new which has not already been discussed.

5.2.2 Comparison of Measured and Predicted Total Local Irradiation

The purpose of comparison of experimental data and analysis on spectral basis was simply to confirm that the directional and bidirectional effects are accounted for correctly in predicting the irradiation accurately. Usually one is interested in calculating the total rather than the spectral radiant energy quantities. Good agreement of the experimental data and the analysis at the two wavelengths shows that the spectral irradiation can be predicted with confidence since the radiation properties of metals in the infrared show only a gradual change with the wavelength.

Results presented in Figure 21 are for an enclosure consisting of all surfaces specular. The nongray DP(S) analysis shows very good agreement with the experimental data. In the worst case the analysis is only 20 percent lower than the data. This difference is much smaller than that determined on a spectral basis. For the same enclosure, but a spacing of $\gamma = 1/2$, the results are shown in Figure 22. Strangely enough the data show equally good or better agreement with the S analysis than with the nongray DP(S) analysis. Some measured local irradiation results are more than three times the values obtained from the diffuse analysis. The predictions based on the D and nongray DP(S) models are lower than those based on the S model. This can be explained in the same way as in the discussion on a spectral basis. At the open end of the system measured, data depart significantly even from the DP analysis, the measured results are about 80 percent higher. Some of the discrepancy may be due to the fact that thermopiles were calibrated at a spacing of $\gamma = 1/6$. For a spacing $\gamma = 1/2$

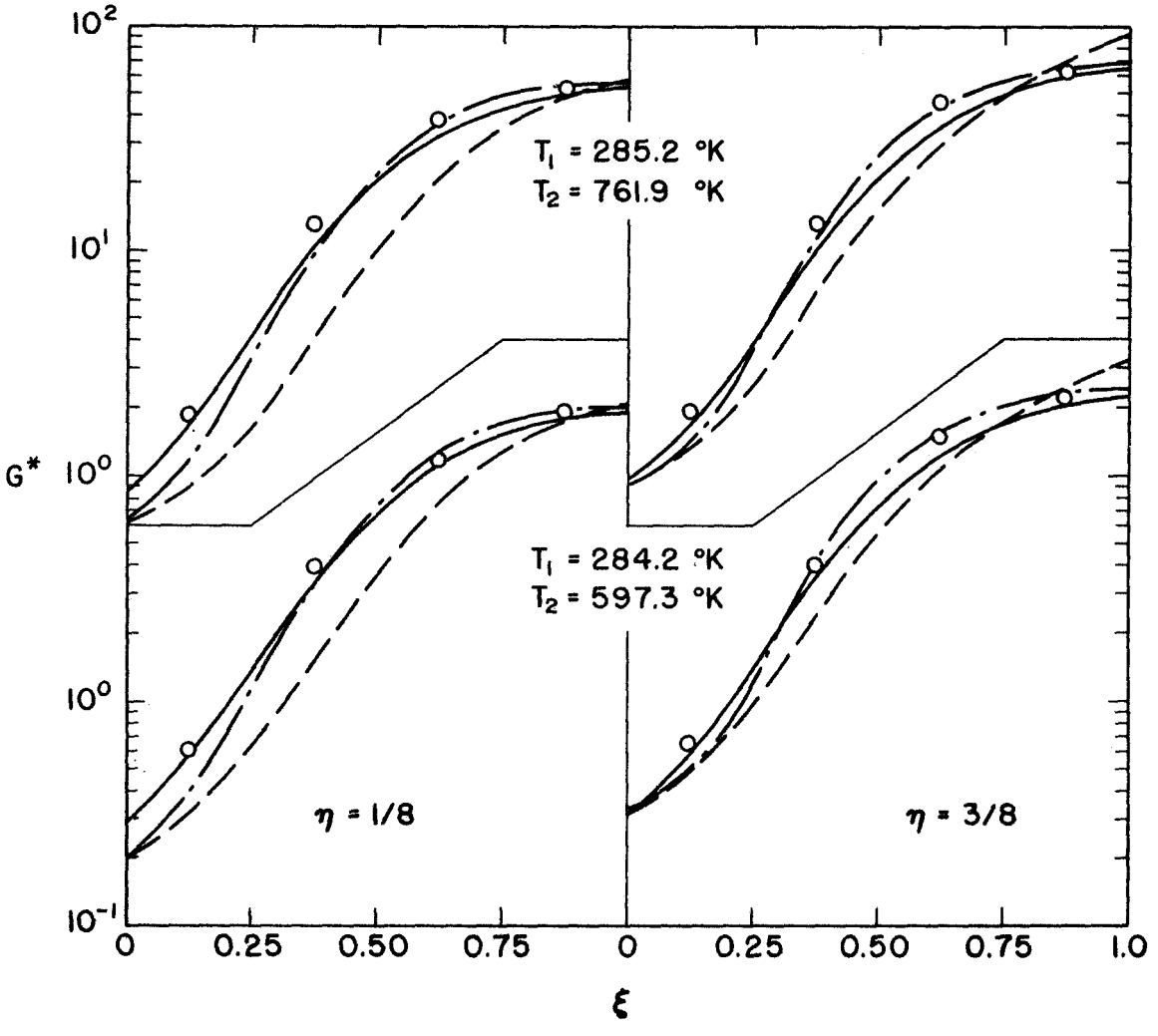

Figure 21. Comparison Between Measured and Predicted Total Irradiation for Different Models, [illegible]face Arrangement S-S-S, $\delta = 1$, $\gamma = 1$

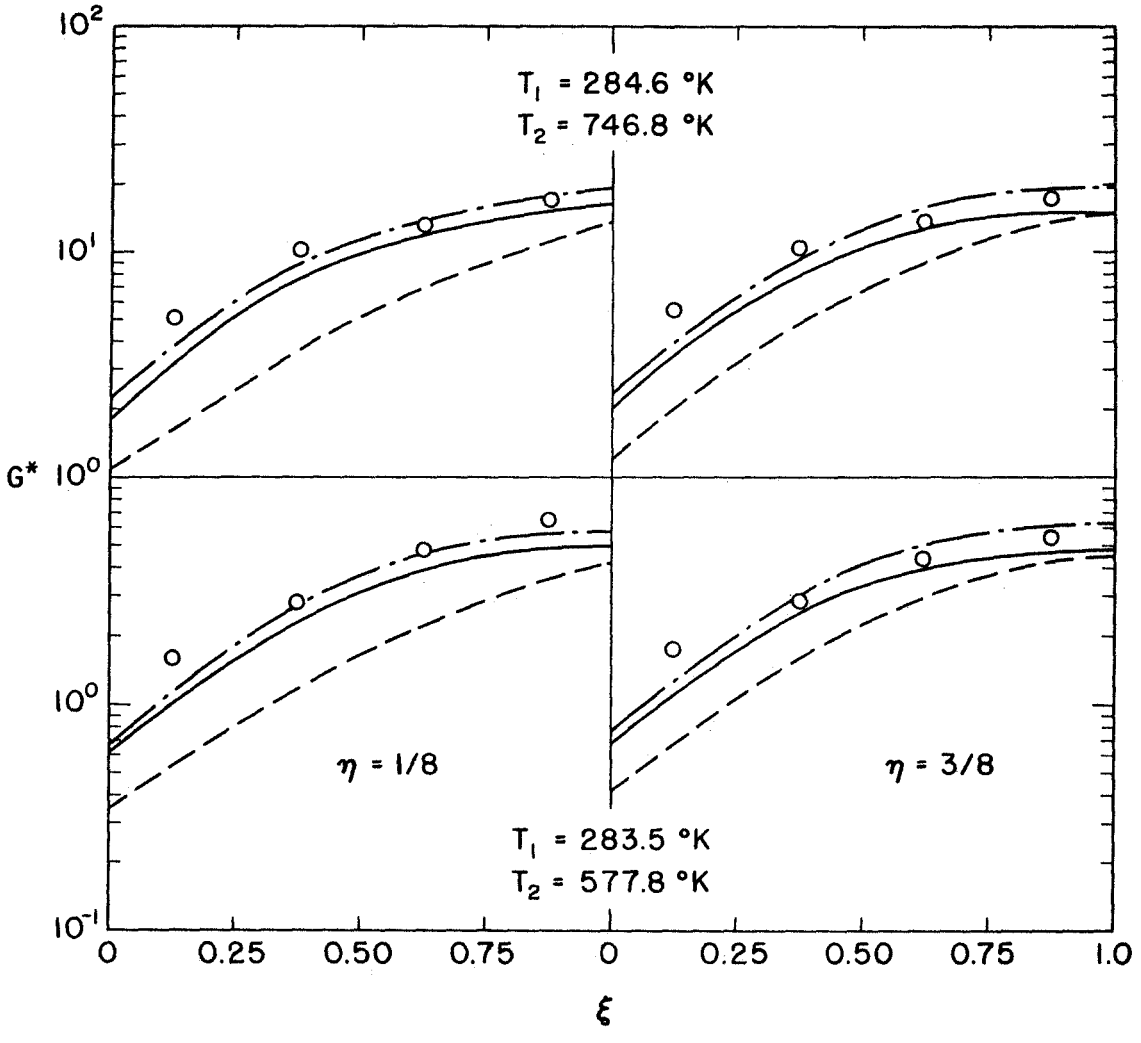

Figure 22. Comparison Between Measured and Predicted Total Irradiation for Different Models, Surface Arrangement S-S-S, $\delta = 1$, $\gamma = 1/2$.

the transmittance of thermopile window is expected to be higher, especially at $\xi = 1/8$ because energy is incident at less oblique angles for that condition.

For the sake of clarity in the figures, the results from the DP(S) semigray and gray analyses are not plotted, but are given in APPENDIX C. It is surprising to note that these results agree with the experiments equally well or better than the nongray DP(S) analysis. This good agreement appears to be due to the fact that for highly reflecting materials the reflectance is not a strong function of wavelength in the infrared part of the spectrum. Hence, in such cases it is the directional effects which are important.

For a system with diffuse surface 3 ($\sigma_m = 7.1\mu$) and specular surfaces 1 and 2, the results (APPENDIX C) show the same trend as those on the spectral basis. The predictions of all the analyses are very close and the experimental data in general agree better than in the spectral case. Surface 3 is not diffuse for the entire spectrum of incident radiation, but there appear to be some compensating effects due to which the agreement of the CP analysis with the measured results is also good. Again, the predictions of the DP(S) semigray and gray analyses agree well with the experiments.

The results for bidirectional surface 3 ($\sigma_m = 0.75\mu$) and specular surfaces 1 and 2 are presented in Figures 23 and 24. The data follow the trend of the B(D+S) analysis. For a spacing of $\gamma = 1/6$ the worst agreement again occurs at the open end of the closed configuration where G^* based on the B(D+S) analysis is about 40 percent lower than the measurements. For $\gamma = 1/2$ the results agree equally well with the D analysis. At some locations the S analysis overpredicts the experimental data by about 140 percent. It is interesting to compare Figure 24 with Figure 22 when surface 3 is specular. For this situation (Figure 22) the measurements agree well with the DP(S) analysis but are also close to the S analysis. For a bidirectional surface 3 the

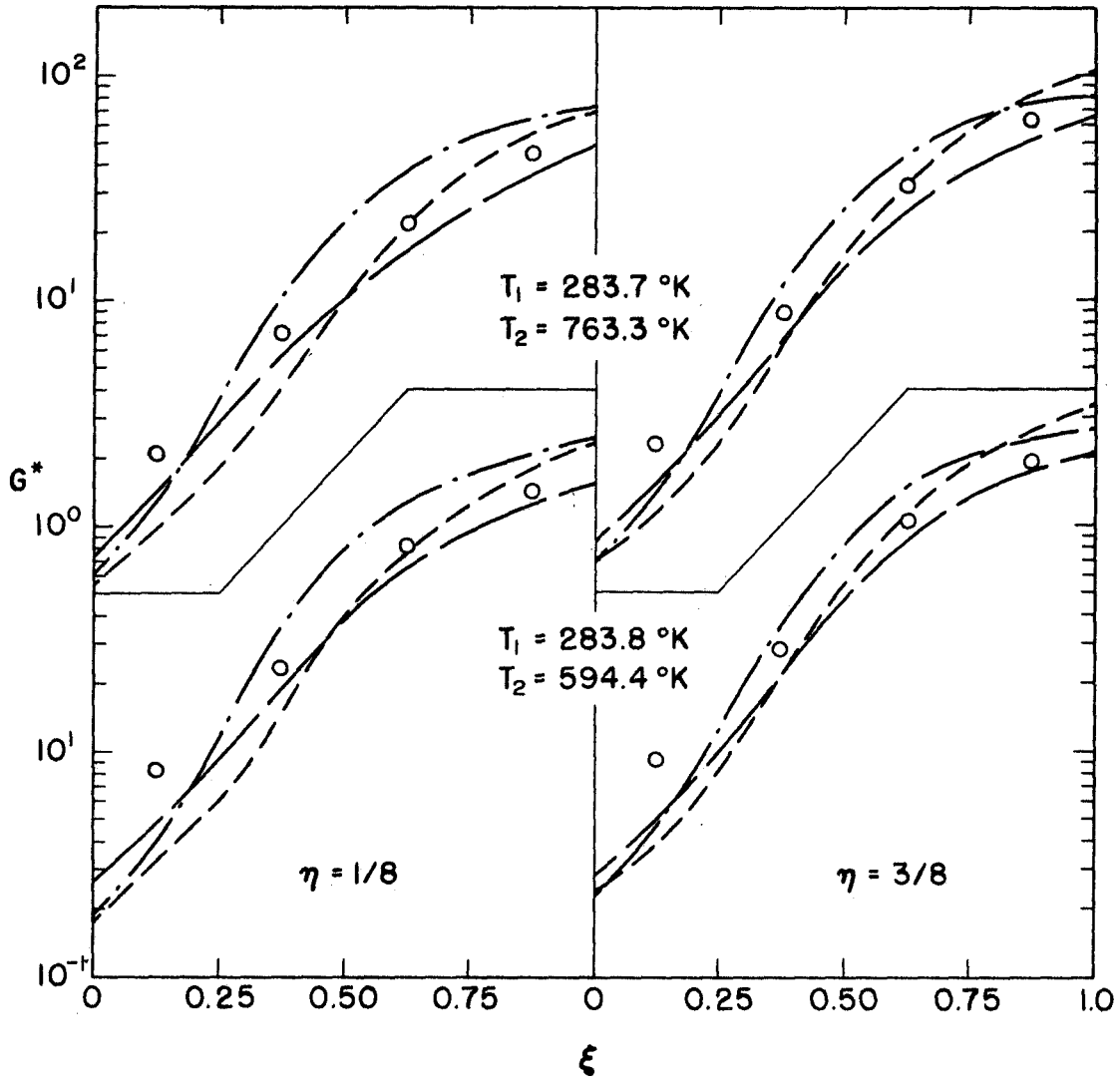

Figure 23. Comparison Between Measured and Predicted Total Irradiation for Different Models, Surface Arrangement S-S-B, $\delta = 1$, $\gamma = 1/6$.

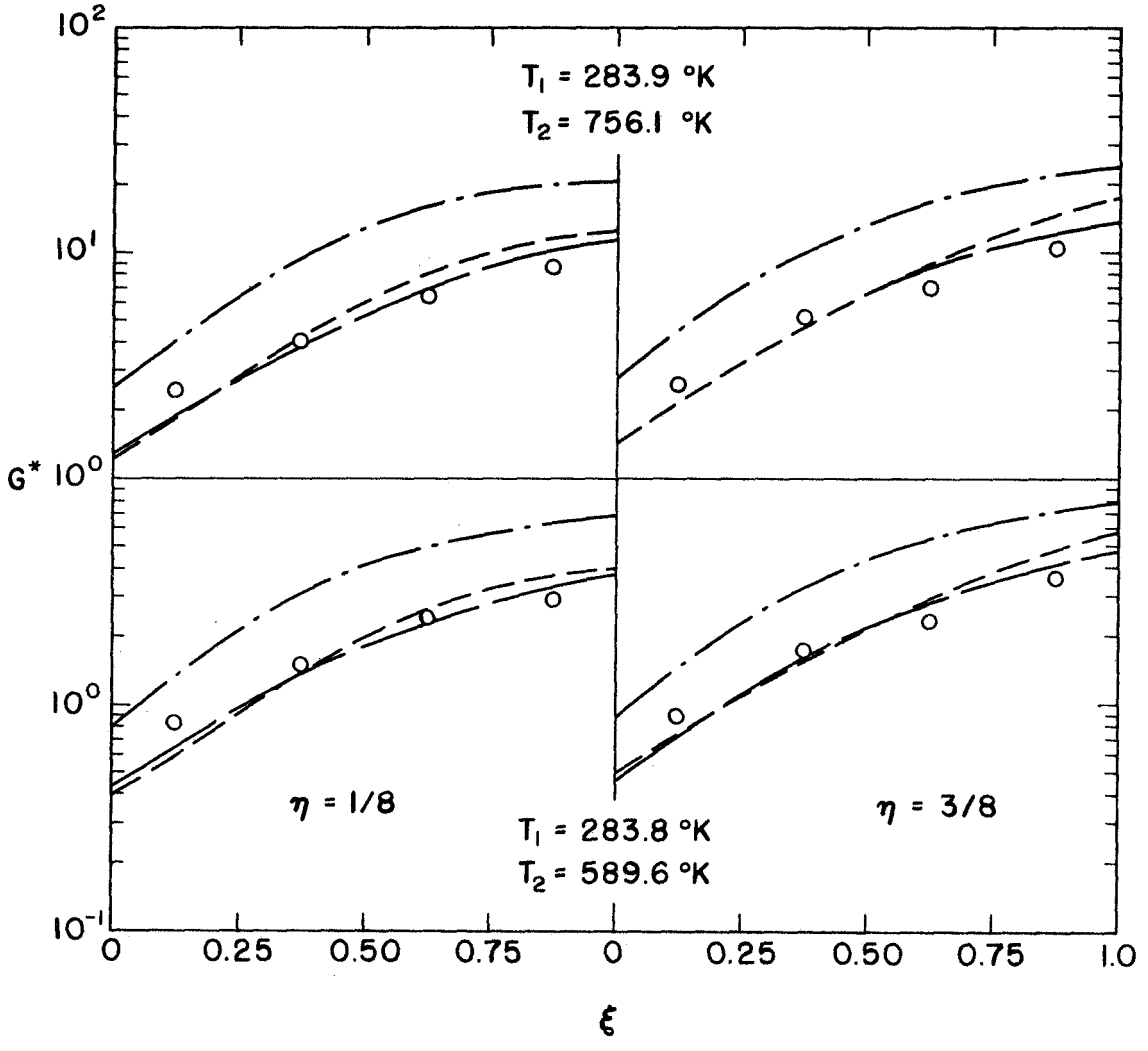

Figure 24. Comparison Between Measured and Predicted Total Irradiation for Different Models, Surface Arrangement S-S-B, $\delta = 1$, $\gamma = 1/2$.

data agree well with the B(D+S) analysis, but are very close to the D analysis. It appears that directional and spectral effects have compensated each other and the appropriate constant property analysis predicts the irradiation quite well. The results of the D+S analysis are not shown in the figures for the sake of clarity, but are given in Table C-3. It is surprising that this simplified analysis agrees with the measurements even better than the detailed directional property analysis for $\gamma = 1/6$. For $\gamma = 1/2$ the agreement is poor, and at some points the analysis is 70 percent higher than the experiments. The results of the semigray and gray DP(D+S) analysis, given in Table C-3, show in general a better agreement with the experiments than the constant property analysis. This again emphasizes the importance of directional effects. The semigray and gray analyses results are also shown in Figure 25 as an example.

For bidirectional surface 2 ($\sigma_m = 1.5\mu$), and with the other surfaces specular, the results (Figure 26) again show better agreement with the B(D+S) analysis. The predictions are about 10 to 30 percent lower than the data. The results based on diffuse analysis are as much as 70 percent lower than the measurements. The D+S analysis results are not shown in the figures but are presented in the tables. It is surprising that this simple analysis shows as good an agreement with the measurements as the more detailed B(D+S) analysis. Also, the predictions of the semigray and gray analysis are in equally good agreement with the B(D+S) analysis on a nongray basis.

For an enclosure consisting of two bidirectional surfaces, and with $\gamma = 1/6$, the data tend to fall more in line with the diffuse analysis. The results are in equally good agreement with the B(D+S) as well as the D analysis, except at the open end of the system where they agree better with the former model. For $\gamma = 1/2$ also the data (Figure 27) agree equally well with the D as well as B(D+S) analysis, but the

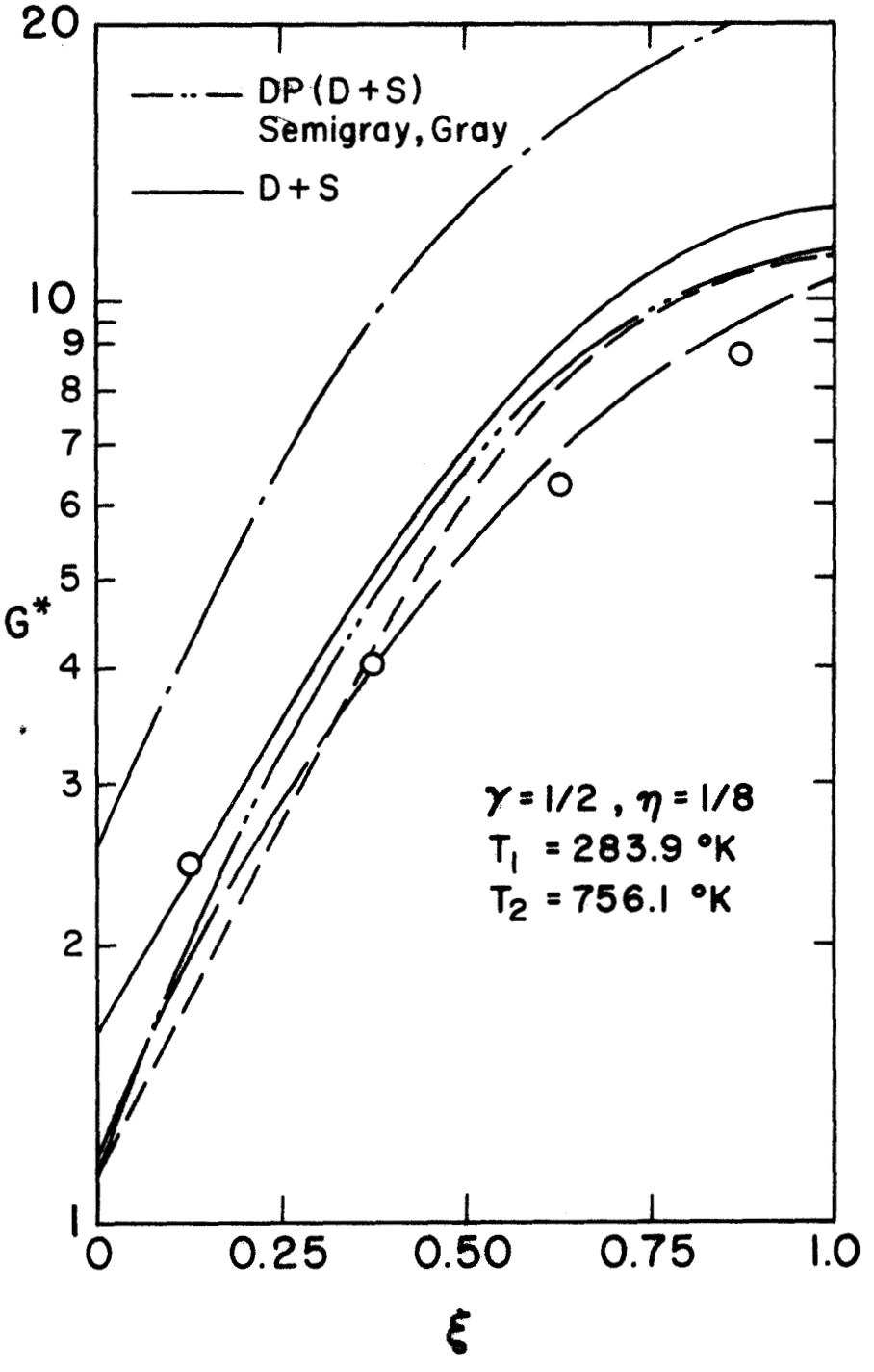

Figure 25. Comparison Between Measured and Predicted Total Irradiation for Different Models, Surface Arrangement S-S-B, $\delta = 1$, $\gamma = 1/2$, $\eta = 1/8$.

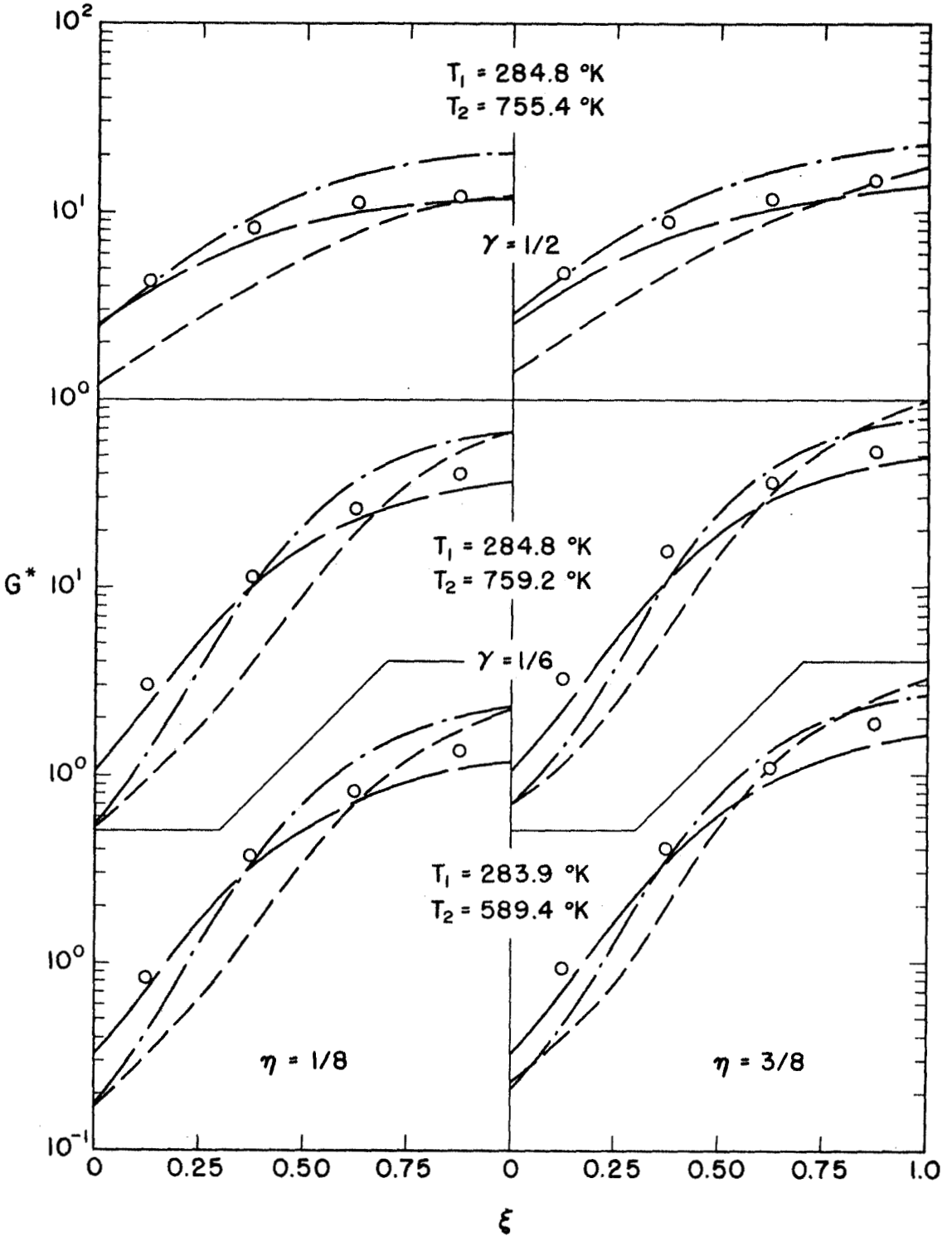

Figure 26. Comparison Between Measured and Predicted Total Irradiation for Different Models, Surface Arrangement S-B-S, $\delta = 1$, $\gamma = 1/6, 1/2$.

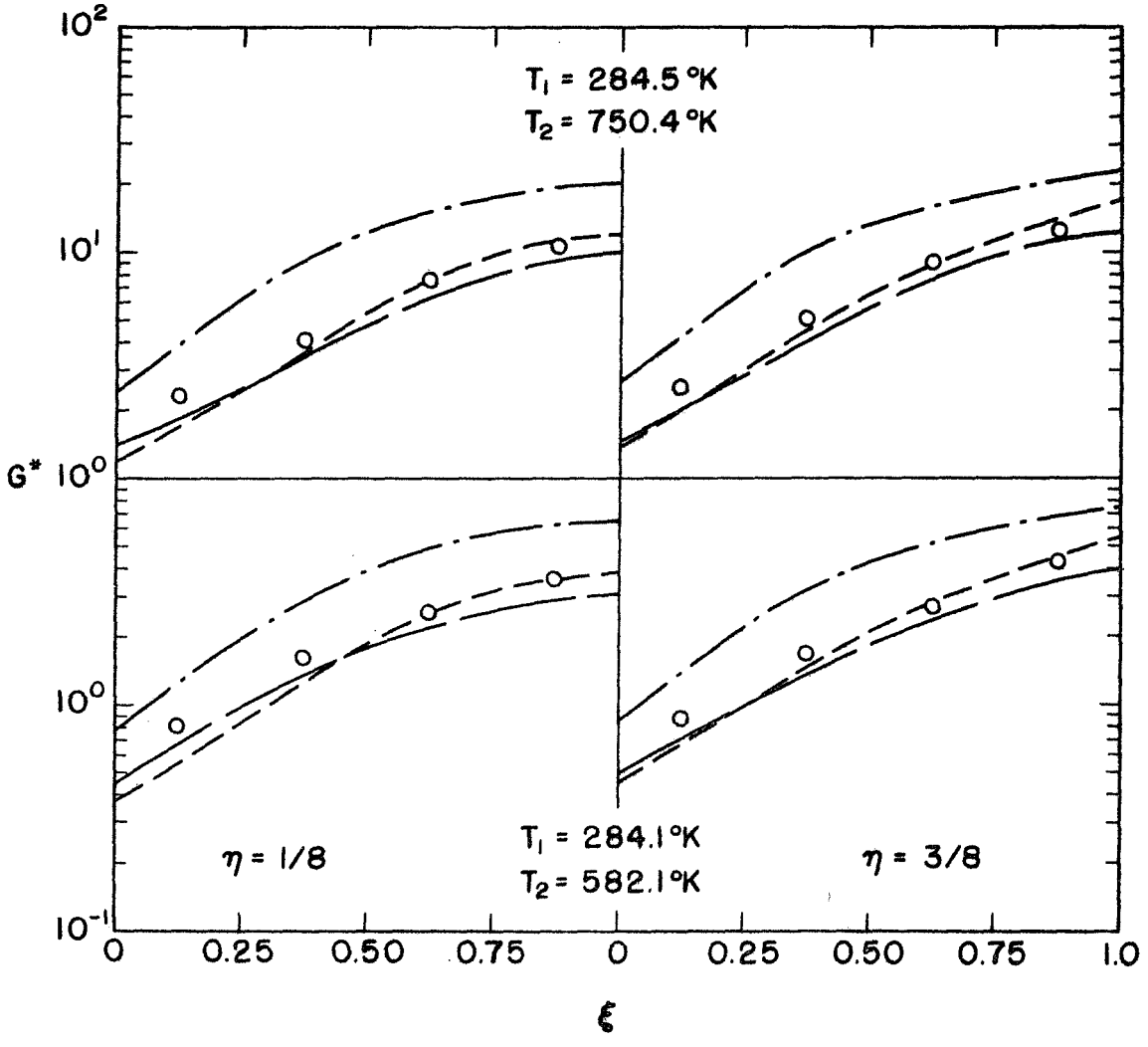

Figure 27. Comparison Between Measured and Predicted Total Irradiation for Different Models, Surface Arrangement S-B-B, $\delta = 1$, $\gamma = 1/2$.

S analysis always predicts higher irradiation. An enclosure with two bidirectional surfaces and a large γ spacing is expected to be more diffuse because the energy is incident at less oblique angles, for which the specular component of reflectance is large. The D+S analysis is in much better agreement with the measurements than the B(D+S) analysis. Semigray and gray B(D+S) calculations are as accurate as the spectral B(D+S) predictions.

5.2.3 Comparison of Measurements and Predictions on Overall (Average) Basis

The results presented in Tables 6 through 8 show that the agreement of measurements and analysis on spectral basis is qualitatively the same as on total basis. Hence the discussion which follows is only for the latter. All constant property models (UR, D, S, D+S) show better agreement with the measurements on overall basis than on local basis. The S analysis always over predicts the irradiation. For a specular enclosure or when surface 3 is diffuse and others specular, the S analysis predicts within 10 percent. However, with bidirectional surfaces in the enclosure, the S analysis for some cases predicts G^* too high by as much as 120 percent. In general, agreement of the D analysis with the measurements is better than that for the S analysis. In the worst case the D analysis is only 44 percent lower than the experiments, and this happens when all the surfaces are specular. For other cases the predictions are within 27 percent. The UR analysis yields equally good agreement with the experiments as the D analysis. Predictions with the D+S model are closer to the experiments than the S analysis, but the agreement is not as good as that of the D analysis. Like the S analysis, the D+S analysis also usually overpredicts the irradiation. Note that predictions of the D+S analysis do not always lie between those of the D and S analyses, but the departure is small.

TABLE 6

Overall Measured Irradiation and Fractional Departure from Experiment for Various Analyses on Spectral Basis, $\lambda = 3.08\mu$

					(Analysis-Experiment)/Experiment				
Surfaces 1-2-3	γ	T_1 °K	T_2 °K	G^*_{EXP}	UR	S	D	DP(S)	B(D+S)
S-S-S	1/6	284.8	594.1	2309	-0.21	-0.03	-0.21	0.09	
		284.3	752.9	9152	0.20	0.45	0.18	0.04	
	1/2	284.1	586.5	1003	-0.38	-0.07	0.73	-0.01	
		283.6	758.5	4323	0.00	0.51	-0.14	0.01	
S-S-D	1/6	283.4	588.0	1573	0.16	0.05	0.15	0.20	
		283.8	750.2	7002	0.58	0.42	0.56	0.03	
	1/2	283.5	590.1	586	0.15	-0.02	-0.01	0.03	
		283.1	754.9	2258	0.92	0.63	0.65	0.06	
S-S-B	1/6	283.7	593.4	1792	0.08	0.33	0.12		-0.02
		283.7	760.9	8662	0.40	0.71	0.45		-0.14
	1/2	283.7	759.5	3403	0.15	0.97	0.07		-0.04
S-B-S	1/6	284.0	596.6	1892	0.04	0.29	0.09		0.15
		284.8	758.6	6753	0.66	1.03	0.71		0.13
	1/2	283.9	594.1	997	-0.30	0.08	-0.41		-0.07
		284.7	755.5	3881	0.02	0.58	-0.14		-0.16
S-B-B	1/6	283.6	596.0	1952	0.03	0.27	0.07		0.10
		284.4	768.5	10087	0.22	0.50	0.27		-0.17
	1/2	283.9	592.8	583	0.17	0.82	-0.01		0.25
		284.4	758.5	2804	0.47	1.28	0.24		-0.16

TABLE 7

Overall Measured Irradiation and Fractional Departure from Experiment for Various Analyses on Spectral Basis, $\lambda = 4.51\mu$

					(Analysis-Experiment)/Experiment						
Surfaces 1-2-3	γ	T_1 °K	T_2 °K	G^*_{EXP}	UR	S	D	D+S	DP(S)	B(D+S)	DP(D+S)
S-S-S	1/6	286.6	596.4	110.5	0.01	0.24	0.01		0.11		
		284.8	757.0	381.2	0.07	0.30	0.06		0.17		
	1/2	285.9	586.2	41.2	-0.09	0.37	-0.22		0.14		
		284.2	758.6	170.9	-0.13	0.32	-0.25		0.10		
S-S-D	1/6	283.5	592.1	90.5	0.33	0.21	0.32		0.10		
		283.6	758.1	308.3	0.40	0.26	0.39		0.14		
	1/2	283.4	590.7	25.4	0.70	0.45	0.46		0.18		
S-S-B	1/6	283.7	598.7	125.6	0.01	0.25	0.06	-0.06		-0.19	-0.13
		283.7	754.3	392.9	0.07	0.32	0.11			-0.16	-0.10
	1/2	283.7	588.6	33.4	0.25	0.95	0.06	0.15		-0.11	-0.10
		283.7	751.8	116.8	0.17	0.99	0.08			-0.09	-0.08

TABLE 8

Overall Measured Irradiation and Fractional Departure from Experiment

for Various Analyses on Total Basis

					(Analysis-Experiment)/Experiment									
Surfaces 1-2-3	γ	T_1 °K	T_2 °K	G^*_{EXP}	UR	S	D	D+S	DP(S)	B(D+S)	$DP(S)_{SG}$	$DP(S)_G$	$DP(D+S)_{SG}$	$DP(D+S)_G$
S-S-S	1/6	284.2	597.3	9.64	-0.19	0.04	-0.14		-0.11			-0.08		
		285.2	761.9	28.71	-0.20	0.00	-0.18		-0.13		-0.11	-0.09		
	1/2	283.5	577.8	3.81	-0.36	-0.02	-0.43		-0.21			-0.20		
		284.6	746.8	11.77	-0.35	-0.01	-0.44		-0.20		-0.16	-0.18		
S-S-D	1/6	283.7	595.7	6.78	0.15	0.10	0.21		-0.03		0.00	0.00		
		283.6	756.8	19.80	0.16	0.07	0.18		-0.05		-0.02	-0.01		
	1/2	283.6	580.6	2.03	0.23	0.07	0.08		-0.16		-0.12	-0.05		
		284.2	752.9	6.41	0.25	0.07	0.08		-0.15		-0.11	-0.10		
S-S-B	1/6	283.8	594.4	7.39	0.04	0.36	0.15	0.06		-0.14				
		283.7	763.3	23.11	0.03	0.31	0.10	0.04		-0.20			-0.12	-0.11
	1/2	283.8	589.6	2.02	0.32	1.07	0.14	0.40		0.04				
		283.9	756.1	5.80	0.41	1.21	0.20	0.41		0.05			0.22	0.21
S-B-S	1/6	283.9	589.4	7.49	-0.01	0.28	0.09	0.07		-0.17				
		284.8	759.2	23.20	-0.01	0.25	0.05	0.03		-0.19			-0.10	-0.09
	1/2	284.8	755.4	9.40	-0.14	0.34	-0.27	0.12		-0.13			-0.09	-0.09
S-B-B	1/6	283.8	594.9	8.06	-0.04	0.25	0.06	-0.00		-0.20				
		284.3	758.2	22.77	0.00	0.28	0.07	-0.04		-0.20			-0.11	-0.10
	1/2	284.1	582.1	2.24	0.12	0.76	-0.03	0.18		-0.16				
		284.5	750.4	6.68	0.17	0.84	-0.00	0.17		-0.14			-0.05	-0.05

In contrast to the S and D+S analysis, the DP analysis usually underpredicts the irradiation. The reason for this has already been given in Section 5.2.1. Although the overall agreement of the DP analysis is better (within 20%) than that of the CP analysis, it does not offer any significant advantage over the appropriate CP analysis. Also, calculations with the nongray B(D+S) or DP(S) models do not yield better results than the corresponding semigray or gray analysis.

The spectral results given in Tables 6 and 7 support the above conclusions qualitatively, but quantitatively the agreement with the experiments is not as good as on total basis.

6. CONCLUSIONS AND RECOMMENDATIONS

As a result of the present analytical and experimental work on radiant heat exchange between simply arranged surfaces the following conclusions may be drawn.

1. Qualitative agreement of measurements and analyses for spectral and total results is the same. Quantitatively, total results show better agreement than the spectral results.
2. Analytical results indicate that the constant property diffuse and specular models do not yield the upper and lower bounds on local radiant heat flux.
3. Both constant property diffuse and specular models can fail badly. The specularity of the surfaces must be considered for more accurate predictions.
4. A diffuse surface in the enclosure appears to destroy the effect of specularity of the other surfaces. Constant property diffuse and specular (with surface 3 diffuse) analyses yield almost identical results.
5. In general, the constant property specular analysis yields higher values of irradiation than the constant property diffuse analysis.
6. When all the surfaces in the enclosure are specular the detailed nongray analysis has no advantage over the simpler semigray or gray analyses, provided that the directional effects are taken into account.
7. In general, the best agreement between analysis and the data is for the B(D+S) model. Assuming the incoherent component of energy to be reflected

diffusely provides appreciable simplicity. However, taking into account the spectral effects makes the computation rather tedious.

8. Semigray and gray analyses predict the irradiation reasonably well provided that the directional properties and the specularity of the surfaces are taken into account.
9. The greatest discrepancy between the data and the analyses occurs at locations which are irradiated at oblique angles. At some locations the experimental results are more than three times the magnitude of the diffuse analysis results and about two times the results from the DP analysis. It remains to be determined whether this discrepancy is due to the limitations of the analyses or the experiments.

The following conclusions can be drawn for evaluation of the overall (average) irradiation on total basis.

1. Calculation of the irradiation on a nongray basis does not yield improved results over the semigray or gray analyses.
2. The appropriate constant property models predict the irradiation reasonably well. The S analysis for a specular enclosure predicts the irradiation within four percent of the measurements. With one or more rough surfaces in the enclosure the D analysis predicts the irradiation within 27 percent and the D+S and UR analyses agree with the data to within 40 percent.
3. The constant property D+S analysis provides better overall agreement with the data than the constant property diffuse or specular analyses.
4. Results of the D+S analysis do not always lie between those of the D and S analyses, but the departure is small.

5. The uniform (UR) and nonuniform (D) radiosity diffuse models are in good agreement with each other (within 20 percent) and with the experimental data (within 45 percent).
6. Overall agreement of measurements and analyses is better for total than for spectral results.

The above conclusions are drawn from the limited results based on a particular combination of geometry, material and temperature levels. This configuration may not be representative of other types of enclosures. Therefore, care should be exercised in extending the results and conclusions to situations very much different from those studied here.

During the course of this research a number of problem areas have evolved. A few areas which need further investigation are briefly discussed below.

1. The gray DP(D+S) model with a direction-independent specular component has proved promising for specularly as well as for bidirectionally reflecting surfaces. This model should be verified for other types of enclosures.
2. More work should be done in determining the specular component of reflectance. Since the incoherently reflected energy is peaked in the specular direction, it appears realistic to assume that a part of this energy is reflected specularly.
3. A need exists for a simple experimental technique to measure the specular and diffuse component of directional reflectance if further studies prove the validity of the diffuse plus specular model. Realistically, the specular component should be larger than the coherent component. The specular component of reflectance can be assumed to be the energy reflected in the specular direction within an arbitrary solid angle.

4. The experimental work has indicated a need for a small thermal (spectral or total) radiation detector with a response independent of the direction or wavelength of the incident energy and with a sensitivity independent of the enclosure pressure.
5. In the present configuration the energy was exchanged in normal as well as oblique directions. Other geometrical arrangements where a surface is primarily irradiated either from some external source, such as a solar simulator or another surface at large angles of incidence relative to the surface normal, should be investigated.
6. The effect of secondary roughness and non-Gaussian roughness on the reflection distribution function should be explored. If this effect is significant, then the effects of surface preparation methods should be examined further.
7. It has been recommended [77] that the Monte Carlo method be used not only to predict the bidirectional reflectance for random surface models, but also to check the validity of the presently available theories. Investigations reported [44, 110] have proved promising, but further work needs to be done. Direct calculation of heat transfer by the Monte Carlo method may be more efficient as compared to first calculating the bidirectional reflectance and then predicting the heat transfer.
8. There is a great incentive to streamline the Monte Carlo method and make it more efficient and economical for engineering calculations. A prediction of the accuracy of the Monte Carlo method with various computational shortcuts is needed.

REFERENCES

1. P. Drude, "Bestimmung der optischen Constanten der Metalle," Ann. Phys. 64, 159 (1898) also available as Air Force Cambridge Research Laboratory Translation "Determination of the Optical Constants of Metals," March 1963, [AD 430 983].

2. E. Hagen, and H. Rubens, "Emissionsvermogen und electrische Leitfahigkeit der Metallegierungen," Verh. Deut. Phys. Ges. 6, 128 (1904).

3. S. Roberts, "Optical Properties of Copper," Phys. Rev. 118, 1509 (1960).

4. S. Roberts, "Optical Properties of Nickel and Tungsten and Their Interrelation According to Drude's Formula," Phys. Rev. 114, 104 (1960).

5. S. Roberts, "Interpretation of the Optical Properties of Metal Surfaces," Phys. Rev. 100, 1667 (1955).

6. G. E. H. Reuter, and E. H. Sondheimer, "The Theory of the Anomalous Skin Effect in Metals," Proc. Roy. Soc. London, Series A, 195, 336 (1948).

7. R. B. Dingle, "The Anomalous Skin Effect and the Reflectivity of Metals," Physica 19, 311, 348, 729 (1953).

8. H. E. Bennett and J. M. Bennett, "Validity of the Drude Theory," Optical Properties and Electronic Structure of Metals and Alloys," (F. Abeles, Editor), pp. 173-188, John Wiley and Sons, Inc., New York (1966).

9. G. A. W. Rutgers, "Temperature Radiation of Solids," Encyclopedia of Physics XXVI Light and Matter II, (Flügge, S., Editor), pp. 129-170, Spring-Verlag, Berlin (1958).

10. N. F. Mott, "The Electrical Conductivity of Transition Metals," Proc. Roy. Soc. London, Series A 153, 699 (1936).

11. J. R. Schronhorst, "The Emissivity and Emittance of Metallic Conductors," MSME Thesis, Purdue University (1962).

12. R. A. Seban, "The Emissivity of Transition Metals in the Infrared," Trans. ASME, Series C, J. Heat Transfer 87, 173 (1965).

13. D. K. Edwards and B. N. de Volo, "Useful Approximations for the Spectral and Total Emissivity of Smooth Bare Metals," Advances in Thermophysical Properties at Extreme Temperatures and Pressures (S. Gratch, Editor), pp. 174-188, ASME, New York (1965).

14. R. B. Dingle, "The Anomalous Skin Effect and the Reflectivity of Metals, I. Theory," Physica 19, 311 (1953); and II. "Comparison between Theoretical and Experimental Optical Properties," Physica 19, 348 (1953).

15. T. Holstein, "Optical and Infrared Reflectivity of Metals at Low Temperatures," Phys. Rev. 88, 1427 (1952).

16. Y. S. Touloukian and D. P. DeWitt, "Thermal Radiation Properties —Metallic Elements and Alloys," Thermophysical Properties of Matter, Vol. 7, Plenum Press, New York (1970).

17. A. F. Houchens, and R. G. Hering, "Real Surface Effects on Radiative Heat Transfer," Technical Report No. ME-TR-661-1, Department of Mechanical and Industrial Engineering, University of Illinois (1970).

18. S. Katzoff, (Editor), Symposium on Thermal Radiation of Solids, NASA SP-55 (1965).

19. D. K. Edwards, "Radiative Transfer Characteristics of Materials," Trans. ASME, Series C, J. Heat Transfer 91, 1 (1969).

20. B. A. Khrustalev, "Radiative Properties of Solids," Heat Transfer —Soviet Research 2, 149 (1970).

21. R. Rolling, "Effect of Surface Roughness on the Spectral and Total Emittance of Platinum," Progress in Aeronautics and Astronautics, Vol. 20, pp. 91-114, Academic Press, New York (1967).

22. D. K. Edwards and I. Catton, "Radiation Characteristics of Rough and Oxidized Metals," Advances in Thermophysical Properties at Extreme Temperatures and Pressures (S. Gratch, Editor), pp. 189-199, ASME, New York (1965).

23. H. E. Bennett, "Influence of Surface Roughness, Surface Damage, and Oxide Films on Emittance," pp. 145-152 in Reference [18].

24. R. C. Birkebak, J. P. Dawson, B. A. McCullough and B. E. Wood, "Hemispherical Reflectance of Metal Surfaces as a Function of Wavelength and Surface Roughness," Int. J. Heat Mass Transfer 10, 1225 (1967).

25. R. C. Birkebak, E. M. Sparrow, E. R. G. Eckert and J. W. Ramsey, "Effect of Surface Roughness on the Total Hemispherical and Specular Reflectance of Metallic Surfaces," Trans. ASME, Series C, J. Heat Transfer 86, 193 (1964).

26. H. J. Keegan, J. C. Schleter, and V. R. Weidner, "Effect of Surface Texture on Diffuse Spectral Reflectance," pp. 165-177 in Reference [18].

27. D. A. Russell, "The Spectral Reflection of Rough Surfaces in the Infrared," MSME Thesis, University of California, Berkeley, California (1961).

28. L. M. Herold and D. K. Edwards, "Bidirectional Reflectance Characteristics of Rough, Sintered Metal, and Wire Screen Surface Systems," AIAA J. 4, 1802 (1966).

29. B. Shyffer, "An Investigation of the Effect of Surface Roughness on Reflectance," MS Thesis, Department of Engineering, University of California, Los Angeles (1963).

30. K. E. Torrance, and E. M. Sparrow, "Directional Emittance of an Electric Nonconductor as a Function of Surface Roughness and Wavelength," Int. J. Heat Mass Transfer 10, 1708 (1967).

31. R. G. Siegfried and R. C. Birkebak, "A Comparative Study of the Total Directional Emittance of a Dielectric and a Metal as a Function of Surface Roughness," AIAA Paper No. 68-778.

32. K. E. Torrance, and E. M. Sparrow, "Off Specular Peaks in the Directional Distribution of Reflected Thermal Radiation," Trans. ASME, Series C, J. Heat Transfer 87, 223 (1966).

33. A. F. Houchens and R. G. Hering, "Bidirectional Reflectance of Rough Metal Surfaces," Progress in Aeronautics and Astronautics, Vol. 20, pp. 65-90, Academic Press, New York (1967).

34. H. Davies, "The Reflection of Electromagnetic Waves from a Rough Surface," Proc. Inst. Elec. Eng., Pt. III, 101, 209 (1954).

35. P. Beckmann, and A. Spizzichino, The Scattering of Electromagnetic Waves from Rough Surfaces, Macmillan Company, New York (1963).

36. R. C. Birkebak, and E. R. G. Eckert, "Effects of Roughness of Metal Surfaces on Angular Distribution of Monochromatic Reflected Radiation," Trans. ASME, Series C, J. Heat Transfer 87, 85 (1965).

37. T. F. Smith and R. G. Hering, "Comparison of Bidirectional Reflectance Measurements and Model for Rough Metallic Surfaces," Proceedings of the Fifth Symposium on Thermophysical Properties (C. F. Bonilla, Editor), pp. 429-435, ASME, New York (1970).

38. T. J. Love and R. E. Francis, "Experimental Determination of Reflectance Function for Type 302 Stainless Steel," Progress in Aeronautics and Astronautics, Vol. 20, pp. 115-135, Academic Press, New York (1967).

39. J. S. Toor, R. Viskanta and E. R. F. Winter, "Radiant Heat Transfer Between Simply Arranged Surfaces with Direction Dependent Properties," AIAA Paper No. 69-624.

40. G. I. Pokrowski, "Zur Theorie der Diffusion Lichtreflexion," Z. Phys., Part I: 30, 66 (1924), Part II: 35, 34 (1925), Part III: 35, 390 (1926), Part IV: 36, 472 (1926).

41. H. Schulz, "Untersuchungen über die Reflexion an teilweise lichtzerstreuenden Flächen," Z. Phys. 31, 496 (1925).

42. W. E. K. Middleton, and A. G. Mungal, "The Luminous Directional Reflectance of Snow," J. Opt. Soc. Amer. 52, 572 (1952).

43. C. H. Treat, and M. W. Wildin, "Investigation of a Model for Bidirectional Reflectance of Rough Surfaces," AIAA Paper No. 69-64.

44. D. C. Look and T. J. Love, "Investigation of the Effects of Surface Roughness upon Reflectance," Progress in Aeronautics and Astronautics, Vol. 24, pp. 123-142, MIT Press, Cambridge, Massachusetts (1971).

45. K. E. Torrance, and E. M. Sparrow, "Biangular Reflectance of an Electric Non-Conductor as a Function of Wavelength and Surface Roughness," Trans. ASME, Series C, J. Heat Transfer 87, 283 (1965).

46. E. M. Sparrow, and S. L. Lin, "Radiation Heat Transfer at a Surface Having both Specular and Diffuse Reflectance Components," Int. J. Heat Mass Transfer 8, 769 (1965).

47. L. F. Daws, "The Emissivity of a Groove," Brit. J. Appl. Phys. 5, 182 (1954).

48. J. Psarouthakis, "Apparent Thermal Emissivity from Surfaces with Multiple V-Shaped Grooves," AIAA J. 1, 1879 (1963).

49. G. A. McCue, "A Note Concerning the Effective Emittance of Certain Grooved Surfaces," AIAA J. 7. 721 (1966).

50. Y. G. Zhulev, "Radiative Power of a Toothed Surface," High Temp. 3, 288 (1965).

51. O. W. Clausen and J. T. Neu, "The Use of Directionally Dependent Radiation Properties for Spacecraft Thermal Control," Astronaut. Acta 11, 328 (1965).

52. R. B. Zipin, "A Preliminary Investigation of the Bidirectional Spectral Reflectance of V-Grooved Surfaces," Appl. Opt. 5, 1954 (1966).

53. R. B. Zipin, "The Apparent Thermal Radiation Properties of an Isothermal V-Groove with Specularly Reflecting Walls," J. Res. Nat. Bur. Stand., Sect. C 70, 275 (1966).

54. M. Perlmutter, and J. R. Howell, "A Strongly Directional Emitting and Absorbing Surface," Trans. ASME, Series C, J. Heat Transfer 85, 282 (1963).

55. W. Z. Black, and R. J. Schoenhals, "A Study of Directional Radiation Properties of Specially Prepared V-Groove Cavities," Trans. ASME, Series C, J. Heat Transfer 90, 420 (1968).

56. J. R. Howell, and M. Perlmutter, "Directional Behavior of Emitted and Reflected Radiant Energy from a Specular, Gray Asymmetric Groove," NASA TN D-1874 (1963).

57. M. Perlmutter and J. R. Howell, "Angular Distribution of Emitted and Reflected Radiant Energy from Diffuse Gray Asymmetric Grooves," NASA TN D-1987 (1963).

58. R. G. Hering and T. F. Smith, "Apparent Radiation Properties of a Rough Surface," AIAA Paper No. 69-622.

59. H. F. Nelson and R. Goulard, "Reflection from Periodic Dielectric Surfaces," J. Opt. Soc. Amer. 57, 769 (1967).

60. E. Lax and M. Pirani, "Temperaturstrahlung Fester Körper," Hanbuch der Physik, Vol. 21, pp. 190-272, Springer Verlag, Berlin (1929).

61. D. K. Edwards and R. D. Tobin, "Effect of Polarization on Radiant Heat Transfer Through Long Passages," Trans. ASME, Series C, J. Heat Transfer 89, 132 (1967).

62. E. M. Sparrow and R. D. Cess, Radiation Heat Transfer, Brooks/Cole Publishing Company, Belmont California (1969).

63. E. M. Sparrow, "On the Calculation of Radiant Interchange Between Surfaces," Modern Developments in Heat Transfer (W. E. Ibele, Editor), pp. 181-212, Academic Press, New York (1963).

64. E. R. G. Eckert and E. M. Sparrow, "Radiative Heat Exchange Between Surfaces with Specular Reflection," Int. J. Heat Mass Transfer 84, 294 (1962).

65. E. M. Sparrow, E. R. G. Eckert and V. K. Jonsson, "An Enclosure Theory for Radiative Exchange Between Specularly and Diffusely Reflecting Surfaces," Trans. ASME, Series C, J. Heat Transfer 84, 294 (1962).

66. S. H. Lin and E. M. Sparrow, "Radiant Interchange Among Curved Specularly Reflecting Surfaces: Application to Cylindrical and Conical Cavities," Trans. ASME, Series C, J. Heat Transfer 87, 299 (1965).

67. B. Munch, "Directional Distribution in the Reflection of Heat Radiation and Its Effect on Heat Transfer," NASA TT F-497 (1968).

68. R. A. Seban, Discussion on Reference [65].

69. A. F. Sarofim and H. C. Hottel, "Radiative Exchange Among Non-Lambert Surfaces," Trans. ASME, Series C, J. Heat Transfer 88, 37 (1966).

70. J. R. Schornhorst and R. Viskanta, "Effect of Direction and Wavelength Dependent Surface Properties on Radiant Heat Transfer," AIAA J. 6, 1450 (1968).

71. P. M. Engstrom, R. Viskanta and J. S. Toor, "Study of Radiation Interchange in an Enclosure Consisting of Plane Isothermal and Adiabatic Surfaces," Wärme-und Stoffübertragung 3, 63 (1970).

72. J. S. Toor and R. Viskanta, "A Numerical Experiment on Radiant Heat Interchange by the Monte Carlo Method," Int. J. Heat Mass Transfer 11, 883 (1968).

73. G. K. Kholopov, "Calculation of Emissivities of Non-Diffuse Cavity-Type Sources," Sov. J. Opt. Technol. 35, 1 (1968).

74. B. M. Golubitskiy, R. U. Gimatutdinova, M. V. Tantashev and G. K. Kholopov, "The Use of the Monte Carlo Method for Calculating the Degree of Blackness of Cavities," Sov. J. Opt. Technol. 37, 296 (1970).

75. J. R. Schornhorst and R. Viskanta, "An Experimental Examination of the Validity of the Commonly Used Methods of Radiant Heat Transfer Analysis," Trans. ASME, Series C, J. Heat Transfer 90, 429 (1968).

76. J. S. Toor and R. Viskanta, "Effect of Direction Dependent Properties of Radiation Interchange," J. Spacecraft Rockets 5, 742 (1968).

77. J. S. Toor, "Radiant Heat Transfer Analysis Among Surfaces Having Direction Dependent Properties by the Monte Carlo Method," MSME Thesis, Purdue University (1967).

78. J. T. Bevans and D. K. Edwards, "Radiation Exchange in an Enclosure with Directional Wall Properties," Trans. ASME, Series C, J. Heat Transfer 87, 388 (1965).

79. S. Goodman, "Radiant Heat Transfer Between Non-Gray Parallel Plates," J. Res. Nat. Bur. Stand. 58, 37 (1957).

80. J. R. Branstetter, "Formulas for Radiant Heat Transfer Between Nongray Parallel Plates of Polished Refractory Metals," NASA TN D-2902 (1965).

81. V. E. Holt, R. J. Grosh and R. Geynet, "Evaluation of Net Radiant Heat Transfer Between Specularly Reflecting Plates," The Bell System Technical J. 41, 1865 (1962).

82. J. R. Howell, "Application of Monte Carlo to Heat Transfer Problems," Advances in Heat Transfer (T. J. Irvine and J. P. Hartnett, Editors), Vol. 5, pp. 1-54, Academic Press, New York (1968).

83. J. T. Bevans, et al., "Prediction of Space Vehicle Thermal Characteristics," Air Force Flight Dynamics Laboratory Technical Report AFFDL-TR 65-139 (1965).

84. K. Elser, "Experimentalle Untersuchung des Strahlungsauatausches zwischen excentrischen Kugelflachen," Institut für Thermodynamik und Verbrennungsmotorebau an der Eidgenossischen Technischen Hochschule in Zurich, Bericht Nr. 205 (1949).

85. T. J. Love and J. S. Gilbert, "Experimental Study of Radiant Heat Transfer Between Parallel Plates," Aerospace Research Laboratories Report ARL 66-0103 (1966).

86. K. Zapf, "Visibility of the LEM with Various Background Luminances," E-1901, Instrumentation Laboratory, Massachusetts Institute of Technology, Cambridge, Mass.

87. J. T. Neu and R. S. Dummer, "Theoretical and Practical Implication of the Bidirectional Reflectance of Spacecraft Surfaces," AIAA J. 7, 484 (1969).

88. J. R. Howell and R. E. Durkee, "Comparison of Analysis and Experiment for Radiative Transfer Between Surfaces with Collimated Incident Radiation," ASME Paper No. 70-HT/SpT-23.

89. W. Z. Black and R. J. Schoenhals, "An Experimental Study of Radiation Heat Transfer from Parallel Plates with Direction-Dependent Properties," Trans. ASME, Series C, J. Heat Transfer 92, 610 (1970).

90. J. S. Toor, R. Viskanta and E. R. F. Winter, "Effects of Polarization on Radiant Heat Interchange Between Simply Arranged Surfaces," AIAA J. 8, 981 (1970).

91. M. Born and E. Wolf, Principles of Optics, Second Edition, Pergamon Press, Oxford (1964).

92. D. K. Edwards and J. T. Bevans, "Effect of Polarization on Spacecraft Radiation Heat Transfer," AIAA J. 3. 1323 (1965).

93. H. J. Nicholas, "Absolute Methods of Reflectometry," J. Res. Nat. Bur. Stand. 1, 29 (1928).

94. G. L. Polyak, "Radiative Transfer Between Surfaces of Arbitrary Spatial Distribution of Reflection," Convective and Radiative Heat Tranfer, pp. 118-31, Academy of Sciences USSR, Moscow, (1960); Translation TT-9, School of Aeronautical and Engineering Sciences, Purdue University.

95. T. J. Love, Radiation Heat Transfer, Charles E. Merrill Publishing Co., Columbus, Ohio (1968).

96. R. P. Bobco, "Analytical Determination of Radiation Interchange Factors," Hughes Aircraft Company, Space Systems Division (1968).

97. R. G. Hering, "Radiative Heat Exchange Between Specularly Reflecting Surfaces with Direction Dependent Properties," Proceedings of the Third International Heat Transfer Conference, Vol. 5, pp. 200-206, AIChE, New York (1966).

98. F. B. Hildebrand, Methods of Applied Mathematics, Prentice-Hall, Inc., Englewood Cliffs, New Jersey (1952).

99. L. Fox, An Introduction to Numerical Linear Algebra, Oxford University Press, New York (1964).

100. Y. P. Chang and V. J. Lunardini, "A Rapid Iteration Method for Radiant Heat Exchange," Trans. ASME, Series C, J. Heat Transfer 91, 581 (1969).

101. A. M. Herbert, Symposium on Monte Carlo Methods, John Wiley and Sons, Inc., New York (1956).

102. B. Gebhart, Heat Transfer, McGraw-Hill, New York (1961).

103. R. L. Merriam, "A Study of Radiative Characteristics of Condensed Gas Deposits on Cold Surfaces," Ph.D. Thesis, Purdue University (1968).

104. McGraw Hill Encyclopedia of Science and Technology, Vol. 12 (1960).

105. "Surface Texture, Surface Measurement and the American Standard ASA B46.1-1962," Technical Bulletin on Surface Texture, Bendix Industrial Metrology Division.

106. W. R. Wade and W. S. Slemp, "Measurements of Total Emittance of Several Refractory Oxides, Cements, and Ceramics for Temperatures from 600°F to 2000°F," NASA TN D-998 (1961).

107. D. L. Stierwalt, "Infrared Spectral Emittance Measurements of Optical Materials," App. Opt. 5, 1911 (1966).

108. "Optical Product Bulletin 28-2," Reflective Products Division 3M Co., Litho (1968).

109. H. E. Bennett, Discussion on "Theoretical and Experimental Studies of the Total Emittance of Metals," by W. J. Parker and G. L. Abbott, pp. 11-28, in Reference [18].

110. R. P. Heinisch and T. S. Chou, "Numerical Experiments in Modeling Diffraction Phenomena," Applied Optics (Submitted for Publication).

111. J. R. Schornhorst, "An Analytical and Experimental Investigation of Radiant Heat Transfer Between Simply Arranged Surfaces," Ph.D. Thesis, Purdue University (1970).

112. "Effects of the Variation of Angle of Incidence and Temperature on Infrared Filter Characteristics," Technical Report, Optical Coating Laboratory, Inc., Santa Rosa, California (1967).

APPENDIX A

SPECULAR COMPONENT OF REFLECTIVITY

For predictions of radiation quantities of interest in an enclosure with some simplified models the specular component of reflectivity over a surface is assumed to be constant. However, in the literature there is no method which incorporates the spectral, directional, roughness and configuration effects for calculating this component. In this appendix the influence of various parameters on the specular component of reflectivity is discussed and expressions are derived for its evaluation.

By definition the overall (averaged over a surface) specular component $\bar{R}$ is written as

$$\bar{R}=\frac{\int_A\int_{\lambda_1}^{\lambda_2}\int_{\phi_1'}^{\phi_2'}\int_{\theta_1'}^{\theta_2'} I_\lambda'(\theta',\phi',\vec{r})\rho_\lambda(\theta')g(\theta',\sigma/\lambda)\cos\theta'\sin\theta'd\theta'd\phi'd\lambda dA}{\int_A\int_{\lambda_1}^{\lambda_2}\int_{\phi_1'}^{\phi_2'}\int_{\theta_1'}^{\theta_2'} I_\lambda'(\theta',\phi',\vec{r})\rho_\lambda(\theta')\cos\theta'\sin\theta'd\theta'd\phi'd\lambda dA} \qquad (A\cdot1)$$

The surface is assumed to be isotropic and to have uniform properties over the area A. It is clear that in general the local specular component $R(\vec{r})$ (Eq. (A·1) without the integral over area A) will vary with location $\vec{r}$ because, in most of the practical problems, the spectral and directional distribution of the incident energy varies with position; also because the reflectance of a surface is dependent on direction and wavelength.

If the incident radiation field is known, then $\bar{R}$ can be evaluated without any difficulty. The purpose of the present discussion is to investigate how to best approximate $\bar{R}$ from the known variables such as the spectral directional emittance, the surface roughness, the prescribed temperatures and the geometry of the enclosure.

For the purpose of discussion the remainder of this appendix is divided into two parts. In the first part the influence of various parameters on the terms or group of terms appearing in Eq. (A·1) is examined. In the second part some approximations are made which reduce Eq. (A·1) to a workable form from which overall (area averaged) specular component of reflectivity can be calculated. An illustrative example is also given at the end.

Influence of Various Parameters on Specular Component of Reflectivity

Before any approximations can be made to simplify Eq. (A·1), it is necessary to examine the influence of various parameters on the terms appearing in Eq. (A·1). Evaluation of $g(\theta',\sigma/\lambda)$ and the product $g(\theta',\sigma/\lambda)\rho_\lambda(\theta')/\rho_\lambda$ for several values of the parameter σ/λ, where $\rho_\lambda(\theta')$ was predicted from Drude's model for gold, yielded almost the same results for values of the angle θ' from 0° up to 80°. This is due to the fact that the reflectivity of gold is high and the percentage change of $\rho_\lambda(\theta')$ with θ' is small. Both of the evaluated quantities (mentioned above) showed a strong dependence on θ' and σ/λ. For some values of σ/λ, $g(\theta',\sigma/\lambda)$ is plotted in Figure A-1.

The effect of the directional variation of the spectral incident intensity on the local specular component was investigated for a perfectly reflecting material as well as gold. The expression evaluated was

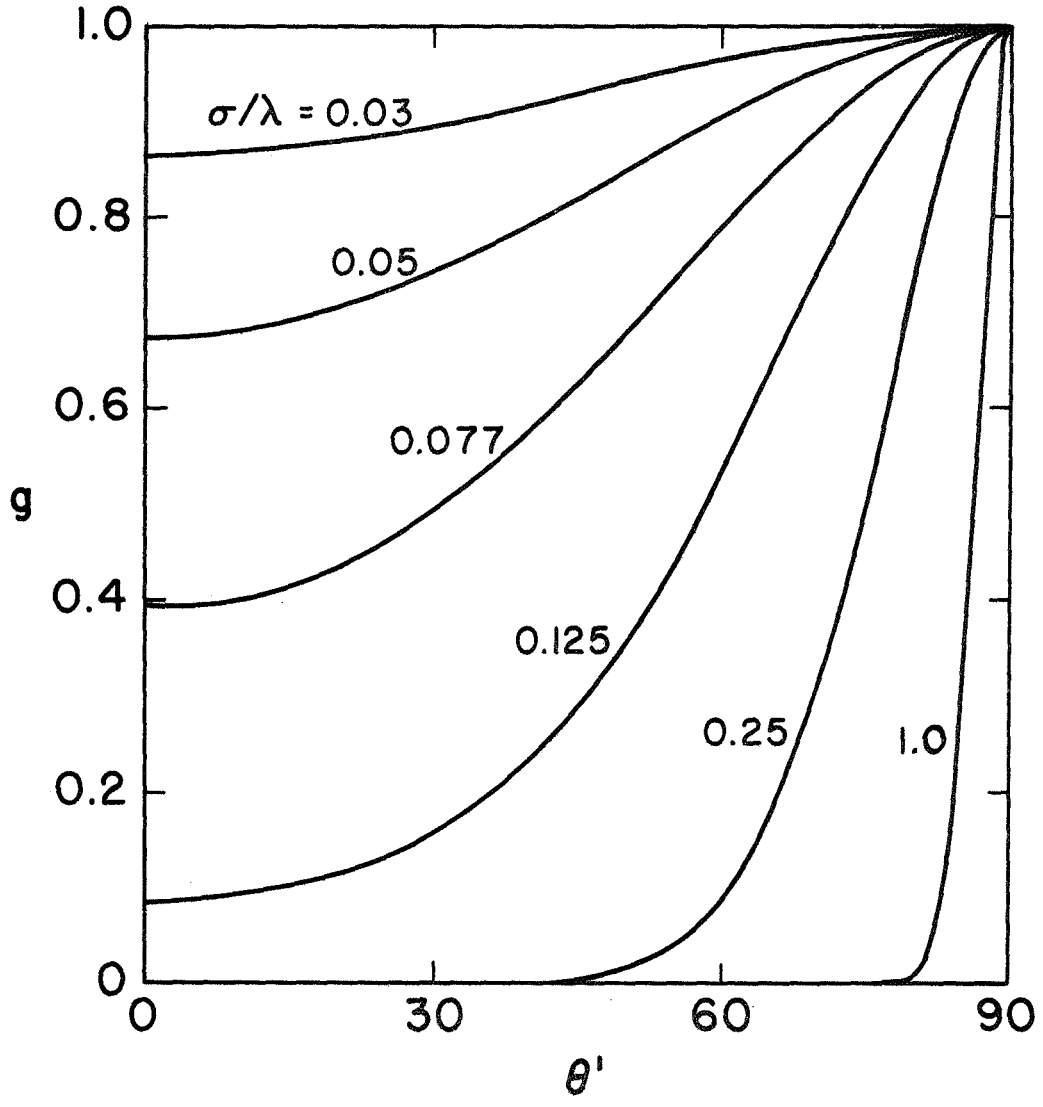

Figure A-1. Specular Component of Reflectivity of Spectral Intensity for a Perfectly Reflecting Material.

$$R_{\lambda\infty}(\theta_1'\to\theta_2') = \frac{\int_{\theta_1'}^{\theta_2'} I_\lambda'(\theta')\rho_\lambda(\theta')g(\theta',\sigma/\lambda)\cos\theta'\sin\theta'd\theta'}{\int_{\theta_1'}^{\theta_2'} I_\lambda'(\theta')\rho_\lambda(\theta')\cos\theta'\sin\theta'd\theta'} \qquad (A\cdot2)$$

where in one case $\theta_1' = 0$ and in the second case $\theta_2' = 0$. The other angle varies from 0 to $\pi/2$. The results are presented in Figure A-2 only for perfectly reflecting material and for θ_2' varying from 0 to $\pi/2$. The variation of I' with θ' is noted on the figure. Comparison of all the results showed that the specular component of reflectivity is a very weak function of the spectral as well as the directional reflectivity. Examination of Figure A-2 shows that the variation of the incident intensity with angle does not have large effect on the specular component of reflectivity.

In view of the above discussion, if I' and ρ are assumed to be independent of direction then Eq. (A·2) reduces to

$$R_{\lambda\infty}(\theta_1'\to\theta_2') = \frac{\int_{\theta_1'}^{\theta_2'} g(\theta',\sigma/\lambda)\cos\theta'\sin\theta'd\theta'}{\int_{\theta_1'}^{\theta_2'} \cos\theta'\sin\theta'd\theta'} \qquad (A\cdot3)$$

This equation can readily be integrated and yields

$$R_{\lambda\infty}(\theta_1'\to\theta_2') = \frac{\frac{1}{2a}\left[e^{-a\cos^2\theta_2'} - e^{-a\cos^2\theta_1'}\right]}{\frac{1}{2}\left[\cos^2\theta_1' - \cos^2\theta_2'\right]} \qquad (A\cdot4)$$

where $a = [4\pi(\sigma/\lambda)]^2$. For limits of integration $\theta_1' = 0$, $\theta_2' = \pi/2$ in Eq. (A·3),

$$R_{\lambda\infty}(0\to\pi/2) = (1-e^{-a})/a \qquad (A\cdot5)$$

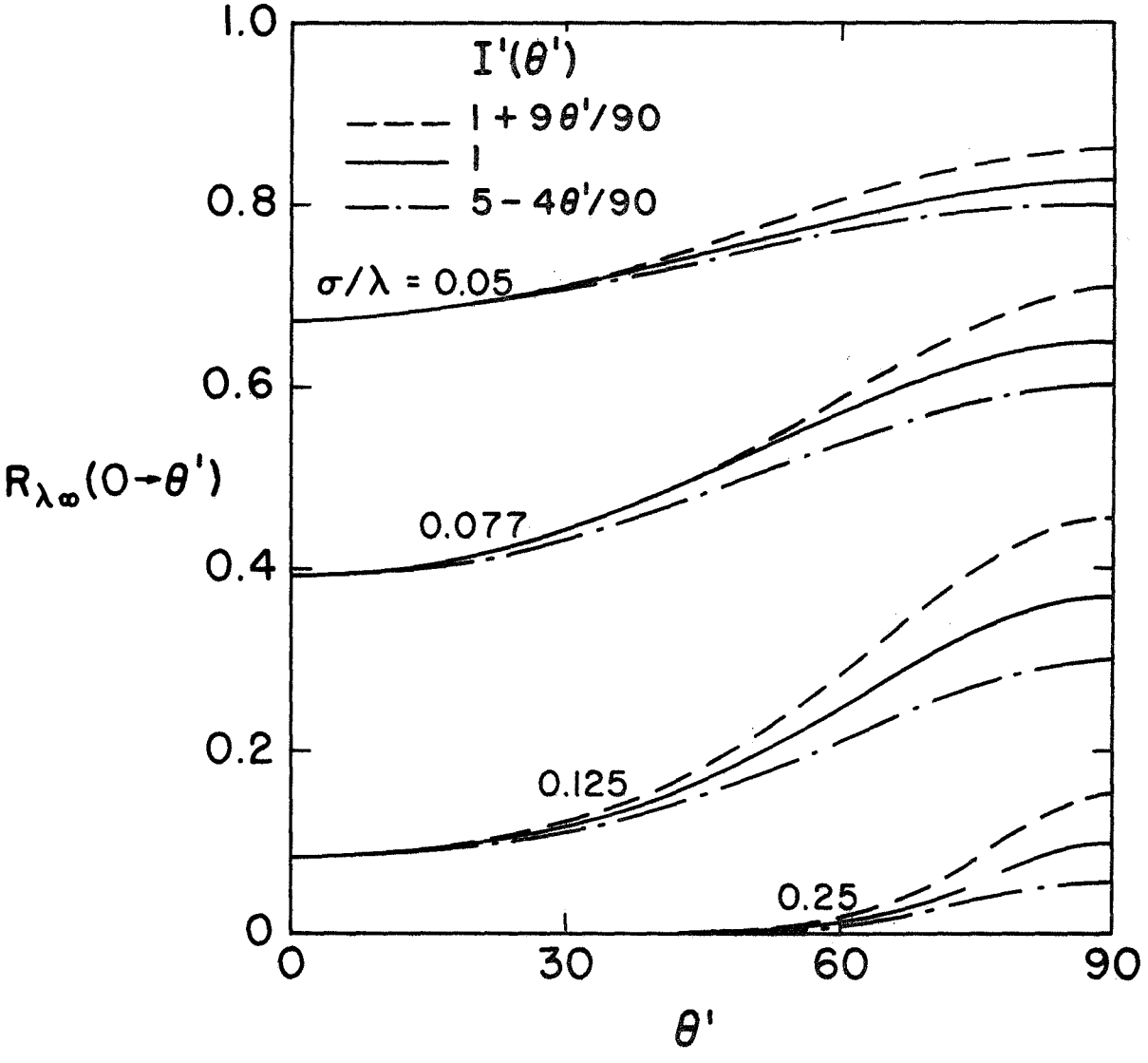

Figure A-2. Effect of Directional Variation of Spectral Intensity on the Specular Component of Reflectivity for a Perfectly Reflecting Material, Eq. (A·2).

Equation (A·4) yields the specular component only for a particular value of optical roughness σ/λ. If the incident intensity is uniformly distributed over the wavelength interval from λ_1 to λ_2, the corresponding specular component can be calculated by integrating Eq. (A·4) over this wavelength interval. Integration of the first term yields

$$\int_{\lambda_1}^{\lambda_2} \frac{1}{2a} e^{-a\cos^2\theta'_2} d\lambda = \frac{1}{2(4\pi\sigma)^2}(-b^{3/2})\left[\frac{e^{-b/\lambda_1^2}}{3\,\frac{b^{3/2}}{\lambda_1^3}} - \frac{e^{-b/\lambda_2^2}}{3\,\frac{b^{3/2}}{\lambda_2^3}} - \frac{2}{3}\left\{\frac{e^{-b/\lambda_1^2}}{\frac{\sqrt{b}}{\lambda_1}} - \frac{e^{-b/\lambda_2^2}}{\frac{\sqrt{b}}{\lambda_2}} - \left(\sqrt{\pi}\ \mathrm{erf}\ \frac{\sqrt{b}}{\lambda_2} - \sqrt{\pi}\ \mathrm{erf}\ \frac{\sqrt{b}}{\lambda_1}\right)\right\}\right] \qquad (A\cdot6)$$

where $b = (4\pi\sigma\cos\theta')^2$. The second term can be written similarly.

The discussion so far has been limited only to the directional effects. The combined spectral and directional effects were investigated in a similar way. Incident intensity was assumed to have a spectral black body distribution at temperatures ranging from 280°K to 760°K (range of temperature in this study). The directional variation of this intensity was assumed the same as is noted in Figure A-2. The following expressions were evaluated:

$$\rho_\infty^s = \frac{\int_0^\infty I'_{b\lambda}(T)g(\theta',\sigma/\lambda)d\lambda}{\int_0^\infty I_{b\lambda}(T)d\lambda} \qquad (A\cdot7)$$

$$R_\infty(0\to\theta') = \frac{\int_0^{\theta'}\int_0^\infty I'_{b\lambda}(T,\theta')g(\theta',\sigma/\lambda)\cos\theta'\sin\theta' d\lambda d\theta'}{\int_0^{\theta'}\int_0^\infty I'_{b\lambda}(T,\theta')\cos\theta'\sin\theta' d\lambda d\theta'} \qquad (A\cdot8)$$

The results from Eq. (A·7) are plotted in Figure A-3. Comparison of all the above mentioned results showed that for the calculation of the specular component of reflectivity the spectral and directional effects appearing in the function $g(\theta',\sigma/\lambda)$ are most important. However, these conclusions should be used with caution for other situations where surfaces may show quite a strong dependence of radiation characteristics on wavelength and direction.

Approximations for Calculating Overall Specular Component of Reflectivity

In practical situations neither is ϕ' independent of θ' nor does the spectral distribution of intensity correspond to a definite temperature, as was assumed in the previous discussion. The former is dependent purely on the configuration studied while the latter depends not only on the system but also on the temperature, roughness and radiation characteristics. The surfaces are usually at different temperatures and, due to unequal spectral emission, absorption and roughnesses of the surfaces, the spectral distribution of energy does not correspond to any weighted mean of blackbody emission corresponding to the surface temperatures. However the intent here is to approximate the spectral distribution in some gross manner so that the specular component of reflectivity can be calculated in a simple way.

If in Eq. (A·1) the incident intensity I' is written as the intensity leaving some other part of the enclosures, then $\bar{R}_i$ can be expressed as

$$\bar{R}_i = \frac{\int_0^\infty \sum_{j=1}^{n} \int_{A_i}\int_{A_j} I_{j\lambda}(\theta,\phi,\vec{r})\rho_{i\lambda}(\theta')g_i(\theta',\sigma/\lambda)K_{ij}\,dA_j\,dA_i\,d\lambda}{\int_0^\infty \sum_{j=1}^{n} \int_{A_i}\int_{A_j} I_{j\lambda}(\theta,\phi,\vec{r})\rho_{i\lambda}(\theta')K_{ij}\,dA_j\,dA_i\,d\lambda} \quad (A\cdot 9)$$

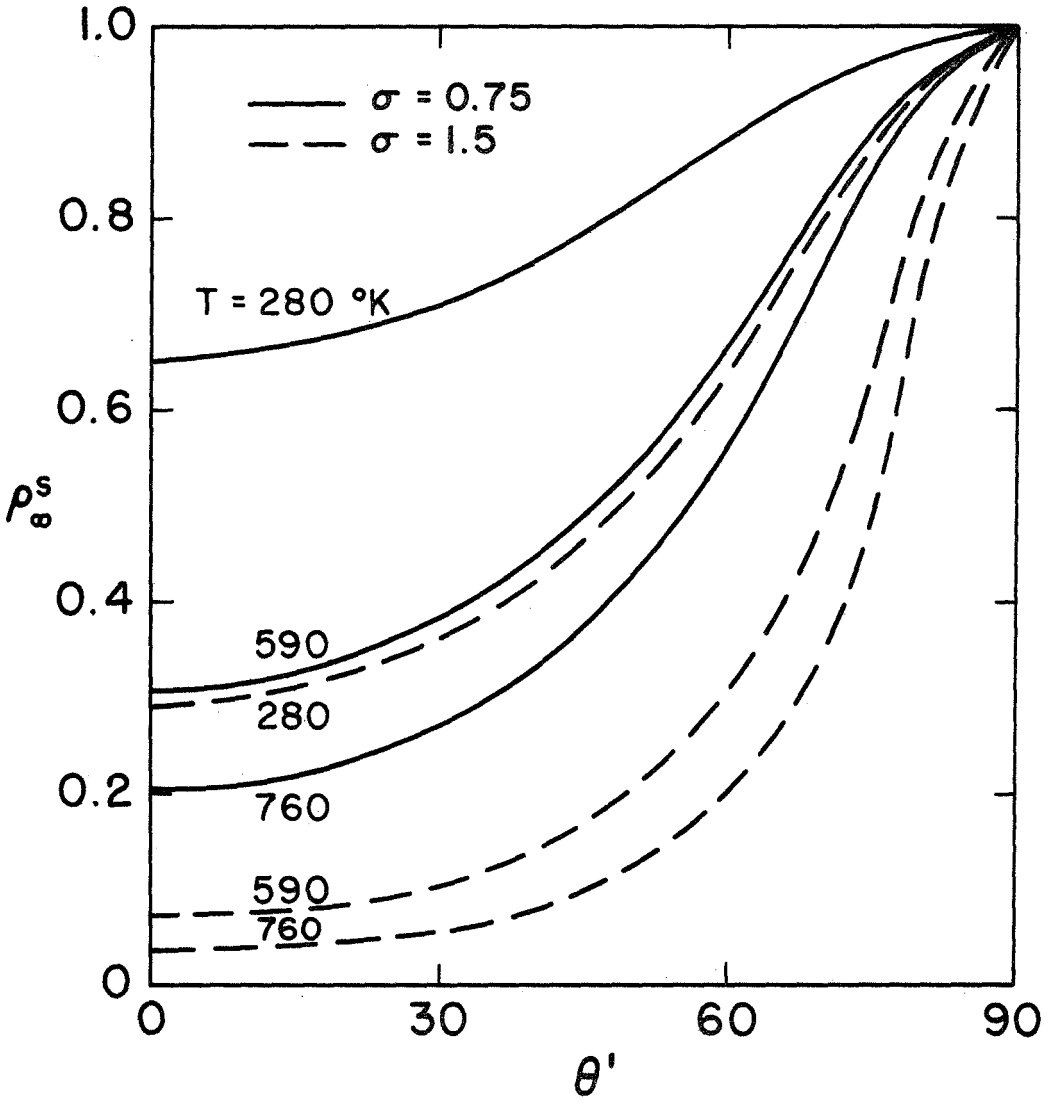

Figure A-3. Specular Component of Reflectivity of Blackbody Intensity for a Perfectly Reflecting Material, Eq. (A·7).

Approximating the intensity I_j as the sum of the emitted and some mean reflected intensity, the above equation becomes

$$\bar{R}_i = \frac{\int_0^\infty \sum_{j=1}^{n} \int_{A_i}\int_{A_j} [\varepsilon_{j\lambda}(\theta) I_{bj\lambda} + \rho_{j\lambda}(\theta') D_{j\lambda}] \rho_{i\lambda}(\theta') g_i(\theta', \sigma/\lambda) K_{ij} dA_j dA_i d\lambda}{\int_0^\infty \sum_{j=1}^{n} \int_{A_i}\int_{A_j} [\varepsilon_{j\lambda}(\theta) I_{bj\lambda} + \rho_{j\lambda}(\theta') D_{j\lambda}] \rho_{i\lambda}(\theta') K_{ij} dA_j dA_i d\lambda} \tag{A·10}$$

where, following Bevans and Edwards [78], $D_{j\lambda}$ represents the mean intensity of the irradiation of the surface j by the surrounding surfaces.

If one term in the bracket in Eq. (A·10) is small compared to the other it can be neglected. For example, the second term can be neglected when the emission from surface j is high and the reflectivity is small.

Introducing geometrical thermal radiation characteristics [78]

$$\int_{A_i}\int_{A_j} \varepsilon_{j\lambda}(\theta) g_i(\theta', \sigma/\lambda) \rho_{i\lambda}(\theta') K_{ij} dA_j dA_i = [\varepsilon_{ji\lambda} g_{ij\lambda} \rho_{ij\lambda}] \pi A_i F_{ij} \tag{A·11}$$

and dropping D_j from Eq. (A·10) gives

$$\bar{R}_i = \frac{\int_0^\infty \sum_{j=1}^{n} I_{bj\lambda} [\varepsilon_{ji\lambda} g_{ij\lambda} \rho_{ij\lambda}] F_{ij} d\lambda}{\int_0^\infty \sum_{j=1}^{n} I_{bj\lambda} [\varepsilon_{ji\lambda} \rho_{ij\lambda}] F_{ij} d\lambda} \tag{A·12}$$

In practical problems it is convenient to evaluate these characteristics at some mean value of the angles. If the surfaces are large and this assumption is poor, the surfaces may be further subdivided.

Assuming ρ to be independent of θ and λ, and evaluating ε and g at some mean angles θ_{ji} (the angle made by normal to A_j with a line joining A_j and A_i), the above equation becomes

$$\bar{R}_i = \frac{\sum_{j=1}^{n} F_{ij} \int_0^\infty \varepsilon_{j\lambda}(\theta_{ji}) E_{bj\lambda} g_i(\theta'_{ij}, \sigma/\lambda) d\lambda}{\sum_{j=1}^{n} F_{ij} \int_0^\infty \varepsilon_{j\lambda}(\theta_{ji}) E_{bj\lambda} d\lambda} \qquad (A\cdot13)$$

For ε independent of θ Eq. (A·13) can be expressed as

$$\bar{R}_i = \frac{\sum_{j=1}^{n} F_{ij} \int_0^\infty \varepsilon_{j\lambda} E_{bj\lambda} g_i(\theta'_{ij}, \sigma/\lambda) d\lambda}{\sum_{j=1}^{n} \varepsilon_j E_{bj} F_{ij}} \qquad (A\cdot14)$$

If it is satisfactory to evaluate g at some mean wavelength λ_m, then Eq. (A·14) reduces to

$$\bar{R}_i = \frac{\sum_{j=1}^{n} \varepsilon_j E_{bj} g_{ij} F_{ij}}{\sum_{j=1}^{n} \varepsilon_j E_{bj} F_{ij}} \qquad (A\cdot15)$$

where g_{ij} stands for g evaluated at some mean angle between surfaces A_i and A_j or calculated from the equation

$$\int_{A_i} \int_{A_j} g_i(\theta', \sigma/\lambda_m) K_{ij} dA_j dA_i = g_{ij} \pi A_i F_{ij} \qquad (A\cdot16)$$

In a highly reflecting enclosure the contribution due to emission is a small fraction of the leaving energy and hence can be ignored. Also, due to large number of

interreflections the radiant energy can be assumed to be well mixed spectrally. The spectral distribution can be assumed the same as the spectral distribution of energy emitted into the enclosure. Under these assumptions and assuming constant ρ, Eq. (A·10) can be written as

$$\bar{R}_i = \frac{\int_0^\infty \left[\sum_{k=1}^{n} \varepsilon_{k\lambda} I_{bk\lambda} A_k\right] \sum_{j=1}^{n} W_j \int_{A_i}\int_{A_j} g_i(\theta',\sigma/\lambda) K_{ij}\, dA_j\, dA_i\, d\lambda}{\int_0^\infty \left[\sum_{k=1}^{n} \varepsilon_{k\lambda} I_{bk\lambda} A_k\right] \sum_{j=1}^{n} W_j \int_{A_i}\int_{A_j} K_{ij}\, dA_j\, dA_i\, d\lambda} \qquad (A\cdot17)$$

where the factors W_j are proportional to the intensity leaving each surface. Note that I_λ over each surface is assumed to be uniform. If this assumption is not valid the enclosure can be further subdivided. Introducing g_{ij} from Eq. (A·16) into Eq. (A·17) leads to

$$\bar{R}_i = \frac{\int_0^\infty \left[\sum_{k=1}^{n} \varepsilon_{k\lambda} E_{bk\lambda} A_k\right] \sum_{j=1}^{n} W_j g_{ij\lambda} F_{ij}\, d\lambda}{\left[\sum_{k=1}^{n} \varepsilon_k E_{bk} A_k\right] \sum_{j=1}^{n} W_j F_{ij}} \qquad (A\cdot18)$$

Further, if it is assumed that g_{ij} can be evaluated at some mean wavelength $\lambda = \lambda_m$, Eq. (A·18) reduces to

$$\bar{R}_i = \left[\sum_{j=1}^{n} W_j g_{ij} F_{ij}\right] \Big/ \sum_{j=1}^{n} W_j F_{ij} \qquad (A\cdot19)$$

Equations (A·17) through (A·19) are of little help unless we can make a good guess about the weighting factor W_j. In a highly reflecting well-enclosed enclosure all of the W_j can be assumed equal because of the large number of interreflections. For other cases only that W_j can be retained whose corresponding surface makes the most contribution to $\bar{R}_i$.

Example.

The quantitative effects of various parameters on the specular component are illustrated by an example. The configuration, roughness and temperatures chosen for the example are the same as for the present study. Surface 1 is assumed to be perfectly reflecting and to have the roughness indicated in Figure A-4. The intensity of radiation leaving surface 3 is assumed diffuse and with the spectral distribution corresponding to blackbody emission at the temperature indicated in the figure. The local as well as the overall specular components were calculated with a variation of intensity as large as a factor of 20 across surface 3. The calculated local specular component is presented in Figure A-4 for the intensity leaving surface 3 uniformly distributed. For other distributions it was similar. The results are given only for $\eta = 7/16$ because for $\eta = 1/16$ the difference was small. The overall specular component of reflectivity is given in Table A-1 for other distributions also.

Comparison of the results (presented and those not presented) shows that the local as well as the overall specular component of reflectivity is not very sensitive to the variation in intensity leaving surface 3. The local specular component of reflectivity shows a large variation across the surface for a relatively close configuration ($\gamma = 1/6$), especially for large roughness and temperature. In spite of the large variation of the local specular component, the overall specular component $\bar{R}$ is very close to the local value at locations where most of the energy is incident in near normal directions. This seems to be due to the fact that the intensity of radiation incident at oblique angles has only a small contribution to the overall specular component. This is due to the presence of the K_{ij} term in the equation for $\bar{R}$. For parallel plates K_{ij} is proportional to $\cos^4\theta$, which decreases very rapidly with increasing θ.

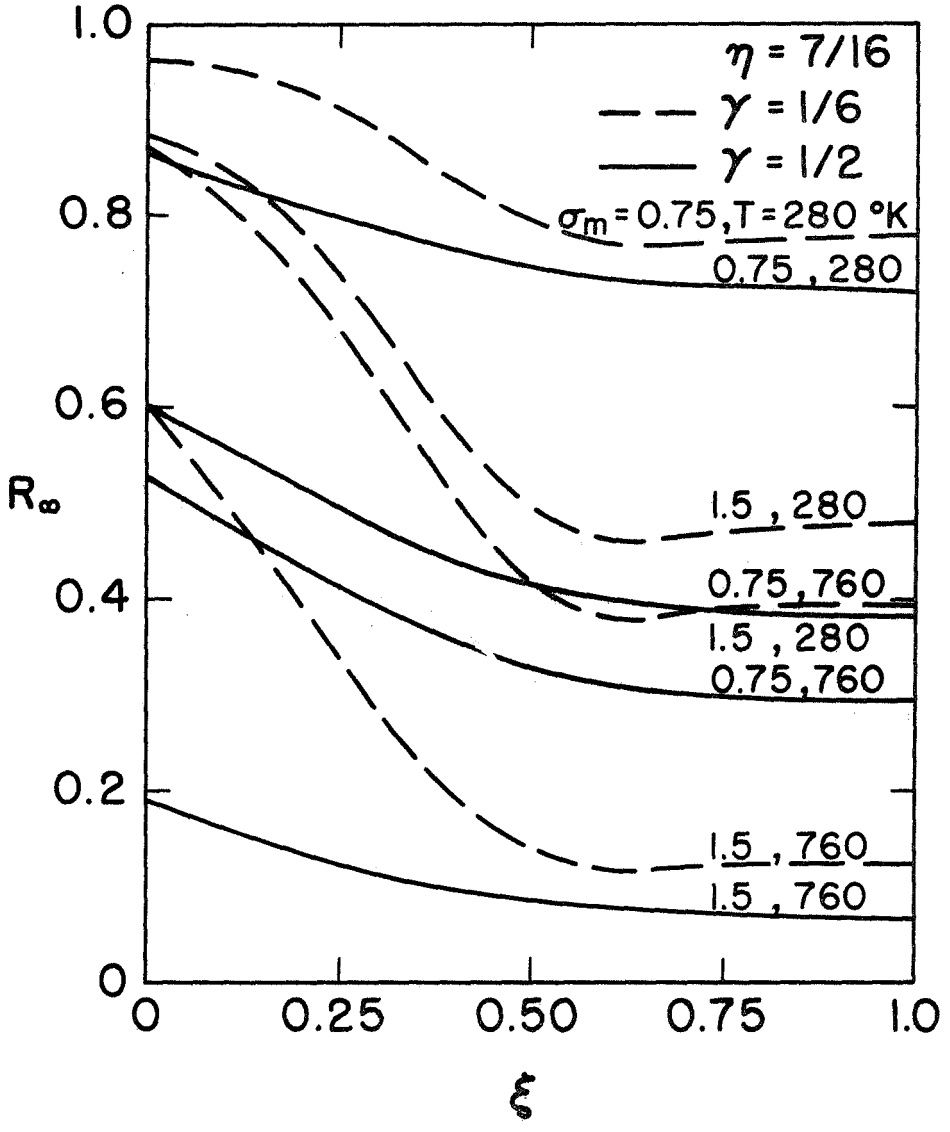

Figure A-4. Specular Component of Reflectivity of Perfectly Reflecting Surface 1. Intensity of Radiation Leaving Surface 3 is Diffuse and Uniform with the Spectral Distribution Corresponding to Blackbody Emission at the Indicated Temperature.

TABLE A-1

Overall Specular Component of Reflectivity of Perfectly Reflecting Surface 1. The Intensity of Radiation Leaving Surface 3 is Diffuse with the Spectral Distribution Corresponding to Blackbody Emission at the Indicated Temperature Varies Linearly with ξ, $I_{3\lambda}(\xi, \eta) = a + b\xi$.

γ	$\overline{R}_\infty$						$I_{3\lambda}(\xi,\eta)$
	σ_m = 0.75μ			1.5μ			a,b
	280°K	590°K	760°K	280°K	590°K	760°K	
	0.785		0.419	0.497		0.150	1,19
1/6	0.774	0.500	0.394	0.474	0.202	0.131	1,0
	0.769		0.383	0.465		0.122	20,-19
	0.764		0.361	0.446		0.101	1,19
1/2	0.747	0.443	0.332	0.419	0.148	0.087	1,0
	0.737		0.315	0.403		0.079	20,-19

APPENDIX B

DISCUSSION OF EXPERIMENTAL ERRORS

There are many factors which contribute in a complicated manner to the evaluation of local irradiation, thus making a quantitative estimate of the error almost impossible; hence what follows is only a qualitative estimate.

Use of some mean temperature instead of considering the actual local temperature variations across the surfaces, inaccuracy in calculating the temperature drop across the plate or paint, and error in the measurement of temperature with thermocouples cause temperature errors which are compounded by T^4-terms in the equations defining irradiation. Maximum non-uniformity of temperature was on the hot plate and was less than 1.0%. The manufacturer claims the performance of Chromel-Alumel thermocouple wires used to be according to NBS standards which is ± 2.22°C up to 550°K and ± 3/4 percent from 550°K to 1533°K. The effect of this error is reduced by using the wire from the same roll for calibration as well as for actual installation. The temperature difference across the paints under high heat loads is estimated to be less than 2°C. Some error is expected in the measured [111] emittances of the 3M Black Velvet and Pyromark paints. The surface temperature errors in both the irradiation and emittance measurements are due to the difficulty in calculating accurately the temperature drop across the paint; therefore, they are compensating and the actual error in the calibration curves is expected to be much lower [111].

The residual gas pressure variation in the system should have had little effect on the measured irradiation

since the radiation flux distribution is only a function of surface temperatures and radiation properties. The measurements were made under vacuum conditions to practically eliminate convection and hence achieve a more uniform temperature over each area as well as to eliminate any condensables from the system.

The errors in the physical geometry are also expected to be small. The estimated errors in the measurement of size of the plates and separation distances are less than 1 percent. The reduction in test surface area due to holes for thermopiles is less than 1.2 percent. Radiation leaving the chamber walls and recorded by the thermopiles is estimated to be less than 4 percent of the measured flux in the worst possible case. Some error is introduced by transmission characteristics of thermopile window since they are functions of not only the temperature but also of the degree of polarization as well as the spectral and directional distribution of the incident radiation field.

Interference filters also contribute to the error because the transmission is direction and polarization dependent. With an increase in the incident angle, not only does the spectral transmittance decrease and the bandwidth increase, but also the peak of the transmittance curve is shifted towards shorter wavelengths. However, the effect is relatively small. For example, for the 4.51μ filter an increase in the angle of incidence from normal to 70° results in a 0.005μ increase in the bandwidth and the peak wavelength of the transmission scan decreases by 0.27μ. The effect of these variations can be examined more clearly by writing the equation for transmittance of the filter. Rigorously, the transmission τ of the filter is given by

$$\tau = \int_{\Omega'} \int_{\Delta\lambda} \tau_\lambda(\theta') I'_\lambda(\theta') \cos\theta' \, d\lambda \, d\Omega' / G \qquad (B\cdot1)$$

The integration is performed over $\Delta\lambda$ because outside this range τ_λ is zero. Although τ is a function of λ and θ', for all practical purposes at not too oblique angles [112]

$$\int_{\Delta\lambda} \tau_\lambda(\theta')d\lambda = C = \text{constant} \qquad (B\cdot 2)$$

Since $\Delta\lambda$ is small, over this interval I_λ can be assumed to be independent of λ. This allows rewriting Eq. (B·1) in the form

$$\tau = C\Delta\lambda \int_{\Omega'} I'_\lambda(\theta')\cos\theta' d\Omega'/G \qquad (B\cdot 3)^*$$

Hence, the error introduced by this simplification arises from the assumption that I_λ is constant over the interval $\Delta\lambda$, which is very small.

It is difficult to evaluate the error introduced in the measurements by the above effects but these effects are expected to a large extent to be calibrated out since the calibration was performed with a similar arrangement of surfaces.

---

* Note that the form of Eq. (B·3) shows that in a relative calibration procedure it is not necessary to know the transmission or the transmission scan of the filter.

APPENDIX C

TABLE C-1

Measured and Predicted Local Irradiation G^*_λ on Spectral Basis, $\lambda = 3.08\mu$

Surfaces 1-2-3, γ	T_1, T_2 °K	Model	G^*_λ							
			η = 1/8				3/8			
			ξ = 1/8	3/8	5/8	7/8	1/8	3/8	5/8	7/8
		EXP	320	1275	3137	4089	289	1307	3643	4502
	284.8	S	94	789	2826	4423	112	927	3476	5203
	594.1	D	69	307	1672	3805	101	501	2252	5624
		DP(S)	183	1088	3220	4810	193	1110	3900	5690
1/6										
		EXP	1107	5057	12192	15141	1098	5744	12361	20867
	284.3	S	564	4727	17001	26082	675	5597	20591	31214
	752.9	D	412	1836	10000	22726	604	2991	13494	33627
		DP(S)	680	4040	12160	18300	718	4110	14800	21400
S-S-S										
		EXP	320	898	1197	1266	459	1041	1503	1503
	284.1	S	307	733	1106	1447	324	788	1269	1537
	586.5	D	131	293	565	901	166	385	758	10770
		DP(S)	330	810	1170	1440	355	876	1410	1650
1/2										
		EXP	2030	4008	4850	5463	2088	4133	6160	6322
	283.6	S	2147	5126	7710	10094	2271	5512	8844	10707
	758.5	D	916	2047	3950	6301	1160	2691	5300	7535
		DP(S)	1430	3520	5130	6350	1540	3820	6190	7250
		EXP	116	471	1453	3181	139	631	1852	4617
	283.4	S	70	274	1600	3600	80	374	2062	4900
	588.0	D	69	305	1664	3787	100	499	2241	5598
		DP(S)	86	360	1705	3960	101	549	2580	5650
1/6										
		EXP	539	1743	6529	12642	602	2695	9412	21716
	283.8	S	423	1652	9639	21661	487	2263	12421	29565
	750.2	D	415	1848	10054	22871	608	3010	13581	33843
		DP(S)	328	1368	6480	15040	385	2095	9860	21450
S-S-D										
		EXP	210	404	630	771	242	473	865	1158
	283.5	S	149	327	588	995	180	403	703	1235
	590.1	D	142	318	614	979	180	418	824	1171
		DP(S)	153	352	606	947	180	407	840	1375
1/2										
		EXP	918	1656	2356	3104	1008	1894	2842	4409
	283.1	S	960	2104	3783	6396	1160	2595	4522	7943
	754.9	D	916	2046	3948	6298	1159	2690	5297	7532
		DP(S)	608	1400	2410	3760	715	1603	3330	5470
		EXP	168	573	1930	3658	171	708	2398	4615
	283.7	S	102	864	3027	4708	116	913	3571	5500
	593.4	D	79	312	1711	4328	88	467	2675	6078
		B(D+S)	125	368	1848	3812	138	472	2573	5381
1/6										
		EXP	825	2841	8970	18266	911	3214	12537	21177
	283.7	S	638	5414	18995	29079	726	5723	22207	34429
	760.9	D	492	1966	10674	26958	548	2912	16670	37818
		B(D+S)	492	1443	7270	15012	542	1855	10157	21210
S-S-B										
		EXP	1322	2502	3953	4970	1428	2706	4479	6016
1/2	283.7	S	2170	5280	7827	10720	2338	5601	8669	11037
	759.5	D	948	1745	4309	6057	1110	2557	4601	7763
		B(D+S)	776	1867	3452	5520	940	2280	4254	7221

TABLE C-1 (cont'd.)

Surfaces 1-2-3, γ	T_1, T_2 °K	Model	G^*_λ							
			η = 1/8				3/8			
			ξ = 1/8	3/8	5/8	7/8	1/8	3/8	5/8	7/8
		EXP	335	1071	2382	3362	378	1166	2578	3877
	284.0	S	104	884	3097	4818	118	935	3654	5628
	596.6	D	81	319	1751	4428	90	478	2737	6219
		B(D+S)	245	1295	2873	3296	264	1500	3037	4598
1/6										
		EXP	1313	3844	8234	10983	1390	4430	9301	14787
	284.8	S	589	5002	17551	26869	671	5288	20519	31812
	758.6	D	455	1816	9863	24909	506	2690	15403	34944
		B(D+S)	868	4578	10148	11610	935	5315	10707	16200
S-B-S										
		EXP	430	823	1213	1434	525	818	1184	1579
	283.9	S	348	847	1260	1728	375	899	1393	1777
	594.1	D	152	280	692	972	178	420	738	1246
		B(D+S)	409	833	1147	1156	438	874	1165	1385
1/2										
		EXP	1818	3225	4377	5386	1893	3683	4768	6076
	284.7	S	1981	4821	7145	9786	2135	5113	7914	10076
	755.5	D	866	1593	3933	5529	1014	2334	4200	7086
		B(D+S)	1435	2917	4016	4046	1532	3060	4077	4850
		EXP	128	663	2092	3985	138	745	2407	5308
	283.6	S	105	897	3142	4887	120	948	3707	5709
	596.0	D	82	323	1776	4492	91	485	2776	6308
		B(D+S)	165	515	1841	4317	174	665	2769	6542
1/6										
		EXP	577	2897	8971	21010	691	3520	13091	29133
	284.4	S	650	5519	19363	29644	740	5834	22638	35097
	768.5	D	502	2004	10881	27481	559	2968	16993	38552
		B(D+S)	643	2012	7175	16790	681	2594	10770	25496
S-B-B										
		EXP	192	373	616	905	220	462	790	1133
	283.9	S	342	833	1238	1698	368	883	1369	1746
	592.8	D	150	275	680	955	175	403	726	1224
		B(D+S)	163	346	739	995	194	427	898	1278
1/2										
		EXP	712	1403	2988	4920	830	1929	3616	6024
	284.4	S	2070	5036	7465	10225	2230	5342	8268	10527
	758.5	D	905	1665	4109	5777	1059	2439	4388	7404
		B(D+S)	611	1294	2762	3721	725	1600	3361	4781

TABLE C-2

Measured and Predicted Local Irradiation G^*_λ on Spectral Basis, $\lambda = 4.51\mu$

Surfaces 1-2-3, γ	T_1, T_2 °K	Model	G^*_λ							
			η = 1/8				3/8			
			ξ = 1/8	3/8	5/8	7/8	1/8	3/8	5/8	7/8
		EXP	15.0	64.0	142.1	182.1	14.6	68.3	178.6	227.8
	286.6	S	5.7	47.9	174.0	272.0	6.8	56.8	213.0	319.0
	596.4	D	4.2	18.9	103.0	233.0	6.2	30.8	138.0	344.0
		DP(S)	8.8	52.0	157.0	234.0	9.2	52.7	190.0	277.0
1/6										
		EXP	49.4	195.5	495.2	684.8	57.9	222.6	602.1	757.2
	284.8	S	21.0	175.0	638.0	973.0	25.0	208.0	775.0	1160.0
	757.0	D	15.4	68.5	373.0	848.0	22.6	112.0	504.0	1254.0
		DP(S)	31.7	189.0	567.0	875.0	33.4	192.0	690.0	1000.0
S-S-S										
		EXP	23.9	42.6	43.5	51.2	22.8	42.1	50.5	55.7
	285.9	S	18.5	44.2	67.0	87.5	19.5	47.6	76.9	93.0
	586.2	D	7.9	17.7	34.0	54.4	10.0	23.3	45.9	65.0
		DP(S)	15.5	38.0	55.1	68.5	16.6	41.1	66.8	78.5
1/2										
		EXP	89.2	165.0	188.9	214.2	81.4	182.8	218.1	243.8
	284.2	S	73.9	177.0	267.0	349.0	78.2	190.0	306.0	371.0
	758.6	D	31.6	70.6	136.0	217.0	40.0	93.0	183.0	260.0
		DP(S)	62.2	152.0	222.0	274.0	67.0	165.0	268.0	314.0
		EXP	7.9	22.6	80.9	186.3	8.5	31.4	119.5	260.0
	283.5	S	4.7	18.3	107.0	239.0	5.4	25.0	137.7	325.6
	592.1	D	4.6	20.4	111.3	252.1	6.7	33.3	149.8	372.5
		DP(S)	4.5	19.0	90.0	210.2	5.3	29.0	137.0	296.0
1/6										
		EXP	26.7	85.1	297.7	609.1	29.1	115.9	450.2	841.2
	283.6	S	16.6	64.8	378.0	849.0	19.1	88.7	487.0	1157.0
	758.1	D	16.3	72.5	395.0	897.2	23.9	118.3	533.2	1326.9
		DP(S)	16.1	67.1	348.0	736.0	18.9	102.5	485.0	1052.0
S-S-D										
		EXP	11.9	17.3	22.8	35.9	13.0	22.9	31.6	48.7
1/2	283.4	S	9.6	20.9	37.7	63.6	11.6	25.8	45.0	79.0
	590.7	D	9.1	20.4	39.3	62.6	11.6	26.8	52.8	74.9
		DP(S)	7.7	17.5	30.1	47.0	9.0	20.2	41.6	68.5
		EXP	10.7	34.9	143.6	245.4	12.0	39.8	163.2	347.2
		S	6.6	56.7	202.1	312.1	7.6	60.2	233.8	363.8
	283.7	D	5.3	20.7	113.5	285.9	5.8	31.0	177.4	401.6
	598.7	B(D+S)	7.8	24.8	108.6	205.0	8.4	30.9	125.1	295.0
		D+S	5.7	25.6	105.9	252.2	6.5	32.8	154.9	342.3
		DP(D+S)	6.1	30.1	101.3	222.9	7.8	32.5	151.5	305.9
1/6										
		EXP	30.7	111.4	454.3	819.6	35.6	142.2	521.8	997.2
		S	22.1	187.8	664.2	1016.2	25.1	198.5	777.2	1195.0
	283.7	D	17.2	68.6	372.4	940.0	19.1	101.7	582.0	1318.0
	754.3	B(D+S)	25.5	80.7	353.0	668.0	27.2	100.4	406.2	961.4
		DP(D+S)	19.8	97.9	329.0	726.3	25.2	105.6	491.9	996.4
S-S-B										
		EXP	13.0	23.3	37.8	56.0	13.9	28.2	40.6	53.9
		S	20.9	50.8	76.1	104.1	22.4	54.2	83.7	108.3
	283.7	D	9.2	16.9	41.7	58.6	10.8	24.8	44.5	75.0
	588.6	B(D+S)	8.3	16.1	29.7	52.3	9.0	21.1	38.5	64.4
		D+S	9.9	22.5	43.6	62.8	11.8	25.4	53.4	76.4
		DP(D+S)	8.9	17.5	34.9	45.5	10.1	21.4	42.2	60.3
1/2										
		EXP	43.1	79.1	129.7	210.4	49.6	90.6	147.4	181.3
	283.7	S	74.9	181.4	271.0	371.0	80.3	194.0	299.0	386.0
	751.8	D	32.7	60.3	149.0	209.0	38.3	88.3	159.0	268.0
		B(D+S)	29.6	57.5	105.7	186.3	32.1	75.2	137.0	230.0
		DP(D+S)	31.9	62.5	124.4	161.9	35.9	76.1	150.3	214.9

TABLE C-3

Measured and Predicted Local Irradiation G^* on Total Basis

Surfaces 1-2-3, γ	T_1, T_2 °K	Model	G^*							
			η = 1/8				3/8			
			ξ = 1/8	3/8	5/8	7/8	1/8	3/8	5/8	7/8
		EXP	0.61	3.96	11.89	19.01	0.67	3.92	14.57	22.32
		S	0.39	3.37	13.24	19.77	0.48	4.01	15.91	23.00
	284.2	D	0.32	1.49	8.04	16.98	0.47	2.41	10.76	25.03
	597.3	DP(S)	0.56	3.37	11.41	17.11	0.55	3.56	12.64	18.93
		$DP(S)_G$	0.61	3.66	11.60	16.88	0.64	3.74	14.21	20.00
1/6										
		EXP	1.89	13.12	38.52	52.97	1.97	13.22	45.96	62.75
		S	1.18	9.98	37.96	56.17	1.43	11.82	45.57	66.40
	285.2	D	0.91	4.08	22.23	49.00	1.33	6.64	29.86	72.37
	761.9	DP(S)	1.69	10.05	32.80	50.04	1.64	10.59	36.06	55.07
		$DP(S)_G$	1.82	10.92	33.62	49.53	1.92	11.13	41.10	58.45
		$DP(S)_{SG}$	1.80	10.13	34.12	45.72	1.97	11.66	39.03	59.77
S-S-S										
		EXP	1.64	2.87	4.70	6.60	1.74	2.86	4.38	5.52
		S	1.18	2.88	4.53	5.79	1.25	3.10	5.19	6.24
	283.5	D	0.54	1.21	2.29	3.60	0.68	1.59	3.11	4.34
	577.8	DP(S)	0.89	2.36	3.96	4.49	1.06	2.33	3.89	5.32
		$DP(S)_G$	1.00	2.41	3.90	4.85	1.10	2.55	4.12	4.71
1/2										
		EXP	5.26	10.59	13.29	17.75	5.54	10.88	13.71	17.42
		S	3.76	9.06	13.95	17.97	3.97	9.74	15.97	19.21
	284.6	D	1.64	3.67	7.03	11.16	2.08	4.83	9.48	13.39
	746.8	DP(S)	2.84	7.49	12.35	14.00	3.36	7.42	12.13	16.55
		$DP(S)_G$	3.21	7.71	12.26	15.17	3.51	8.14	12.95	14.85
		$DP(S)_{SG}$	3.36	7.81	12.33	15.12	3.53	8.15	13.67	15.76
		EXP	0.28	0.87	5.17	15.24	0.34	1.54	8.81	21.16
		S	0.32	1.33	7.56	15.92	0.38	1.82	9.87	21.68
	283.7	D	0.32	1.48	8.01	16.91	0.47	2.40	10.72	24.93
	595.7	DP(S)	0.26	1.35	6.39	13.50	0.38	1.92	8.93	19.30
		$DP(S)_G$	0.31	1.36	6.45	13.88	0.37	2.06	9.70	19.80
		$DP(S)_{SG}$	0.29	1.64	6.17	14.65	0.38	1.97	8.26	20.33
1/6										
		EXP	0.79	3.48	18.25	41.54	0.95	5.64	28.28	58.12
		S	0.91	3.62	20.94	45.81	1.05	4.97	27.11	62.46
	283.6	D	0.90	4.05	22.07	48.65	1.32	6.60	29.66	71.86
	756.8	DP(S)	0.73	3.78	17.92	39.18	1.07	5.32	25.05	56.07
		$DP(S)_G$	0.89	3.79	18.05	40.43	1.05	5.77	27.15	57.80
		$DP(S)_{SG}$	0.81	4.61	17.08	42.48	1.08	5.45	22.83	58.90
S-S-D										
		EXP	0.58	1.21	2.15	3.31	0.80	1.40	2.71	4.15
		S	0.57	1.26	2.26	3.73	0.70	1.56	2.70	4.64
	283.6	D	0.55	1.23	2.33	3.67	0.70	1.63	3.17	4.43
	580.6	DP(S)	0.43	1.02	1.77	2.81	0.55	1.22	2.37	3.62
		$DP(S)_G$	0.45	1.06	2.13	3.51	0.61	1.28	2.58	3.90
		$DP(S)_{SG}$	0.47	1.02	2.17	2.77	0.58	1.14	2.64	3.61
1/2										
		EXP	2.14	3.93	6.15	9.94	2.81	4.63	7.91	13.81
		S	1.79	3.93	7.05	11.83	2.17	4.84	8.43	14.70
	284.2	D	1.71	3.82	7.34	11.65	2.17	5.04	9.88	13.97
	752.9	DP(S)	1.34	3.20	5.57	9.00	1.74	3.84	7.49	11.60
		$DP(S)_G$	1.41	3.34	6.81	8.08	1.93	4.03	8.21	12.56
		$DP(S)_{SG}$	1.47	3.21	6.88	8.85	1.82	3.57	8.37	11.55

TABLE C-3 (cont'd.)

Surfaces 1-2-3, γ	T_1, T_2 °K	Model	G*							
			η = 1/8				3/8			
			ξ = 1/8	3/8	5/8	7/8	1/8	3/8	5/8	7/8
		EXP	0.83	2.36	8.10	14.30	0.91	2.80	10.30	19.20
		S	0.39	3.44	13.38	19.60	0.45	3.68	15.41	22.91
	283.8	D	0.35	1.42	7.60	17.90	0.39	2.12	11.83	25.21
	594.4	B(D+S)	0.47	1.87	6.82	12.09	0.53	2.05	9.15	17.18
		D+S	0.40	2.58	7.93	15.01	0.44	3.00	11.89	20.55
1/6										
		EXP	2.10	7.40	22.30	45.80	2.30	8.90	31.80	63.16
		S	1.23	10.70	39.60	59.20	1.41	11.32	46.12	69.00
	283.7	D	1.01	4.05	22.05	54.21	1.13	6.09	34.47	76.30
	763.3	B(D+S)	1.42	5.92	17.05	34.65	1.51	6.59	25.96	52.00
		D+S	1.31	5.94	22.46	49.97	1.29	8.60	34.17	67.16
		$DP(D+S)_G$	1.33	6.12	19.43	43.08	1.59	7.47	27.21	56.70
		$DP(D+S)_{SG}$	1.29	5.97	18.70	42.37	1.58	7.23	26.46	56.17
S-S-B										
		EXP	0.84	1.51	2.40	2.90	0.89	1.75	2.30	3.65
		S	1.32	3.18	5.00	6.73	1.37	3.50	5.50	6.94
	283.8	D	0.60	1.13	2.72	3.78	0.71	1.64	2.94	4.83
	589.6	B(D+S)	0.67	1.34	2.37	3.18	0.70	1.63	2.63	4.33
		D+S	0.90	1.80	3.06	4.52	0.95	2.33	3.90	5.17
1/2										
		EXP	2.45	4.05	6.60	8.70	2.60	5.23	6.92	10.05
		S	4.13	9.84	15.17	20.49	4.29	10.80	16.70	21.03
		D	1.81	3.35	8.21	11.49	2.13	4.90	8.81	14.72
	283.9	B(D+S)	1.94	3.73	7.24	9.23	2.14	4.75	7.88	11.62
	756.1	D+S	2.31	5.09	8.82	14.41	2.89	6.35	10.49	15.17
		$DP(D+S)_G$	2.09	4.37	8.48	10.87	2.43	5.50	8.97	12.94
		$DP(D+S)_{SG}$	2.06	4.35	8.69	11.08	2.37	5.52	9.08	13.11
		EXP	0.83	3.72	8.29	13.11	0.92	4.01	10.92	18.32
		S	0.38	3.31	12.74	18.84	0.43	3.54	14.75	22.12
	283.9	D	0.33	1.37	7.34	17.24	0.37	2.05	11.41	24.27
	589.4	B(D+S)	0.63	3.16	7.85	9.97	0.64	3.66	9.45	14.02
		D+S	0.50	4.10	11.01	13.13	0.58	4.45	12.61	17.13
1/6										
		EXP	3.01	11.22	26.34	39.82	3.24	15.43	35.28	52.54
		S	1.18	10.27	38.03	56.82	1.35	10.87	44.32	66.27
	284.8	D	0.97	3.90	21.20	52.07	1.08	5.83	33.13	73.24
	759.2	B(D+S)	2.00	10.25	23.07	31.22	1.90	11.31	28.57	39.61
		D+S	1.51	12.20	31.81	39.52	1.83	13.89	36.08	52.82
		$DP(D+S)_G$	2.10	11.46	26.40	34.95	2.49	13.14	31.97	43.87
		$DP(D+S)_{SG}$	2.11	11.36	25.94	34.57	2.48	13.11	31.52	43.06
S-B-S										
		EXP	4.31	8.27	11.13	11.95	4.72	8.89	11.87	14.85
		S	4.06	9.68	14.93	20.16	4.22	10.63	16.44	20.70
		D	1.78	3.30	8.08	11.31	2.09	4.82	8.66	14.49
1/2	284.8	B(D+S)	3.60	7.66	9.61	10.44	3.63	7.82	9.87	12.71
	755.4	D+S	3.82	9.51	10.22	15.18	4.36	10.18	14.25	16.06
		$DP(D+S)_G$	3.66	7.78	9.88	11.00	4.02	8.35	10.80	13.14
		$DP(D+S)_{SG}$	3.67	7.76	10.07	10.78	4.00	8.34	10.75	13.26

TABLE C-3 (cont'd.)

Surfaces 1-2-3, γ	T_1, T_2 °K	Model	G*							
			η = 1/8				3/8			
			ξ = 1/8	3/8	5/8	7/8	1/8	3/8	5/8	7/8
		EXP	0.72	2.43	8.62	15.20	0.78	3.31	12.11	21.22
		S	0.39	3.45	13.44	19.65	0.45	3.70	15.47	23.00
	283.8	D	0.35	1.43	7.63	17.98	0.39	2.13	11.88	25.31
	594.9	B(D+S)	0.55	2.07	7.22	11.89	0.59	2.65	9.40	16.73
		D+S	0.47	2.48	8.62	15.70	0.57	3.38	11.43	21.11
1/6										
		EXP	2.12	7.31	23.22	44.20	2.21	8.92	33.41	60.13
		S	1.18	10.28	38.07	56.89	1.35	10.88	44.37	66.34
		D	0.97	3.90	21.22	52.12	1.09	5.84	33.17	73.32
	284.3	B(D+S)	1.55	5.59	18.42	35.30	1.67	6.84	26.71	47.02
	758.2	D+S	1.34	7.30	22.82	43.34	1.74	8.22	30.07	59.10
		$DP(D+S)_G$	1.56	6.56	19.70	39.76	1.67	8.33	28.68	54.07
		$DP(D+S)_{SG}$	1.53	6.33	19.31	40.84	1.65	8.16	28.39	53.48
S-B-B										
		EXP	0.81	1.61	2.53	3.51	0.87	1.69	2.69	4.23
		S	1.24	2.99	4.71	6.34	1.29	3.29	5.17	6.54
	284.1	D	0.57	1.06	2.56	3.56	0.67	1.55	2.78	4.55
	582.1	B(D+S)	0.68	1.34	2.07	3.00	0.73	1.45	2.27	3.48
		D+S	0.86	1.76	2.79	4.30	0.98	2.18	3.57	4.70
1/2										
		EXP	2.33	4.12	7.56	10.60	2.52	5.13	9.20	12.24
		S	3.95	9.43	14.54	19.63	4.11	10.35	16.01	20.15
		D	1.74	3.21	7.87	11.01	2.04	4.69	8.44	14.10
	284.5	B(D+S)	1.80	3.50	6.56	9.16	2.10	4.18	7.24	11.48
	750.4	D+S	2.32	4.96	8.54	12.32	2.82	5.57	9.73	16.26
		$DP(D+S)_G$	2.03	4.43	7.15	8.80	2.39	4.58	8.45	12.45
		$DP(D+S)_{SG}$	2.03	4.29	7.42	8.60	2.35	4.55	8.46	12.64

APPENDIX D

RECIPROCITY RELATION FOR RADIATION EXCHANGE

In this appendix the reciprocity relation for absorption factors is discussed. The assumptions under which the relation is valid are described. The effect of change in radiation characteristics or temperatures of participating surfaces is mentioned. In the end a reciprocity relation is derived which is valid for arbitrary radiation characteristics and temperatures of surfaces.

The reciprocity relation on spectral basis between an elementary area dA_i and a surface A_j of an enclosure is written as

$$dA_i \varepsilon_{i\lambda} B_{\lambda di-j} = A_j \varepsilon_{j\lambda} B_{\lambda j-di} \qquad (D\cdot1)$$

This relation is valid if two conditions are satisfied while calculating the absorption factors: 1) the spectral directional absorptance is assumed equal to the spectral directional emittance, $\alpha_\lambda(\theta) = \varepsilon_\lambda(\theta)$, and 2) the reflection distribution function satisfies the Helmholtz reciprocity relation, $f(\vec{\Omega}',\vec{\Omega},\lambda) = f(\vec{\Omega},\vec{\Omega}',\lambda)$.

It can be shown that a change in radiation characteristics of surfaces other than i and j does not effect the reciprocity relation although it will change the value of absorption factors. Similarly, any change in $\varepsilon_{i\lambda}(\theta)$ or $\varepsilon_{j\lambda}(\theta)$ would alter the value of absorption factors only.

Since the effect of change in temperature appears in Eq. (D·1) only through the radiation characteristics, it does not need any separate discussion.

The reciprocity relation on total basis can be obtained by dropping λ from Eq. (D·1). It is easy to see that validity of the reciprocity relation on spectral basis is a necessary but not a sufficient condition for the validity of this relation on a total basis. Hence, the two conditions mentioned previously must be satisfied by the analytical procedure for calculating the absorption factors. Other conditions are discussed below.

Equation (D·1) on total basis is effected by the change in temperature in two ways: firstly, through the effect of temperature on radiation characteristics, and secondly, due to the change in the spectral distribution of black body emission. One can easily conclude that for unequal temperatures of surfaces i and j, the reciprocity relation holds only if all the participating surfaces in the enclosure are gray. For equal temperatures of surfaces i and j any change in the radiation characteristics alters the value of absorption factors, but the reciprocity relation remains valid. Note that the situations mentioned above are the only two situations in which this relation is valid. However, a general reciprocity relation can be derived with a slightly different definition of absorption factors. If the absorption factor B_{di-j} is calculated by considering the radiation characteristics of dA_i at temperature T_i, while considering the blackbody emission at temperature T_j, then Eq. (D·1) on total basis is valid for arbitrary radiation characteristics of surfaces. This can be easily shown by writing the radiation interchange between dA_i and A_j, Eq. (3·37). Since both surfaces are at the same temperature, the net interchange $Q_{di\rightleftarrows j}$, from second law of thermodynamics, must be zero,

$$Q_{di\rightleftarrows j} = dA_i \varepsilon_i E_{bj} B_{di-j} - A_j \varepsilon_j E_{bj} B_{j-di} = 0$$

or

$$dA_i \varepsilon_i B_{di-j} = A_j \varepsilon_j B_{j-di}$$

The absorption factors so defined reduce to their usual definition under the gray assumption.